Cell division in Mycobacteria: the role of septal factor, SepIVA

By: Angela H. Freeman

Presented to the faculty of the graduate school of
The University of Texas at Arlington
In partial fulfillment of the requirements for the degree of

Doctor of Philosophy

Department of Biology

May 2023

Supervising Committee

Cara Boutte
Supervising Professor

Joseph Boll
Woo-Suk Chang
Matt Fujita
Laura Mydlarz

Table of Contents

Table of Figures

Abstract

Today, about a quarter of the world's population are infected with *Mycobacterium tuberculosis (Mtb)* and therefore, are at risk of developing tuberculosis (TB) disease. Tuberculosis, on average, takes about six months to treat, and even longer for those with drug resistant *Mtb* infections (World Health Organization, 2022). Extended treatment times for these infections are caused by the inherent tolerance to antibiotics conveyed by mycobacteria's distinct cell wall. Mycobacteria have a wide variety of cell wall regulators that help the cell adapt to stress, such as antibiotics. By understanding how these regulators work, we can learn how mycobacteria evade killing by antibiotics.

This work aims to further investigate cell wall regulation. Specifically, we characterize the cell division regulator, SepIVA. We begin by analyzing the post-translational modifications on SepIVA and how they affect SepIVA function. We also study the effects of SepIVA protein depletion on different cytoplasmic cell wall precursor enzymes and polar elongation. Finally, we determine how SepIVA helps mycobacterial cells adapt to certain stressors, mainly DNA damage.

Our data led us to conclude that SepIVA is an activator of cell division and that arginine methylation on the N-terminus and C-terminus of SepIVA have differing roles in the cell cycle. We find that arginine methylation near the N-terminus of SepIVA promotes its role in polar elongation, while the C-terminus largely functions in septation. We characterize specific arginine residues that are crucial to SepIVA's function in cell division as well as its response to DNA damage. Our results support the importance of cell wall regulation on the mycobacterial cell cycle and the treatment of TB.

Chapter 1: Introduction

1.1 Challenges facing the tuberculosis epidemic

The genus *Mycobacteria* includes the pathogens *Mycobacterium tuberculosis* and *Mycobacterium leprae*. *Mycobacterium tuberculosis* (Mtb) causes the lung infection tuberculosis (TB). Prior to the coronavirus pandemic, TB was the leading cause of death due to a single pathogen (World Health Organization, 2022). A key challenge to the TB epidemic is antibiotic resistance and tolerance to current drug regimens. In fact, current TB drug regimens include 6 months of first-line antibiotic treatment and anywhere from 9-20 months of treatment for those with drug-resistant TB infections (World Health Organization, 2022).

Many of the leading antibiotics used to treat infections are cell wall antagonists, meaning they cause bacterial cell walls to lose integrity and eventually cause cell lysis. To create effective antibiotics, scientists aim to understand the organisms they are fighting against. A key part of this understanding includes how bacterial cells adapt in environmental stress. When mycobacteria encounter stress, the cell wall is heavily remodeled, and cells decrease in size (Wu *et al.*, 2016). Responses to stressful environments, such as inside the human lungs, require strict regulation of the cell wall to maintain the balance between cell elongation and cell division. To understand the response of mycobacteria to stress, many scientists use mycobacterial model organism, *Mycobacterium smegmatis* (*Msmeg*). *Msmeg* is not only non-pathogenic but has a population doubling time that is significantly less than *Mtb*, making it a much more pliable relative of *Mtb*. Examining the regulation of the mycobacterial cell wall will

expand knowledge of how mycobacterial cells respond to stressful environments and are tolerant to front-line antibiotics.

1.2 Balancing elongation and division

All bacteria face the same challenges when regulating cell elongation and division: how to organize cell wall machinery spatially and temporally for one cell to elongate and eventually divide into two daughter cells. This includes efforts of the cell to elongate by incorporating newly synthesized cell wall components, replicate and segregate the chromosome, build new cell wall assembly of the division apparatus (known as the divisome), septal cell wall synthesis and then bisect the septum to separate the two cells (Baranowski *et al.*, 2019). To fully layout bacterial cell division, scientists focus on model organisms, such as *E. coli*, and then apply the principles of division in model organisms to other species. By detailing what is known about mechanisms of division in *E. coli*, scientists can understand mechanisms in division of organisms that are tiresome or even harmful to work with, such as *Mycobacterium tuberculosis (Mtb).*

1.3 Elongation in *E. coli*

Before one bacterial cell divides into two daughter cells, the cell must elongate to approximately twice as long as its original size. Elongation can be separated into three stages, 1) peptidoglycan (PG) synthases building new cell wall material, 2) newly synthesized PG incorporation into the cell wall and 3) hydrolases to cleave the PG to create space for nascent PG incorporation. Peptidoglycan is composed of alternating

glycan sugars, N-acetylglucosamines and N-acetylmuramic acid, referred to as GlcNAc and MurNAc, respectively, strung together by glycosyltransferases (Heijenoort, 2001; Vollmer and Bertsche, 2008). These glycan strands are attached to each other by D,D-transpeptidases crosslinking peptide chains stemming from the lactyl group on MurNAc glycans (Born *et al.*, 2006).

1.3a Lipid II synthesis

Before the PG layer can be assembled, the cell has to synthesis the monomeric precursor for peptidoglycan, lipid II (Fig. 1.1). Lipid II is synthesized by the Mur pathway beginning with a single MurNAc residue synthesized by MurA and MurB. A pentapeptide chain consisting of L-alanine, meso-diaminopimelic acid (m-DAP), D-glutamate, and D-alanine dipeptide are added sequentially by ATP-dependent ligases, MurC to MurF, to the MurNAc residue (Benson *et al.*, 1996; Gegnas *et al.*, 1998; Zeng *et al.*, 1998; Yan *et al.*, 2000; Reck *et al.*, 2001; Baum *et al.*, 2001; El Zoeiby *et al.*, 2003). The peptide chain is attached and the MurNAc is tethered to the plasma membrane by MraY through an undecaprenyl phosphate tail, creating lipid I (Ikeda *et al.*, 1991; Boyle and Donachie, 1998). A second glycan residue, GlcNAc, is attached to lipid I by MurG, resulting in lipid II (Mengin-Lecreulx *et al.*, 1991). This precursor molecule then must be flipped into the periplasm by lipid II flippase, MurJ (Ruiz, 2008; Sham *et al.*, 2014).

Once in the periplasm, lipid II is polymerized into glycan strands by glycosyltransferases and then crosslinked to other glycan strands by D,D-transpeptidases. Peptidoglycan synthases, often referred to as penicillin-binding proteins (PBPs), are classified into three groups, 1) class A PBPs, bifunctional

glycosyltransferases and transpeptidases, catalyzing both reactions, 2) class B PBPs, which are monofunctional transpeptidases (TPases) or 3) monofunctional glycosyltransferases (GTases) (Suginaka *et al.*, 1972; Typas *et al.*, 2012; Garde *et al.*, 2021). By utilizing different PG synthases, there are two main routes for lipid II to be incorporated into the PG layer that are needed for elongation to occur.

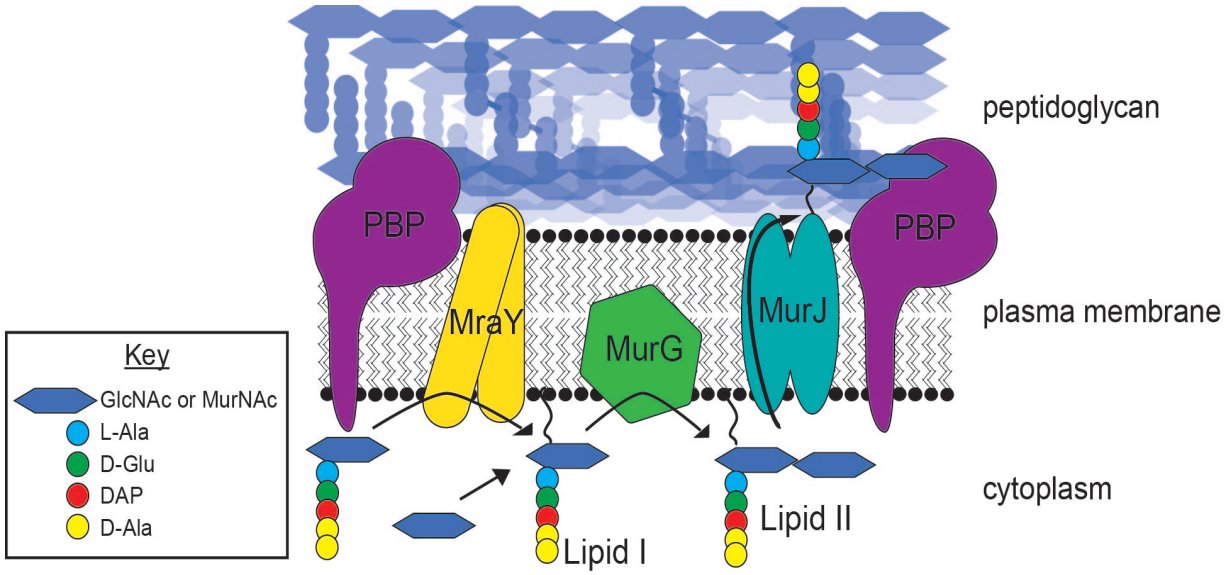

Figure 1.1. Lipid II synthesis in E. coli.

1.3b The Rod complex

The Rod complex consists of RodA, a GTase that is coupled to PBP2, a monofunctional TPase (Rohs *et al.*, 2018). RodA and PBP2 associate with scaffold proteins, MreBCD through MreB's interaction with RodZ (Morgenstein *et al.*, 2015). RodA and PBP2 build new PG, while MreB governs where new PG is incorporated into the sidewall. MreB localizes in small structures that move along the inner perimeter of the cell membrane, resulting in even distribution of new PG into the lateral wall (van Teeffelen *et al.*, 2011; Shi *et al.*, 2018). The incorporation of PG into the lateral wall maintains cell wall integrity and rod shape (Wachi *et al.*, 1987). MreB even interacts with

MurG, directing where the PG precursor molecule, lipid II is synthesized (Mohammadi *et al.*, 2007). MreC is a membrane bound protein that binds to both MreB and PBP2 (Kruse *et al.*, 2005; Contreras-Martel *et al.*, 2017) connecting Mre proteins to PG synthases, in addition to MreB's interaction with RodZ. MreC interacts with transmembrane protein, MreD, and tethers MreB to the membrane (Kruse *et al.*, 2005). Together, MreBCD associate with the Rod complex to spatially regulate PG layer synthesis along the lateral wall of the cell, resulting in elongation of the cell.

1.3c Class A PBPs

Class A PBPs, PBP1a and PBP1b are functionally redundant, and at least one of them has to be present for proper cell growth in *E. coli* (Kato *et al.*, 1985). Before the discovery of the Rod complex, these high molecular weight, bifunctional PBPs were thought to be the sole major peptidoglycan synthases within the cell (Typas *et al.*, 2012; Garde *et al.*, 2021). However, characterization of the Rod complex lead to the discovery that class A PBPs more often fill in gaps in the PG layer (Cho *et al.*, 2016). PBP1a and PBP1b are linked to the outer membrane (OM) of the cell wall through their interactions with lipoproteins, LpoA and LpoB (Typas *et al.*, 2010). LpoA simulates TPase activity of PBP1a (Jean *et al.*, 2014) and LpoB stimulates PBP1b activity (Egan *et al.*, 2014). Put simply, as the Rod complex is assembling PG during elongation, there are holes left behind along the layer. LpoA and LpoB span the periplasm and recruits and associates with their respective PBPs through holes in the PG layer to repair them (Egan *et al.*, 2014; Jean *et al.*, 2014). Through cooperation of the Rod complex and class A PBPs, the PG layer maintains cell wall integrity and shape as the cell elongates before initiating division.

1.3d Peptidoglycan hydrolysis

Once complete, the peptidoglycan (PG) layer appears to be a mesh-like covering encapsulating the cell. For newly synthesized PG to be incorporated, hydrolase enzymes must break the mesh-like PG to make room for new glycan strands. To make room for new glycan strands, endopeptidases, like MepS, MepM and MepH, cleave D-ala and m-DAP crosslinks, creating space for crosslinks with new PG material to be made (Chodisetti and Reddy, 2019). D,D-carboxypeptidases, such as PBP5 (Nelson and Young, 2001), cleave the terminal D-alanine on lipid II after it has been added to a glycan strand. This allows for transpeptidases to then crosslink the newly free m-DAP peptide to the D-ala from the new glycan strand (Egan *et al.*, 2020; Garde *et al.*, 2021). The balance of hydrolysis and PG synthesis results in elongation of the cell wall before the cell is ready to divide.

1.3e Chromosome replication & segregation

Elongation continues until the cell reaches the correct size to trigger initiation of chromosome replication (Katayama *et al.*, 2017). As cell mass increases, so does the amount of the initiator protein, DnaA (Kleckner *et al.*, 2018). When the threshold amount of active DnaA has accumulated, DnaA promotes DNA unwinding at the origin of replication (*oriC*), allowing DNA replication to begin (Katayama *et al.*, 2017; Hansen and Atlung, 2018). While chromosome replication and segregation are happening, the division apparatus is being assembled. However, the chromosome must fully replicate and segregate before cell wall synthesis at the septum occurs. Chromosome segregation is the one of the checkpoints the cell needs to pass before cell constriction (Kleckner *et al.*, 2018).

1.4 Division in *E. coli*

FtsZ is widely understood as the initiator and master regulator of bacterial cell division. The earliest step of cell division is polymerization of FtsZ along the circumference of the cytoplasmic membrane, resulting in a ring-like structure called the Z-ring (Ma *et al.*, 1996; Tsang and Bernhardt, 2015b). After this step, several division factors are recruited to the Z-ring, located at the midcell. These factors, both essential and non-essential, form and regulate the division apparatus, the divisome. An estimated dozen conserved proteins are thought to be recruited to the midcell as part of the divisome (Mahone and Goley, 2020). Recruitment of division factors can be sectioned into early and late divisome assembly.

1.4a Early divisome assembly

Factors considered early divisome proteins are those that directly interact with FtsZ. Once the Z-ring formation begins, FtsZ polymers are anchored to the cell membrane via ZipA and FtsA (Hale and de Boer, 1997). FtsA co-localizes with FtsZ and is required for FtsZ localization (Ma *et al.*, 1996). ZipA stabilizes FtsZ polymers through its interaction with the C-terminus domain of FtsZ. ZipA helps bundle FtsZ polymers, allowing the Z-ring to form circumferentially along the inner membrane of the cell (Hale *et al.*, 2000). Overproduction of ZipA causes inhibited division, implying that ZipA is a negative regulator of FtsZ (Hale and de Boer, 1997; Geissler *et al.*, 2003). However, overproduction of both ZipA and FtsZ leads to normal cell division. This implies that FtsZ and ZipA binding is a checkpoint of cell division, as unbound ZipA could signal to the cell that the Z-ring has not yet formed (Hale and de Boer, 1997). While both FtsA

and ZipA are considered Z-ring anchor proteins, FtsA serves as the communication center between FtsZ and the rest of the divisome (Liu *et al.*, 2015; Pichoff *et al.*, 2015).

The next divisome factors to be recruited are FtsE and FtsX. FtsEX is an ATP-binding cassette (ABC), with FtsE possessing as the nucleotide binding domain and FtsX as the transmembrane domain (Corbin *et al.*, 2007). FtsE interacts with FtsZ and FtsX interacts with FtsA (Corbin *et al.*, 2007; Du *et al.*, 2019). FtsEX recruits peptidoglycan (PG) amidase regulators, such as EnvC and NlpD, to the division site, eventually leading to septation of the cell (Schmidt *et al.*, 2004; Yang *et al.*, 2011). EnvC localizes with the inner membrane while NlpD localizes to the outer. Here, EnvC and NlpD activate cell wall amidases, AmiA, AmiB, and AmiC (Yang *et al.*, 2011). These amidases are PG hydrolases that break PG crosslinks and split apart cell materials shared by the two developing cells, leading to separation of the daughter cells (Yang *et al.*, 2012; Tsang *et al.*, 2017). Outer membrane invagination lead by NplD is regulated by the Tol-Pal system. This system connects the outer membrane to the PG layer and then to the inner membrane to pinch the cell closed with the help of NplD and amidases (Gerding *et al.*, 2007). FtsEX is required for recruitment of late divisome proteins, beginning with the DNA translocase, FtsK.

1.4b Late divisome assembly

Late-stage divisome assembly starts with the DNA translocase, FtsK. FtsK is multifunctional, playing a role in both chromosome segregation and cell division (Sherratt *et al.*, 2010). With the help of FtsEX, FtsK also completes anchoring of FtsA/ZipA to the cell membrane (Hale and de Boer, 2002; Villanelo *et al.*, 2011). Before division can continue, FtsK acts as a checkpoint to ensure the chromosome has fully

replicated and segregated to ensure no DNA is trapped as the new cell envelope is constructed (Mahone and Goley, 2020). FtsK localization leads to recruitment of FtsQ, which then cascades into the recruitment of the remaining divisome proteins (Villanelo *et al.*, 2011).

FtsQLB is part of a highly conserved, transmembrane, regulator of division that also acts as a scaffold for maintaining the structure of the divisome as it matures (Liu *et al.*, 2015). FtsL recruits FtsW and FtsQ recruits FtsI, with stabilization through the FtsQLB subcomplex (Villanelo *et al.*, 2011; Park *et al.*, 2020). When FtsQLB is depleted, cells become filamentous, meaning septation is inhibited (Goehring *et al.*, 2005). FtsL has been implicated as an activator of the cytokinetic ring, based on a FtsL mutant that caused accelerated division (Tsang and Bernhardt, 2015a). FtsQLB is assumed to be a regulator of septal PG synthesis, possibly activating FtsW and FtsI, which are the PG synthases building the septum (Marmont and Bernhardt, 2020). FtsW is a glycosyltransferase, polymerizing lipid II, while FtsI is a transpeptidase, crosslinking glycan strands together to form the new PG (Pogliano *et al.*, 1997; Taguchi *et al.*, 2019; Marmont and Bernhardt, 2020). As FtsEX recruits PG hydrolases to the Z-ring to break apart the PG layer, FtsWI has room to synthesize new PG and build the septum (Marmont and Bernhardt, 2020; Attaibi and den Blaauwen, 2022). FtsWI enlist other PG synthases, like PBP1b and lipid II synthases, to help create the new cell septum before cell constriction can occur (Boes *et al.*, 2019).

The final protein recruited to the divisome is FtsN (Addinall *et al.*, 1997). Despite all other divisome components already localizing, active cell constriction is not triggered until the accumulation of FtsN at the Z-ring (Liu *et al.*, 2015). FtsN interacts with FtsA

and FtsQLB, conformationally changing them from an “off” state to an “on” state (Liu *et al.*, 2015; Weiss, 2015). Additionally, FtsN activates PBP1b, further supporting FtsN accumulation at the Z-ring as the licensing step for septal PG synthesis and launching cell constriction (Boes *et al.*, 2020).

1.4c Regulation of cell division

Cell division is regulated via two pathways: the Min system and nucleoid occlusion (Noc). The Min system is made up of MinC, MinD and MinE. MinCD cooperate to prevent Z-ring formation, while MinE topologically regulates MinCD by keeping it from inhibiting septation at the midcell (de Boer *et al.*, 1989; Raskin and de Boer, 1997). MinC inhibits FtsZ polymerization, stopping the Z-ring from forming (Hu *et al.*, 1999; Pichoff and Lutkenhaus, 2001). Additionally, MinC functionality results lower integrity Z-rings, by unbundling FtsZ polymers (Dajkovic *et al.*, 2008). MinC is activated by MinD, which recruits MinC to the membrane (de Boer *et al.*, 1991; Raskin and de Boer, 1999b; Hu *et al.*, 2003). To determine the correct site of septation, MinD oscillates from cell pole to cell pole, inhibiting division from occurring at the poles (Raskin and de Boer, 1999a). Finally, MinE localization follows MinD oscillation, inhibiting MinD polymerization at the septation site, therefore, allowing the Z-ring to form and division to occur (Hale *et al.*, 2001).

Cell division and chromosome segregation are coordinated by the nucleoid occlusion (Noc) protein, SlmA (Cabré *et al.*, 2015). While DnaA kicks off replication, SlmA makes sure a single, complete copy of the chromosome ends up in each daughter cell. SlmA interacts directly with FtsZ to antagonize polymerization and inhibit cytokinesis before chromosome replication and segregation can be complete (Cho *et*

al., 2011; Cabré *et al.*, 2015). In fact, ΔSlmA + ΔMin cells had even greater number of Z-rings compared to ΔMin cells, implying that the two systems work together to inhibit Z-ring assembly at non-septal sites (Bernhardt and de Boer, 2005). Without regulation through the Min and Noc systems, bacterial cell division would often result in irregularly sized daughter cells with different sized chromosomes. Since misregulation of cell division would often lead to non-viable daughter cells, regulation of division is equally essential to the division process itself.

1.5 Mycobacterial growth and division

While PG synthesis is the core of most bacterial cell division, mycobacteria must account for an additional two layers of cell wall. The three main layers of the mycobacterial cell wall include a thick layer of peptidoglycan (PG), a layer of highly-branched arabinogalactans, and a bilayer of long-chained mycolic acids (Fig. 1.2) (Jankute *et al.*, 2015). The synthesis of distinct cell wall features creates a need for machinery that is also distinct to mycobacteria. Mycobacteria also differ from many of the hallmark features of cell division as described in model organisms, such as elongation mode and regulation of division. While cell division is well characterized in *E. coli*, there is much still unknown about mycobacteria.

1.5a Division in Mycobacteria

Because of the distinct features of mycobacteria, such as the extra layers of the cell wall, mechanisms and factors of division must be distinct from model organisms as well. Within the cassette of division factors in mycobacteria, homologs of FtsA, ZipA and FtsN are missing, despite their essentiality to division in *E. coli.* Homologs of other

divisome factors (FtsZ, FtsEX, FtsK, FtsQLB, FtsI and FtsW) have been found in mycobacteria (Hett and Rubin, 2008). In E. coli, the Z-ring is stabilized by FtsA and ZipA, the lack of these two proteins brings into question how the Z-ring is stabilized in mycobacteria. Investigation into this mystery revealed that, in mycobacteria, FtsW and FtsI create a ternary structure with FtsZ, implying that in addition to the PG synthesis roles these proteins play, they also stabilize the Z-ring, covering the functionalities of FtsA and ZipA (Datta *et al.*, 2006). Mycobacteria stabilize their Z-ring with help of SepF, another FtsZ interacting protein found in Gram-positive bacteria. SepF has been named as the best candidate divisome component that fulfills the function of FtsA and ZipA (Gola *et al.*, 2015).

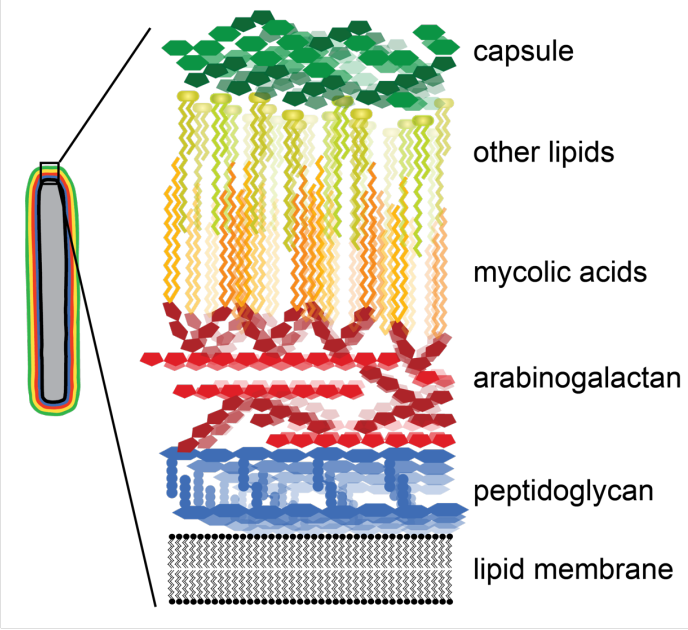

Figure 1.2. The mycobacterial cell wall.

Mycobacteria also lack a homolog of the division protein, FtsN, which is considered a negative regulator of cell division in *E. coli*. In *E. coli*, FtsN is the last protein to be recruited to the divisome and is required for initiation of cell constriction (Weiss, 2015). Without FtsN, cells cannot balance elongation and division. Since this

balance is highly regulated in mycobacteria, it can be assumed that mycobacteria possess distinct factors performing the functions of FtsN.

Mycobacteria lack negative regulators of cell division, such as the nucleoid occlusion (Noc) and Min systems, that are found in both Gram-positive and negative bacteria. Noc, proteins ensure that chromosome segregation has completed, and no DNA will be lost due to the splitting of the cell septum at the end of division (Wu and Errington, 2012). Mycobacteria also lack the Min system, which negatively regulates division by inhibiting FtsZ polymerization at non-division sites (Hu *et al.*, 1999). Considering mycobacterial chromosomes are successfully segregated and FtsZ rings are only present at the midcell before normal cell division, there must be division regulatory systems distinct to mycobacteria.

1.5b Polar elongation

Mycobacteria incorporate new cell wall material at the cell poles, denoted as polar elongation (Logsdon and Aldridge, 2018). This is different from *E. coli,* which incorporates new cell wall along the lateral body of the cell with the help of MreB. Mycobacteria, lacking a known MreB orthologue, need a different set of tools to incorporate recently synthesized cell wall precursors into the already existing cell wall. While some of these tools have been discovered, such as Wag31, which regulates new cell wall synthesis at sites of polar elongation (Kang *et al.*, 2008), much of the machinery accounting for the differences between mycobacteria and other rod-shaped bacteria is still unknown.

Mycobacteria possess LamA, which has been shown to inhibit growth at the new pole, causing elongation from one cell's two poles to occur at different rates (Rego *et*

al., 2017). In mycobacteria, the newer pole, created by the last division, grows at a slower rate compared to the older pole. Because of variable elongation rate, daughter cells will be variable in size after cytokinesis, with the daughter cell inheriting the older pole being longer in length. This helps create a phenotypically heterogenous population of cells of different sizes (Aldridge *et al.*, 2012; Kieser and Rubin, 2014). It has also been shown that heterogeneity conveys antibiotic tolerance or provides advantages in survival within certain conditions (Rego *et al.*, 2017).

When mycobacteria divide at the midcell, a new pole is created. The division machinery at this new pole must then switch modes and begin elongating from the same site. This switch requires additional spatiotemporal regulation that is not needed in lateral growers. How the cell pole regulates the switches from division to elongation is unknown. One way the cell could be regulating growth modes at the poles, although speculative, is through cell wall enzymes like the lipid II synthase, MurG. In *E. coli*, MurG interacts with both divisome and elongasome proteins (Mohammadi *et al.*, 2007). The switch from division to elongation at the poles in mycobacteria could be regulated by cell wall enzymes' interactions with either division or elongation proteins.

1.5c Extra layers of the cell wall

For most bacterial species, cell wall synthesis is centered around PG construction. In mycobacteria, the PG layer is just the first cell wall component to be established. Covalently attached to the PG layer is a thick layer of arabinogalactan, a highly branched polysaccharide assembled by specified transglycosylases (Fig. 1.3) (Alderwick *et al.*, 2015; Shen *et al.*, 2020). The arabinogalactan layer attaches to the outer membrane layer, the inner leaflet of which is composed of mycolic acids. Mycolic

acids are long-chain, two-branched, three-hydroxylated fatty acids that have been observed in every mycobacterial species to date (Marrakchi *et al.*, 2014). Mycolic acids are key to virulence of mycobacteria and are even targeted by front-line anti-tubercular drugs such as isoniazid (Takayama *et al.*, 2005; Puffal *et al.*, 2018). Mycolic acids primarily make up the inner leaflet of the outer membrane. While the outer leaflet of the outer membrane has mycolic acids, it is also rich in glycans and lipids, such as lipoarabinomannan and trehalose dimycolate, but a wide variety of lipids can be found in outer membranes across the mycobacteria genus (Jankute *et al.*, 2015; Zhou *et al.*, 2019).

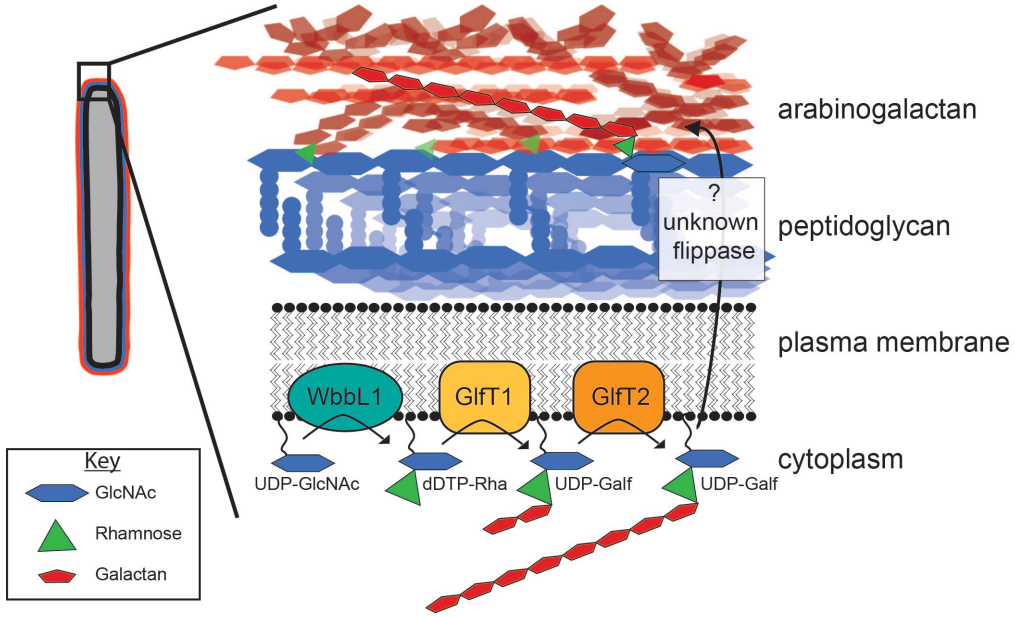

Figure 1.3. Arabinogalactan synthesis in mycobacteria.

Each of the extra layers of the mycobacterial cell wall requires machinery to be made, regulated, set in place and often ends up being remodeled. The tight regulation of the cell wall to constantly adapt these extra layers to the environment contributes significantly to failed treatment of pathogenic mycobacteria with antibiotics. While the biosynthetic pathways of the individual components of the mycobacterial cell wall have

been well-studied, the coordination that results in a well-organized cell wall remains elusive.

1.5d DivIVA and Wag31

In *B. subtillis*, a Gram-positive model organism, the DivIVA protein interacts with and is functionality dependent on MinCD (Cha and Stewart, 1997). MinCD acts as a septation repressor and DivIVA functions as a pilot protein, guiding MinCD to primary septation sites. Here, MinCD can inhibit FtsZ polymerization, preventing division from occurring at that septation site. Essentially, MinCD tells the cell where *not* to divide and ensures that division occurs at the mid-cell with help from DivIVA. Mycobacteria lack the Min system, but possess a DivIVA homolog, Wag31. Since DivIVA piloting MinCD is essential to growth mechanisms in lateral growers, it's possible that Wag31 is acting as a pilot but with different cargo. Wag31 localizes to the cell poles as well as the cell septum (Meniche *et al.*, 2014). When Wag31 is depleted, cells become spherical, meaning they are unable to sustain their rod shape, first at the poles, and then throughout the cell (Kang *et al.*, 2008). This, along with data that suggests Wag31 abundance correlates to the growing cell pole, implies that Wag31 plays a key role in polar elongation. Specifically, Wag31 regulates polar elongation at the new pole (Habibi Arejan *et al.*, 2023).

Wag31 is regulated via phosphorylation. Phosphomimetic and non-phosphorylatable mutants were still able to grow, suggesting that while Wag31 is essential for survival, the phosphorylation of Wag31 is not essential to the protein's function. Modification of Wag31 regulates PG synthesis at the new cell pole (Habibi Arejan *et al.*, 2023). This suggests that the activation of Wag31 coincides with the need

for new cell wall to be built, conceivably in reaction to environmental stimulus (Jani *et al.*, 2010). In fact, Wag31 interacts with FtsI in oxidative stress but not in stress-free log phase environments (Mukherjee *et al.*, 2009; Habibi Arejan *et al.*, 2023). Wag31 interacts with several essential cell wall synthesis proteins, like those involved in PG synthesis and mycolic acid biosynthesis, implicating Wag31 as a major regulator of the cell wall (Plocinski *et al.*, 2011; Hammond *et al.*, 2019).

1.5e SepIVA, another DivIVA homolog

Novel protein, SepIVA, is an essential division factor first identified as a new septal factor that interact with FtsQ in mycobacteria (Wu *et al.*, 2018; Jain *et al.*, 2018). SepIVA contains a DivIVA-domain and when it is depleted, cells display an elongated, filamentous phenotype, like FtsQ depletion phenotypes (Goehring *et al.*, 2005). This also suggests that SepIVA plays a role in cell division (Wu *et al.*, 2018). This phenotype is incompatible with what is seen when DivIVA in *B. subtillis* is depleted, suggesting that SepIVA is not involved in septal site establishment. Unlike the DivIVA homolog Wag31, SepIVA primarily functions as part of the divisome, versus at the cell poles (Wu *et al.*, 2018).

SepIVA does interact with FtsQ, which has been shown to modulate cell length and cell division in mycobacteria (Jain *et al.*, 2018). Based on this interaction, and evidence that SepIVA is likely a regulator (Lu *et al.*, 2020), it's possible that SepIVA plays a role in regulating FtsQ. SepIVA could transmit information to FtsQ, such as environmental changes, leading to cell wall modifications. However, any additional information about this interaction is still being investigated. Data presented here shows that SepIVA is post-translationally modified via protein arginine methylation. The effects

of this modification in prokaryotes have yet to be elucidated. In theory, arginine methylation of SepIVA could be involved in a signaling cascade leading to cell wall modulation via interaction with FtsQ and other cell wall factors.

1.6 Arginine methylation

Post-translational modifications (PTMs) are critical in cell signal transduction and in mediating protein interactions (Biggar and Li, 2015). Protein methylation is equally as relevant as phosphorylation for the regulation of cell physiology in eukaryotes. Arginine methylation is known to be involved in various cell functions, such as membrane association/disassociation (Fig. 1.4a), protein transport (Fig. 1.4b), DNA binding (Fig. 1.4c) and protein-protein interactions (Fig. 1.4d). Arginine methyltransferases are overexpressed in cancer, a disease of the cell cycle. In fact, many of the interactors of protein arginine methyltransferases (PRMTs) are known cell cycle regulators (Raposo and Piller, 2018).

Even though methylated amino acids were first discovered in bacterial flagellar proteins (Weibull and Koffler, 1959), much of what is known of this PTM is based on the methylation of histone proteins in eukaryotes. There is enough evidence to establish protein arginine methylation as a PTM within bacteria, yet further evidence is needed to determine its regulatory and functional potential as a PTM (Lassak *et al.*, 2019). In fact, bioinformatic studies in *E. coli* revealed 37 methylated proteins (Zhang *et al.*, 2018). Additionally, lysine methylation of a histone-like protein in mycobacteria has been linked to isoniazid resistance but arginine methylation has yet to be investigated (Sakatos *et al.*, 2018). Understanding the role that arginine methylation plays in prokaryotes will

provide insight on how information is transduced in bacterial cells to regulate the cell wall in response to environmental changes.

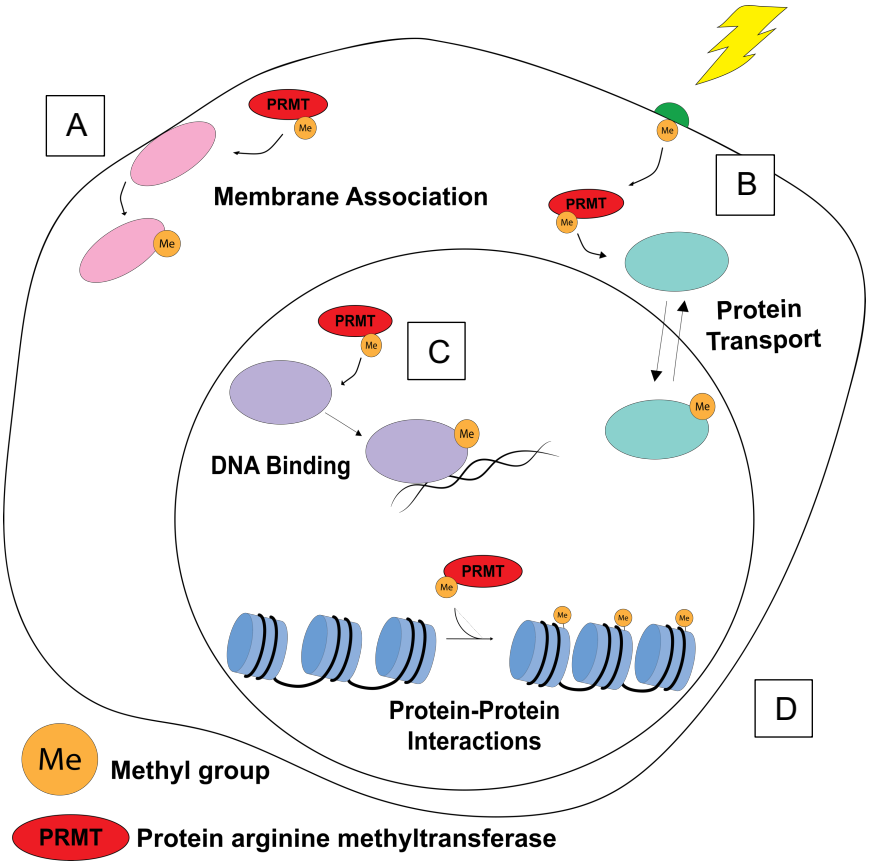

Figure 1.4. Various functions of protein arginine methylation. (1.4a) Arginine methylation can cause association or disassociation to the cell membrane. **(1.4b)** Methylation of proteins can facilitate protein transport. **(1.4c)** Methylation can increase a proteins ability to bind to DNA. **(1.4d)** Methylation can mediate protein-protein interactions, such as the tight compaction of eukaryotic histones.

1.7 Questions asked in this dissertation

Mycobacteria are inherently tolerant to many antibiotics due to their distinct cell wall. This cell wall requires strict regulation to persist in the presence of antibiotics. We ask what the molecular function of the cell wall regulator, SepIVA, is and how it regulates mycobacterial growth. We also ask how post-translational modifications on SepIVA may regulate SepIVA's function. We address these questions in chapter 2.

Once mycobacteria divide at the midcell, a new cell pole is created. The new pole then must switch growth modes to begin elongating from the pole. We ask what factors are involved in mediating this switch. We propose potential factors involved in this process in chapter 2.

Our results from investigating arginine methylation sites on SepIVA that are important to its function showed that residue R230, near the C-terminus of SepIVA, is crucial for SepIVA to function properly. We then asked what mutating R230K and R230M could inform us about the molecular mechanism of SepIVA. We address this question in chapter 3.

Since the molecular mechanism of SepIVA function is unknown, we ask what environmental stressors may elicit a regulatory response from SepIVA. Specifically, we ask how SepIVA arginine methylation site mutant strains tolerate DNA damage. We also ask how potential SepIVA interactor, UvrA, which recognizes DNA damage as part of the nucleotide excision repair system, affects SepIVA's ability to regulate cell division. We address this question in chapter 4.

1.7a Approaches

To investigate the molecular function of SepIVA, we looked for changes in different cell wall precursor enzymes upon SepIVA depletion. Since it is already known that SepIVA depletion inhibits division, we measured the effects of SepIVA depletion on polar elongation. To deplete SepIVA, we used a strain of *Mycobacterium smegmatis (Msmeg)* that contains a tetracycline-regulated gene depletion system. This system requires the protein to be degraded be labeled with a das tag, which is recognized by adapter protein, SspB (Kim *et al.*, 2011). SspB delivers the das-tagged protein to the

protease, ClpXP, where proteolysis occurs. SspB expression is controlled through an inducible tetracycline promoter. In short, upon addition of anhydrotetracycline (ATc), SspB will be expressed, and das-tagged proteins will be degraded (Kim *et al.*, 2011). I will also use this strain without the addition of ATc as a negative control.

To look for localization changes in cell wall precursor enzymes upon SepIVA depletion, we fluorescently labeled MurG, the lipid II synthase, and GlfT2, the final cytoplasmic protein in arabinogalactan synthesis. To measure polar elongation, we dyed the PG layer with fluorescent D-amino acid (FDAA) stains. I first stained log phase cells with hydroxycoumarin-carboxylic acid D-alanine (HADA) stain, which consists of a small fluorophore bound to D-amino acids that is incorporated into the PG layer as it is metabolized (Kuru *et al.*, 2015). I let cells grow in the 37° C roller for 1.5 hours before staining them again with a different FDAA stain. This allowed us to manually measure the elongation of the PG layer between the two staining events.

We investigated how SepIVA's post-translational modifications affect its molecular function. Our collaborators provided us with data suggesting that SepIVA in *Mtb* is arginine methylated on multiple residues. We found, via mass spectrometry, that all 24 arginine residues on SepIVA from *Msmeg* can be methylated. I constructed many different strains of *Msmeg* with mutated arginine methylation sites. I grouped together 2-5 arginines at a time to narrow down which methylation sites are important to SepIVA function. I mutated arginine to alanine, to remove the positive charge found on arginine residues. I also mutated arginine to lysine, to act as a methyl-ablative mutant, as lysine retains the positive charge but is unable to be methylated by the same

methyltransferase. To create methyl-mimetic strains, I mutated arginine to methionine, as methionine's side chain mimics that of a methylated residue.

To create these strains, I used the L5-phage integrase site allelic exchange system (Pelicic *et al.*, 1997; Pashley and Parish, 2003) (Fig. 1.5). Beginning with a strain of *Msmeg* with *sepIVA* at its native locus (Fig. 1.5a), we integrated a copy of *sepIVA* fused to a nourseothricin resistance cassette into the L5 phage integration site on the chromosome (Fig. 1.5b). Then, via recombineering, we replaced *sepIVA* at its native locus with a zeocin resistance cassette (Fig. 1.5c). The next step in this exchange system can produce three different results, depicted in Fig. 1.5d-f. The desired result, a mutant allele of *sepIVA* fused to a kanamycin resistance cassette with the WT *sepIVA* excised from the integration site (Fig. 1.5e). To guarantee I isolated strains with a single copy of *sepIVA* at the L5 site, I selected for kanamycin-resistant but nourseothricin-sensitive colonies.

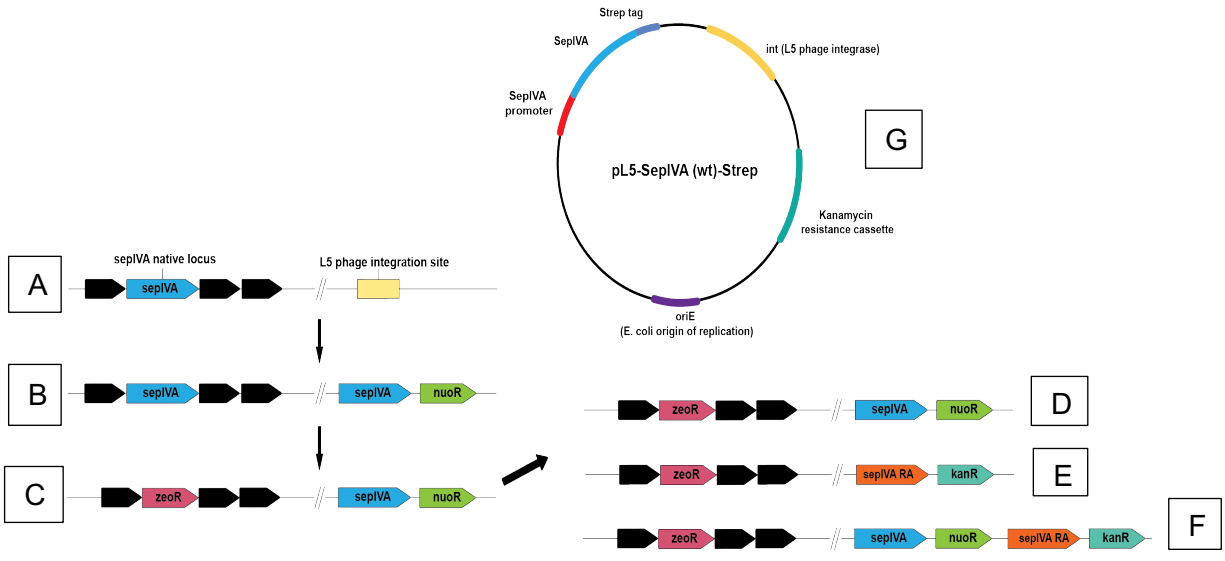

Figure 1.5. Schematic of L5-phage integrase allelic exchange system. (1.5a) Gene arrangement with WT *sepIVA* (blue) at its native locus. **(1.5b)** Gene arrangement with *sepIVA* at its native locus as well as *sepIVA-nuoR* at the L5 phage integration site. **(1.5c)** Gene arrangement after recombineering, resulting in *zeoR* at the *sepIVA* native site. **(1.5d)** Possible

gene arrangement after unsuccessful allele exchange, resulting in no change in gene arrangement. **(1.5e)** Possible gene arrangement after successful excision of WT *sepIVA-nuoR* and integration of mutant *sepIVA* (orange) fused to *kanR.* **(1.5f)** Third possible gene arrangement after unsuccessful excision of *sepIVA-nuoR* but successful integration of mutant *sepIVA-kanR.* **(1.5g)** Depiction of plasmid containing WT *sepIVA* and *nuoR.*

With these arginine methylation site mutants, I looked for phenotypic differences in population doubling time, cell length, polar elongation (as previously described), PG layer staining, and changes in localization of SepIVA and cell wall precursor enzymes, MurG and GlfT2. With help from collaborators, we also assessed SepIVA's membrane association using sucrose density gradients.

To further elucidate SepIVA's molecular function we looked for potential SepIVA interactors via immunoprecipitation and mass spectrometry. One possible interactor was UvrA, a non-essential, DNA damage response protein. I constructed a *uvrA* knockout strain using recombineering, which replaces *uvrA* on the chromosome with a hygromycin-resistance cassette (Murphy *et al.*, 2015). I constructed Δ*uvrA* L5::*sepIVA* with all methylation site mutant versions of *sepIVA.* To induce DNA damage, I used mitomycin C, a cancer drug that crosslinks the chromosome, inhibiting DNA synthesis (Peh *et al.*, 2001; Sinawe and Casadesus, 2022). We used the Δ*uvrA* strains and mitomycin C to investigate changes in cell length, SepIVA localization, growth rate and PG layer staining.

1.7b Co-author contributions

Each of the following data chapters including collaborative work between the author of this dissertation, Angela H. Freeman, and co-authors. In chapter 2, conceptualization was done by Angela H. Freeman and Cara C. Boutte. The manuscript was written by Angela H. Freeman and reviewed and edited by Cara C. Boutte. This

chapter was based on preliminary data curated by Sarah M. Fortune and Michael R. Chase. All data was curated and analyzed by Angela H. Freeman with the exceptions of figure 2.9a, which was done by Yasu S. Morita and James R. Brenner, and figure 2.10abcd, which was done by Karen Tembiwa. Funding acquisition and project administration were done by Cara. C. Boutte.

Chapter 3 was conceptualized by Angela H. Freeman and Cara C. Boutte. Data curation, formal analysis and writing was done by Angela H. Freeman. Funding acquisition and project administration were done by Cara. C. Boutte.

Chapter 4 was conceptualized by Angela H. Freeman, Cara C. Boutte, and Anusuya Nepal. All data was curated and analyzed by Angela H. Freeman apart from figure 4.3ab, which was done by Anusuya Nepal. Writing was done by Angela H. Freeman. Funding acquisition and project administration were done by Cara. C. Boutte.

Chapter 2: Arginine methylation sites on SepIVA help balance elongation and septation in *Mycobacterium smegmatis*†

By Angela H Freeman[1], Karen Tembiwa[1], James R Brenner[2], Michael R Chase[3], Sarah M Fortune[3], Yasu S Morita[2], Cara C Boutte[1*]

[1]Department of Biology, University of Texas at Arlington, Arlington, Texas, USA

[2]Department of Microbiology, University of Massachusetts, Amherst, Massachusetts, USA

[3]Department of Immunology and Infectious Disease, Harvard TH Chan School of Public Health, Boston, Massachusetts, USA

Molecular Microbiology, Volume 119, Issue 2, 23 November 2022.

https://doi.org/10.1111/mmi.15006

2.1 Abstract

Growth of mycobacterial cells requires successful coordination between elongation and septation. However, it is not clear which factors mediate this coordination. Here, we studied the function and post-translational modification of an essential division factor, SepIVA, in *Mycobacterium smegmatis*. We find that SepIVA is arginine methylated, and that alteration of its methylation sites affects both septation and polar elongation of *Msmeg.* Furthermore, we show that SepIVA regulates the localization of MurG, and that this regulation may impact polar elongation. Finally, we map SepIVA's two regulatory functions to different ends of the protein: the N-terminus regulates elongation while the C-terminus regulates division. These results establish SepIVA as a regulator of both elongation and division and characterize a physiological role for protein arginine methylation sites for the first time in mycobacteria.

2.2 Introduction

The cell cycle of rod-shaped bacteria requires coordination of elongation and division. Elongation involves incorporation of newly synthesized cell wall components, including peptidoglycan (PG) into the existing cell wall. In the well-studied species *B. subtilis* and *E. coli*, this incorporation occurs along the lateral cell walls and is directed by the cytoskeletal factor MreB (Egan *et al.*, 2020). However, some rod-shaped bacteria, including many Actinobacteria and some Alpha-proteobacteria, lack MreB-like proteins and elongate by incorporating new cell wall near the cell poles (Thanky *et al.*, 2007; Aldridge *et al.*, 2012; Brown *et al.*, 2012; Cameron *et al.*, 2015; Zupan *et al.*, 2019; Zupan *et al.*, 2021). Polar elongation in mycobacteria, which includes the

pathogen *Mycobacterium tuberculosis* (*Mtb*), requires the DivIVA homolog, Wag31 (Kang, 2005; Kang *et al.*, 2008; Melzer *et al.*, 2018), through mechanisms that are currently unclear.

Many essential cell division factors are conserved from *E. coli* to mycobacteria (Hett and Rubin, 2008; Wu *et al.*, 2018). However, because of the extra layers of the cell wall (Jankute *et al.*, 2015) and polar growth (Thanky *et al.*, 2007) in mycobacteria, we expect that some aspects of cell division must be different. In mycobacteria, polar elongation occurs at the site of previous septation; while in lateral growers, elongation and septation are spatially distinct. Because division creates the site of polar growth for the next generation of mycobacterial cells, we expect there to be proteins involved in transitioning the new pole from the septal mode of cell wall metabolism (orthogonal to the long axis of the cell) to the elongative mode of cell wall metabolism (parallel to the long axis of the cell) - though such factors have not been described.

The intracellular membrane domain (IMD) is likely shared by the elongation and division processes. The IMD is a membranous hub for generation of lipid-linked cell wall precursors and it localizes to sites of cell wall synthesis: the subpolar region and septum (Hayashi *et al.*, 2016). Cell wall precursors assembled in the IMD are thought to be translocated into the plasma membrane associated with the cell wall (PM-CW) before assembly into the cell wall (García-Heredia *et al.*, 2021). How precursor enzymes associate with the IMD, and how that affects their activity is unknown.

SepIVA is essential for division and interacts with the conserved divisome protein, FtsQ (Wu *et al.*, 2018; Jain *et al.*, 2018). *sepIVA* has also been implicated as a determinant of beta-lactam susceptibility, indicating that it may affect peptidoglycan

metabolism (Flores *et al.*, 2005). Like Wag31, SepIVA comprises a DivIVA domain and aligns to DivIVA from *B. subtillis*. DivIVA homologs are often involved in recruitment of other proteins to cell poles or septa (Marston and Errington, 1999; Halbedel and Lewis, 2019; Hammond *et al.*, 2019; Hammond *et al.*, 2021). However, none of the confirmed interactors of DivIVA-domain proteins interact with residues that are conserved in SepIVA. Depletion of Wag31 and SepIVA have opposite effects: depletion of SepIVA leads to continued elongation and defective division (Wu *et al.*, 2018), while depletion of Wag31 leads to elongation arrest but continued division (Kang *et al.*, 2008).

Here, we show that SepIVA is arginine methylated. Arginine methylation is known to be involved in various cell functions in eukaryotes, such as membrane association, protein transport, DNA binding and protein-protein interactions (Biggar and Li, 2015; Raposo and Piller, 2018). Protein arginine methylation has been identified using mass spectrometry in *E. coli* (Zhang *et al.*, 2018), mycobacteria (Sakatos *et al.*, 2018) and *Salmonella* (Su *et al.*, 2021). Arginine methylation sites have been shown *in vitro* to affect DNA binding of transcription factors in *Salmonella* (Su *et al.*, 2021) and mycobacteria (Singhal *et al.*, 2020). However, the physiological roles of protein arginine methylation have barely been studied in bacteria. Currently, there are no characterized protein arginine methyltransferases in mycobacteria. Recent work has suggested that the protein glutamate methyltransferase CheR in *Salmonella enterica* can somehow also methylate arginines (Su *et al.*, 2021); there is no homolog with a predicted CheR methyltransferase domain in mycobacteria.

In this work, we show that SepIVA is arginine methylated, and that methyl-ablative and methyl-mimetic mutations at certain arginine methylation sites on SepIVA

regulate SepIVA's localization, peptidoglycan metabolism, polar growth, and division. We also show that SepIVA is involved, likely indirectly, in regulating the localization of peptidoglycan precursor enzyme MurG, and that arginine methylation site mutations of *sepIVA* affect MurG's localization to the poles. This work establishes SepIVA as a regulator of both elongation and division and indicates that it may have a role in regulating MurG.

2.3 Results

2.3a Methylation site mutations on SepIVA affect growth and cell length of *Msmeg*

Post-translational modifications are critical for regulating the physiology of *Mtb* and other mycobacteria (Kang *et al.*, 2008; Prisic *et al.*, 2010; Garces *et al.*, 2010; Prisic and Husson, 2014; Boutte *et al.*, 2016; Sakatos *et al.*, 2018; Iswahyudi *et al.*, 2019; Shamma *et al.*, 2020). Most studies thus far have focused on phosphorylation. To identify proteins that could be regulated by other types of post-translational modification, we re-analyzed a mass spectrometry data set of *Mtb* peptide masses that we had previously published (Garces *et al.*, 2010) to search for post translational modifications. We found evidence of four arginine methylations on SepIVA (Rv2927c), as well as on many other proteins from *Mtb*. The four methylated arginines from *Mtb* SepIVA were R19, R105, R111, R199 and all are conserved in SepIVA from *Msmeg*.

To see if SepIVA in *M. smegmatis* is also arginine methylated, we immunoprecipitated SepIVA-strep from *Msmeg* lysates and used LCMS-IT-TOF mass spectrometry to measure the post-translational modifications. We found evidence of widespread arginine methylation on SepIVA's 24 arginine residues.

To identify arginine residues in SepIVA for which methylation might have a physiological role in *Msmeg*, we used L5 allele swapping to make mutants of all the arginines in *sepIVA* (Pashley and Parish, 2003). First, we integrated a wild-type *sepIVA* at the L5 site on a nourseothricin-marked vector and deleted the endogenous copy of *sepIVA.* Then, we cloned various *sepIVA* arginine mutants into kanamycin-marked vectors, and transformed these into the Δ*sepIVA* L5::*sepIVA* WT strain, and selected for allele swaps. Because there were so many arginines with potential methylation sites, we made mutants with several clustered arginines mutated at once. We grouped arginines based on their location and orientation on the SepIVA protein, as predicted by AlphaFold (Jumper *et al.*, 2021) (Pettersen *et al.*, 2021) (Fig. 2.1).

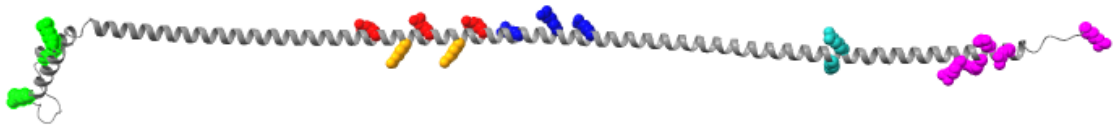

Figure 2.1. Predicted SepIVA structure with colored arginine residues. Tertiary structure of SepIVA protein as predicted by AlphaFold and visualized using UCSF ChimeraX. Arginine residues with methylations identified by mass spectrometry are grouped and colored to reflect fig. 2.2. We grouped arginines by their proximity to each other and their position on the SepIVA predicted structure. Arginine labels: green (R3, R19, R31; also referred to as the N-terminus mutants); red (R105, R116, R127); orange (R111, R122); dark blue (R134, R142, R149); teal (R199, R201); and pink (R224, R228, R230, R234, R245; also referred to as the C-terminus mutants).

We made R->M methionine mutants to represent methyl-mimetic mutations, as methionine is the closest structural mimic to a methylated arginine (Singhal *et al.*, 2020). We made R->A alanine mutations to test the function of the positive charge of arginines and R->K lysine mutations to serve as methyl-ablatives that retain the positive charge on the residue. We found that several groups of arginines were essential for *sepIVA*

function, as the alanine mutant strains did not grow (R->A mutants, Fig. 2.2a) in liquid culture.

Our analysis of clustered arginine mutants of *sepIVA* (Fig. 2.2ab) identified two sets of mutants with interesting phenotypes. If the lysine and methionine mutants mimic the different arginine methylation states, and if that methylation has a physiological role, then we expect to see opposing phenotypes in the methyl-ablative (R->K) and methyl-mimetic (R->M) strains compared to the wild-type. The *sepIVA* R3K, R19K, R31K mutant, hereafter called the NT-K mutant, as these are the most N-terminal arginines, had a comparable growth rate, and shorter cells than the wild-type, while the NT-M mutant (*sepIVA* R3M, R19M, R31M) had slower growth (Fig. 2.2ab). The allele swap mutant *sepIVA* R224K, R228K, R230K, R234K, R245K, hereafter called the CT-K mutant, had slow growth and (Fig. 2.2a) and very short cell length (Fig. 2.2b). The C-terminal methionine mutant (*sepIVA* R224M, R228M, R230M, R234M, R245M) was not viable, likely because the protein was unstable (Fig. 2.2c).

To examine whether individual arginine residues were responsible for these growth and cell length defects, we generated allele swap *Msmeg* strains with single methylation site mutations in the N-terminal and C-terminal arginines. We found that single methylation site mutations near the N-terminus of *sepIVA* did not have the same effects on growth and cell length as the triple mutant (Fig. 2.2de). Since more than one methylation site mutant near the N-terminus was needed for these phenotypes to be apparent, we used the NT-K and NT-M triple mutants to study the potential role of arginine methylation on SepIVA's N-terminus. The single methylation site mutations on

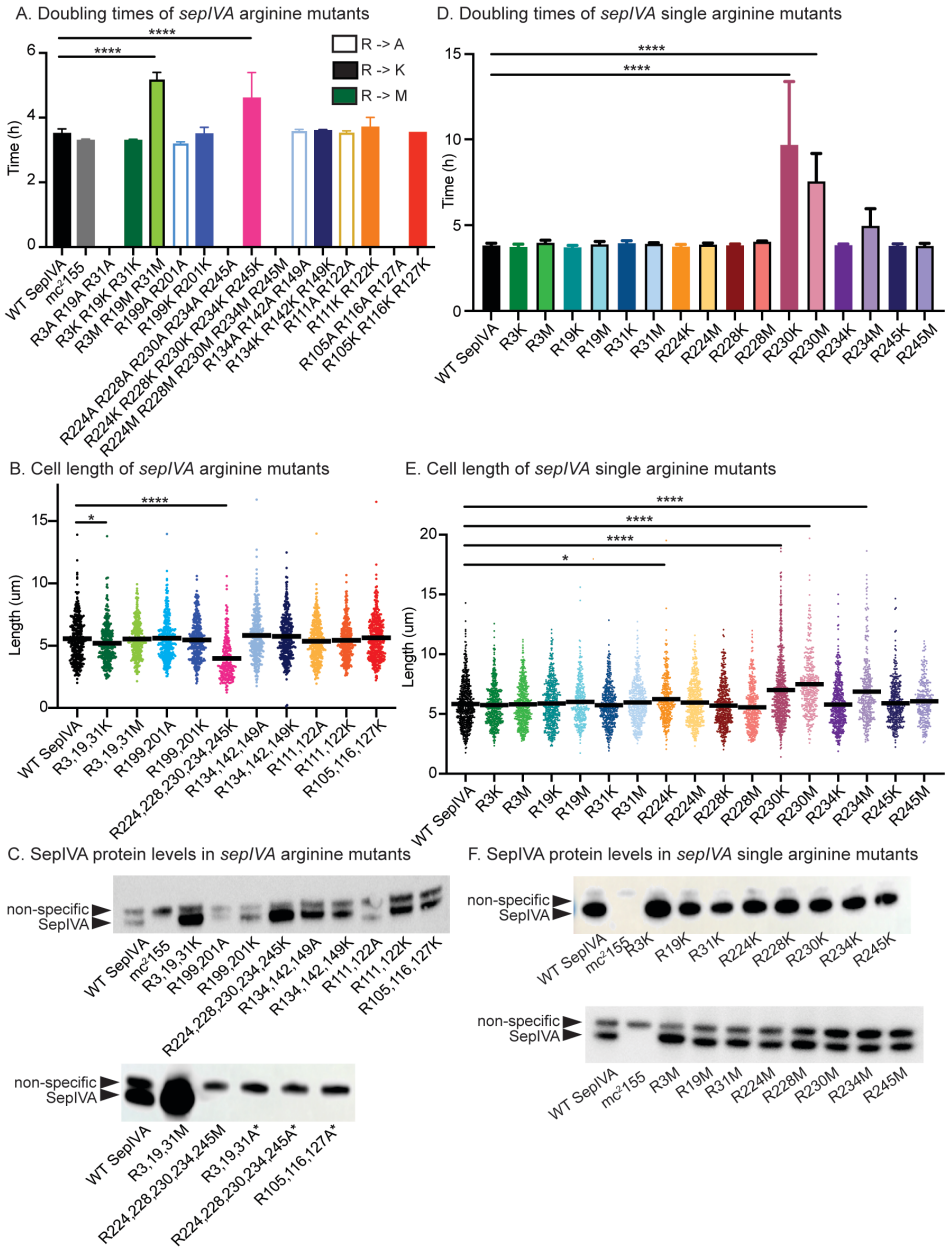

Figure 2.2. Methylation site mutations on SepIVA affect growth and cell length of Msmeg. **(2.2a)** Doubling time of allele-swap *M. smeg* cells expressing WT or arginine methylation site mutants of SepIVA. WT SepIVA represents the L5 complemented strain. Lighter color outlined bars represent arginine to alanine mutants. No outline, darker color bars represent methyl-ablative methylation site mutants. Black outline bars represent methyl-mimetic methylation site mutants. Strains without bars were non-viable. At least 3 biological replicates of each strain were used. Error bars represent standard deviation. ****, *P = <0.0001.* **(2.2b)** Cell lengths of SepIVA WT or arginine methylation site mutants. Bars represent mean. At least 300 cells over three biological replicates of each strain were analyzed. *, *P = 0.0439;* ****, *P = <0.0001.* **(2.2c)** α-strep western blot of L5::*sepIVA*-strep WT or arginine methylation site mutants. mc^{2}155

without a strep tag was used as a negative control (lane 2). The non-specific band serves as a loading control. '*' denotes merodiploid strains. Merodiploid strains were used for SepIVA variants did not support growth as allele swaps. **(2.2d)** Doubling time of allele-swap *M. smeg* cells expressing WT or single arginine methylation site mutants of SepIVA. WT SepIVA is the strain with WT *sepIVA*-strep at the L5 site and *sepIVA* deleted from its native locus – this is the isogenic control. No outline, darker color bars represent methyl-ablative methylation site mutants. Black outline bars represent methyl-mimetic methylation site mutants. Strains without bars were non-viable. At least 3 biological replicates of each strain were used. Error bars represent standard deviation. ****, *P = <0.0001.* **(2.2e)** Cell lengths of SepIVA WT or single arginine methylation site mutants. Bars represent mean. At least 300 cells over three biological replicates of each strain were analyzed. *, *P = 0.0351; ****, P = <0.0001.* **(2.2f)** α-strep western blot of L5::*sepIVA*-strep WT or single arginine methylation site mutants. mc^2155 without a strep tag was used as a negative control (lane 2). The non-specific band serves as a loading control. P-values were calculated using ordinary one-way ANOVA, Dunnett's multiple comparisons test, with a single pooled variance in GraphPad Prism (v9.2). At least two western blots were performed for each strain shown, and representative results are displayed.

the C-terminus of SepIVA had different phenotypes from the quintuple CT-K allele swap mutant (Fig. 2.2abde), suggesting that the quintuple mutant may be genetically unstable. Both the *sepIVA* R230K and R230M exhibited slow growth and long cells (Fig. 2.2de): this indicates that these mutations likely do not represent different methylation states and are instead both loss-of-function mutations. Another methylation site, R234, only showed growth defects in the methionine mutant (Fig. 2.2de).

We made all the mutants described above with C-terminal strep tags so we could test for protein stability using western blotting. (Fig. 2.2cf). To test the stability of mutant proteins that did not support growth in allele swap strains (Fig. 2.2a – missing bars), we transformed the vectors carrying the mutant *sepIVA*-strep into wild-type *Msmeg* with the wild-type *sepIVA* allele at its native locus to support growth. Using these merodiploid strains, we found that SepIVA-strep alanine mutant proteins that did not support growth were unstable (Fig. 2.2c, '*' indicates merodiploid strain). Several of the mutants had significantly higher levels of SepIVA than the wild-type, including the NT-K, NT-M and

CT-K mutants (Fig. 2.2c) which exhibited phenotypes. To test whether high levels of SepIVA protein might be responsible for the slow growth, we tested how overexpression of the WT or CT-K mutant SepIVA protein affected growth rates (Fig. 2.3). We found that overexpression of these proteins did not slow growth in either WT *sepIVA* or *sepIVA* CT-K genetic backgrounds. This result shows that the increased protein levels are not responsible for the slow growth and short cell length of the *sepIVA* CT-K mutant, and that overexpression of SepIVA alone does not inhibit growth rate. Other variants of SepIVA-strep are stable; though protein levels between the lysine and alanine mutants vary (Fig. 2.2c), these variations do not correlate with phenotypes (Fig. 2.2abde).

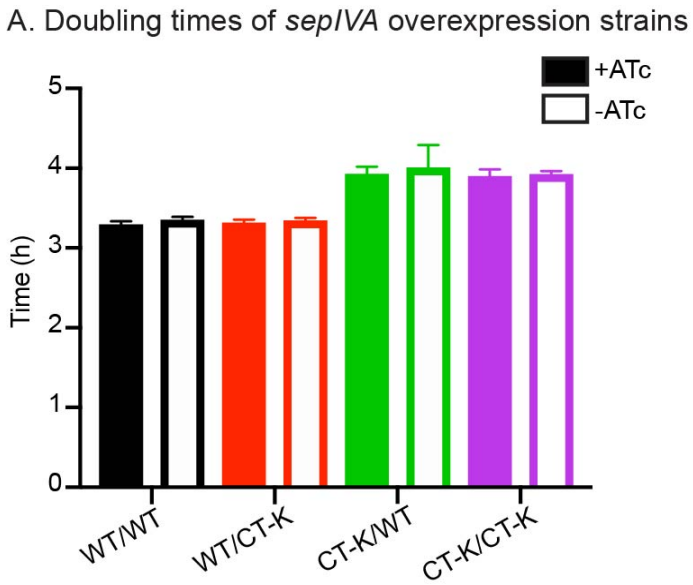

Figure 2.3. Overexpression of sepIVA has no effect on population doubling time. Overexpression of *sepIVA* was controlled by a tetracycline inducible promoter found on an episomal plasmid. +ATc denotes addition of anhydrotetracycline causing overexpression of SepIVA. Strains are labeled based on the *sepIVA* allele at the L5 integration site followed by the *sepIVA* allele overexpressed via episomal plasmid. At least two biological replicates were used per strain. Error bars represent standard deviation.

These data suggest that methylation sites on SepIVA play a role in how SepIVA regulates growth and division. Near the N-terminus, methyl-mimetic site mutations cause slow growth and lead to slightly shorter cells (Fig. 2.2). However, near the C-

terminus of SepIVA, both R230 mutants are defective in division. At R234 the methyl-mimetic mutation results in slow growing, long cells, while the methyl-ablative mutation results in cells like the WT. For the remainder of this chapter, we focus on the N-terminal triple mutants and the single site mutants of R234.

According to TnSeq experiments and our previous work, *sepIVA* is an essential gene (DeJesus *et al.*, 2017; Wu *et al.*, 2018; Dragset *et al.*, 2019). In another recent study, a mutant of *sepIVA* missing only residues 156-245, the C-terminus, was characterized and the authors described cell division defects (Pickford *et al.*, 2020). We generated this C-terminus truncation mutant using L5 allele swapping and were able to generate colonies on plates. However, once in liquid culture, these mutants exhibited highly variable or no growth (Fig. 2.4). We interpret this to mean that the deletion of the *sepIVA* C-terminus leads to severe growth defects that result quickly in suppressor mutants.

A. Gene arrangement of WT *sepIVA* and *sepIVA* C-terminus truncation mutant

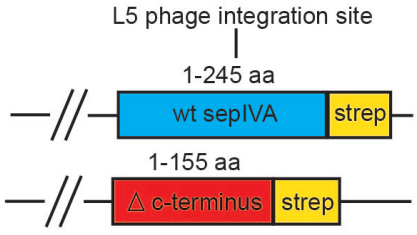

B. Doubling times of WT *sepIVA* and *sepIVA* C-terminus truncation mutant

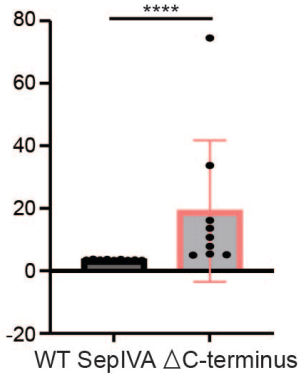

C. Growth chart of *sepIVA* C-terminus truncation mutants

Isolate	Days before growth	Avg doubling time (h)
1	7	39.971
2	4	16.13
3	8	6.492
4	No growth	
5	9	4.292
6	No growth	
7	3	33.7
8	11	44.2
9	No growth	
10	No growth	
11	No growth	
12	2	29.16
13	7	5.674
14	No growth	
15	7	13.6
16	5	5
17	No growth	
18	7	10.76
19	No growth	
20	7	19.75

Figure 2.4. The C-terminus of SepIVA affects growth rate of Msmeg. (2.4a) Gene arrangement of WT *sepIVA* and *sepIVA* truncation mutant strains. The C-terminus truncation mutant only contains the first 155 amino acids of SepIVA. **(2.4b)** Doubling times of WT *sepIVA*

and *sepIVA* truncation mutants. Doubling times were only calculated for C-terminus isolates that were able to grow in liquid culture. At least 3 biological replicates of each strain were used. Error bars represent standard deviation. ****, *P = <0.0001.* P-value calculated by unpaired t-test using GraphPad Prism (v9.2). **(2.4c)** Growth chart of *sepIVA* C-terminus truncation mutants. Twenty biological replicates were individually grown in liquid culture. “Days before growth” represents number of days rolling at 37C before visible growth occurred. Cultures that did not show visible growth after two weeks were deemed “no growth.” Doubling time was calculated only on isolates that grew in liquid culture.

2.3b Methylation site mutations on SepIVA affect its polar localization

We sought to determine if alterations at the arginine methylation sites could affect SepIVA’s localization. SepIVA normally localizes at the poles and septum, with stronger localization to the old pole, and spotty localization along the lateral walls in a pattern (Wu *et al.*, 2018) that is seen in proteins that associate with the Intracellular Membrane Domain (IMD) (Meniche *et al.*, 2014; Hayashi *et al.*, 2016). To test this, we made merodiploid strains of *Msmeg* with GFPmut3-SepIVA methyl-mutant alleles expressed from the L5 site. We were unable to generate strain of *Msmeg* carrying GFPmut3-*sepIVA* as the only *sepIVA* allele, so merodiploid strains were used. Because the fusion protein does not complement, we will be cautious in drawing conclusions from these localization data. However, we note that FtsZ-FP fusions do not complement in any species, and yet still give valuable information (Ma *et al.*, 1996; Fu *et al.*, 2010). We also note that protein aggregates of overexpressed protein in mycobacteria tend to accumulate at the poles and septum (Zhang *et al.*, 2019), and we do not observe this localization pattern for GFP-SepIVA.

We grew these strains in log. phase, and stained the cells with the fluorescent D-amino acid HADA, which preferentially labels sites of new peptidoglycan synthesis, and allows us to identify the faster growing, old pole, as the pole that stains more brightly

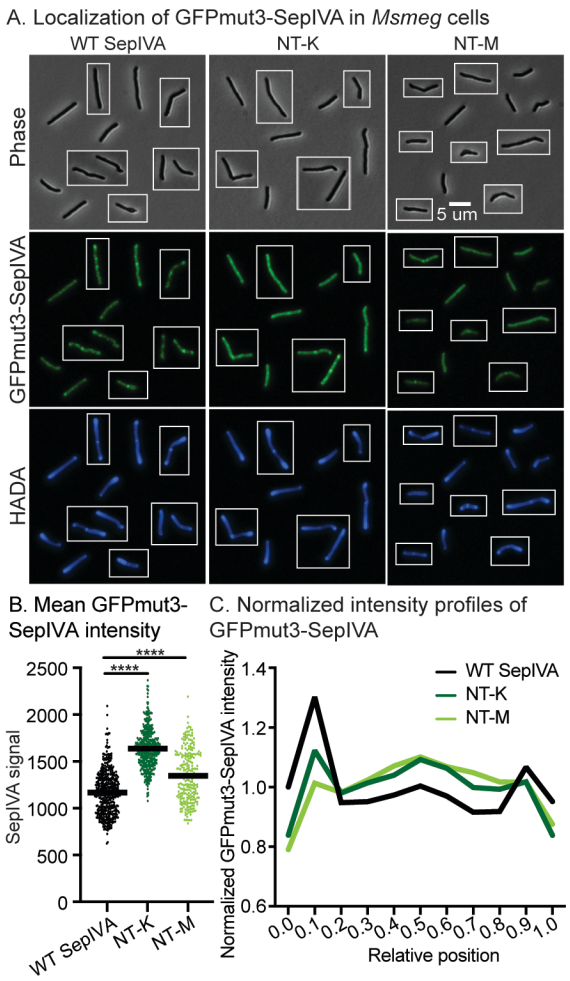

Figure 2.5. Methylation site mutations affect polar localization of SepIVA. (2.5a) Images of *Msmeg* cells expressing L5::*GFPmut3-sepIVA* WT and methylation site mutants. Strains are merodiploid. Phase images are on the top row. Fluorescence images of GFPmut3-SepIVA are in the middle panel. HADA images are on the bottom row. Scale bar applies to all images. Pictures of several cells from images processed identically were pasted together. **(2.5b)** Mean intensity values per cell of cells expressing L5::*GFPmut3-sepIVA* WT and methylation mutants. At least 250+ cells across three biological replicates of each mutant were analyzed in MicrobeJ. Bar represents mean intensity value between cells. ****, *P = <0.0001.* P-values were calculated using ordinary one-way ANOVA, Dunnett's multiple comparisons test, with a single pooled variance in GraphPad Prism (v9.2). **(2.5c)** Normalized Intensity profiles of GFP-SepIVA signal of WT and methylation site mutants. The solid line represents the mean intensity value across the relative position of the cell. Normalized intensity values were generated by dividing each position's intensity value by the mean intensity value. Cells were pole-sorted such that the brighter pole in the HADA channel was set to 0 on the X axis.

(Kuru *et al.*, 2012; Baranowski *et al.*, 2018). Upon imaging the cells, we found that methylation site mutations on SepIVA affect its distribution and total intensity (Fig. 2.5).

Specifically, both NT-K and NT-M mutants showed inhibited localization of SepIVA to the fast-growing pole, and increased localization to the cell septum (Fig. 2.5c). This suggests that regulation of these methylation sites affects SepIVA distribution throughout the cell. Methylation site mutants also exhibit differences in GFPmut3-SepIVA intensity broadly (Fig. 2.5b), however, we cannot conclude whether mean GFPmut3-SepIVA signal is an indicator of protein levels within the cell. Our findings suggest that SepIVA's localization to the cell poles is affected by changes in the methylation sites on the N-terminus of SepIVA. We cannot discount the possibility that GFPmut3-SepIVA localizes differently from the untagged protein, but these results show at least that these mutations can affect the distribution of the fusion in a merodiploid background.

2.3c Methylation site mutations on SepIVA affect peptidoglycan metabolism

SepIVA's essentiality for cell division and sequence similarity to DivIVA proteins suggests that it regulates cell wall synthesis. To determine if the methylation sites on SepIVA impact metabolism of cell wall components, we stained the allele swap *sepIVA-strep* arginine-mutant strains with NADA (Kuru *et al.*, 2015), which is incorporated into peptidoglycan mostly by periplasmic amino acid exchange by L,D-transpeptidases (LDTs) (Kuru *et al.*, 2012; Baranowski *et al.*, 2018), but also through new peptidoglycan incorporation (García-Heredia *et al.*, 2018). We found that the N-terminal methyl-mimetic site mutant, NT-M, showed slightly decreased NADA signal at the cell poles compared to the wild-type (Fig. 2.6). We also found that the NT-K mutant showed increased overall NADA incorporation compared to the wild-type (Fig. 2.6b). To observe differences in distribution of NADA, we looked at NADA incorporation across the length

of the cell. Based on normalized polar NADA intensities, there is less NADA incorporation at both poles in the NT-M mutant (Fig. 2.6cd). These data suggest SepIVA affects peptidoglycan metabolism, though they do not address whether these effects are direct or indirect. SepIVA had previously been shown to be essential for division (Wu *et al.*, 2018), but these differences in polar NADA incorporation indicate that SepIVA may also be a regulator of polar peptidoglycan metabolism.

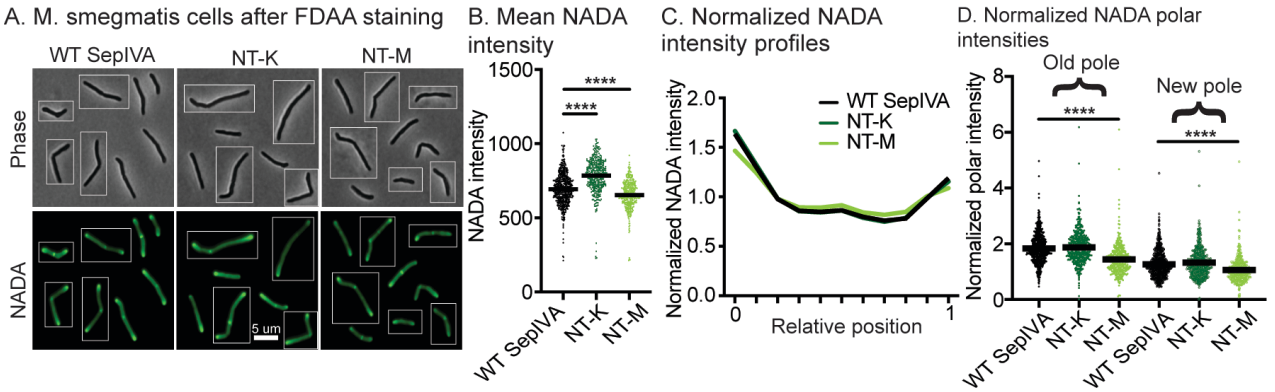

Figure 2.6. Methylation site mutations of SepIVA affect peptidoglycan metabolism. (2.6a) Images of M. smeg cells expressing *L5::sepIVA* WT and methylation site mutants. Scale bar applies to all images. Pictures of several cells from images processed identically were pasted together. **(2.6b)** Mean NADA intensity values of *M. smeg* cells expressing *L5::sepIVA* WT and methylation site mutants. At least 250+ cells across three biological replicates of each mutant were analyzed in MicrobeJ. Bar represents mean intensity value. ****, *P* = <0.0001.* P-values were calculated using ordinary one-way ANOVA, Dunnett's multiple comparisons test, with a single pooled variance in GraphPad Prism (v9.2). **(2.6c)** Normalized intensity profiles of NADA signal of WT and methylation mutants. The solid line represents the mean intensity value across the relative position of the cell. Intensity values were normalized by dividing each strain's intensity value by its mean intensity value. Cells were pole-sorted such that the brighter pole in the NADA channel was set to 0 on the X axis. **(2.6d)** Normalized polar NADA intensities of WT and methylation site mutants. Intensity values were normalized by dividing each cell's maximum polar intensity value by the mean intensity of the whole cell. ****, *P* = <0.0001.* P-values were calculated using ordinary one-way ANOVA, Dunnett's multiple comparisons test, with a single pooled variance in GraphPad Prism (v9.2).

2.3d Methylation site mutations on SepIVA affect polar elongation

To determine if the changes in NADA staining in the *sepIVA* methyl-mutants were due to alterations in LDT-mediated peptidoglycan remodeling (Baranowski *et al.*,

2018) or due to insertion of new cell wall at the poles, we measured polar elongation in the *sepIVA* wild-type and mutant strains. We developed a method of measuring elongation using a pulse of HADA (blue), 1.5 hours of outgrowth in media, and another pulse of NADA (green) stain. We then measured the distance of the NADA-stained but HADA-clear poles, which represents the polar growth during the 1.5-hour outgrowth (Fig. 2.7a).

First, we used this method to determine if depletion of SepIVA affects cell elongation. SepIVA depletion leads to a slight increase in net polar elongation (Fig. 2.7b). Because cell division is inhibited in the SepIVA-depletion condition, the increase in net polar elongation could be due to the increased age of the poles in non-dividing cells: older poles in mycobacteria grow faster (Aldridge *et al.*, 2012), so cells that are not creating new poles through division will have older poles overall. From these data we conclude that SepIVA is not essential for elongation.

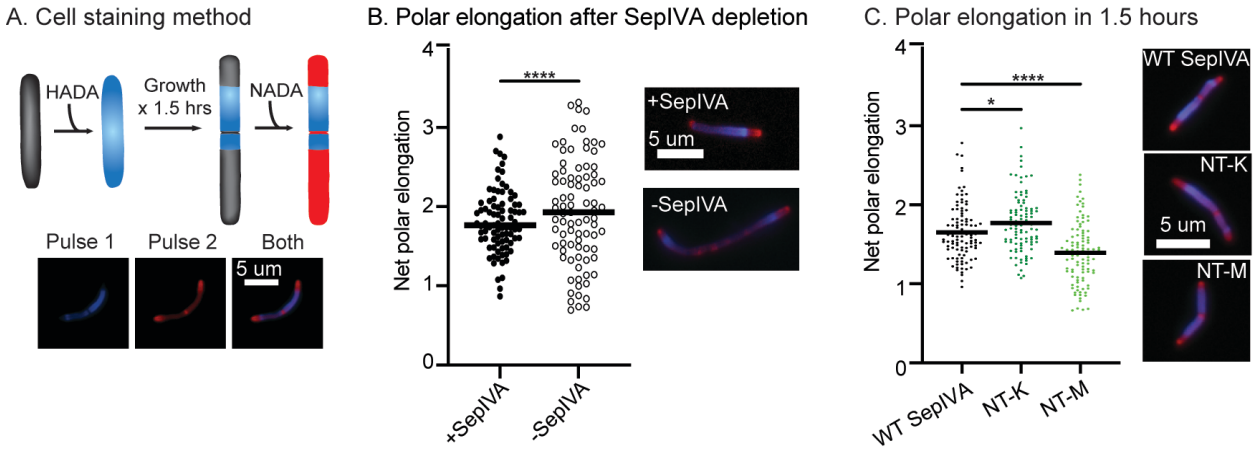

Figure 2.7. Methylation site mutations on SepIVA affect polar elongation. (2.7a) Schematic of pulse-chase-pulse staining method. We stained growing cells with blue peptidoglycan dye HADA, then returned them to media for another 1.5 hours of growth, then stained them again with green dye NADA. We false-colored the green signal as red in these images to make the contrast clearer. **(2.7b)** Length of poles after SepIVA depletion. +SepIVA (black dots) represent cells expressing SepIVA, -SepIVA (black-outlined dots) represent cells with depleted SepIVA

protein. At least 100 cells across three biological replicates were analyzed. Bar represents median. Scale bar applies to all images. *****, P = <0.0001.* P-value calculated by unpaired t-test using GraphPad Prism (v9.2). **(2.7c)** Length of poles elongation after 1.5 hours in cells expressing *sepIVA* WT and methylation site allele swap mutants. At least 100 cells across three biological replicates were analyzed. Bar represents mean polar elongation. **, P = 0.0461, ****, P = <0.0001.* P-values were calculated using ordinary one-way ANOVA, Dunnett's multiple comparisons test, with a single pooled variance in GraphPad Prism (v9.2).

To determine if methylation sites on SepIVA could affect elongation, we performed pulse-chase-pulse staining on *sepIVA-strep* wild-type and methylation site mutant allele swap strains. We observed increased elongation in the NT-K methyl-ablative mutants, while the NT-M methyl-mimetic mutant showed decreased polar

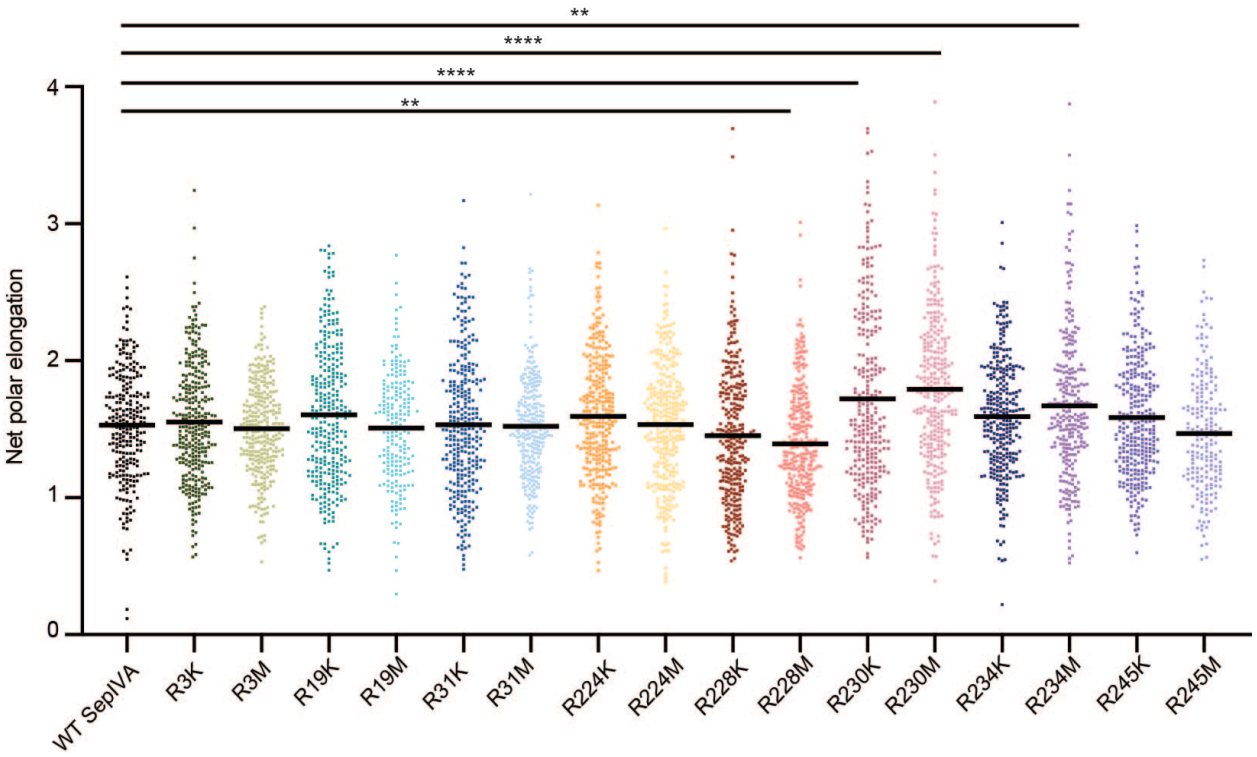

Figure 2.8. Net polar elongation of single methylation site mutants. Length of poles elongation after 1.5 hours in cells expressing *L5::sepIVA* WT and single methylation site mutants. At least 250 cells across three biological replicates were analyzed. Bar represents mean polar elongation. The adjusted p-values of the mutant compared to the WT are: R3M = 0.0009; R19M = 0.0066; and R31K = 0.0143*;* R31M = 0.0051; R224M = 0.0163; R228K = <0.0001; R228M = <0.0001; R230M = 0.0086; R234K = <0.0001; R245M = 0.0002. P-values were calculated using ordinary one-way ANOVA, Dunnett's multiple comparisons test, with a single pooled variance in GraphPad Prism (v9.2).

elongation (Fig. 2.7c). Since our methyl-ablative and methyl-mimetic site mutations show opposing effects on polar elongation, this suggests that methylation of SepIVA at these sites regulates polar elongation. We also performed this elongation assay on single methylation site mutants (Fig. 2.8). We found that individual N-terminal arginines had a similar trend - with the lysine mutants exhibiting greater elongation than the methionine mutants – but none of the single mutants had a statistically significant effect. From these results, we conclude that methylation at the R3, R19 and R31 residues work together in regulating elongation. These results show that SepIVA is an elongation regulator; since it is not required for elongation (Fig. 2.7b) we suggest that its function may be to help toggle growth between the poles and septum.

2.3e SepIVA affects MurG localization

The Intracellular Membrane Domain (IMD) is a membrane domain that can be separated by sucrose density centrifugation from the cytoplasmic fractions and from the PM-CW (plasma membrane attached to the cell wall) fraction, which contains PBPs and other periplasmic cell wall enzymes (Hayashi *et al.*, 2016). Microscopy from our previous study showed that GFPmut3-SepIVA has a similar localization pattern as the IMD-associated arabinogalactan precursor enzyme GlfT2 (Wu *et al.*, 2018). To determine if SepIVA is biochemically associated with the IMD, we performed sucrose gradient fractionation on an *Msmeg* strain with a C-terminal strep tag on SepIVA (Fig. 2.9a). We found that SepIVA was found in the cytoplasmic fractions 1-2, as well as fraction 3, which shows that SepIVA is not biochemically associated with the IMD. GlfT2 is found in the IMD in fractions 4-6 (Hayashi *et al.*, 2018). MurG, the final cytoplasmic enzyme in PG precursor synthesis, which also has a typical IMD-localization pattern

(Meniche *et al.*, 2014; García-Heredia *et al.*, 2021), is in both the IMD and the cytoplasmic fractions (García-Heredia *et al.*, 2021). Thus, SepIVA and MurG have some overlap in their biochemical fractionation in this assay. These results show that SepIVA is not an IMD-associated protein; however, the microscopic co-localization of GFPmut3-SepIVA and IMD-associated proteins suggests (Wu *et al.*, 2018) that it may associate indirectly.

Because other DivIVA homologs are involved in recruiting proteins to their site of activity (Marston and Errington, 1999; Halbedel and Lewis, 2019), we hypothesized that perhaps SepIVA could be involved in recruiting proteins to its locations near the IMD and at the septum. To test this, we looked at the effects of SepIVA depletion on localization of GlfT2-mRFP and MurG-Dendra2, which have a similar localization pattern (Meniche *et al.*, 2014; Wu *et al.*, 2018). We built an *Msmeg* strain where the only copy of *sepIVA* has a C-terminal DAS degradation tag, which targets a protein to be proteolyzed by ClpP when the SspB protease adaptor is induced by adding Atc (Kim *et al.*, 2011; Wu *et al.*, 2018). We transformed this depletion strain with either of the localization constructs. We then added Atc to induce *sspB* expression, leading to degradation of SepIVA-DAS, or did not add Atc in the control, and imaged the cells. We found that depletion of SepIVA had mild effects on GlfT2-mRFP localization (Fig. 2.9bc). However, we found that MurG-Dendra2 localization was highly sensitive to SepIVA degradation. In the strain with SepIVA-DAS and no *sspB*, MurG-Dendra2 had a localization pattern similar to the normal IMD pattern that has been described before (Meniche *et al.*, 2014; Hayashi *et al.*, 2016; García-Heredia *et al.*, 2021) (Fig. 2.9df). When we transformed the *sspB* vector into this strain but did not induce *sspB*

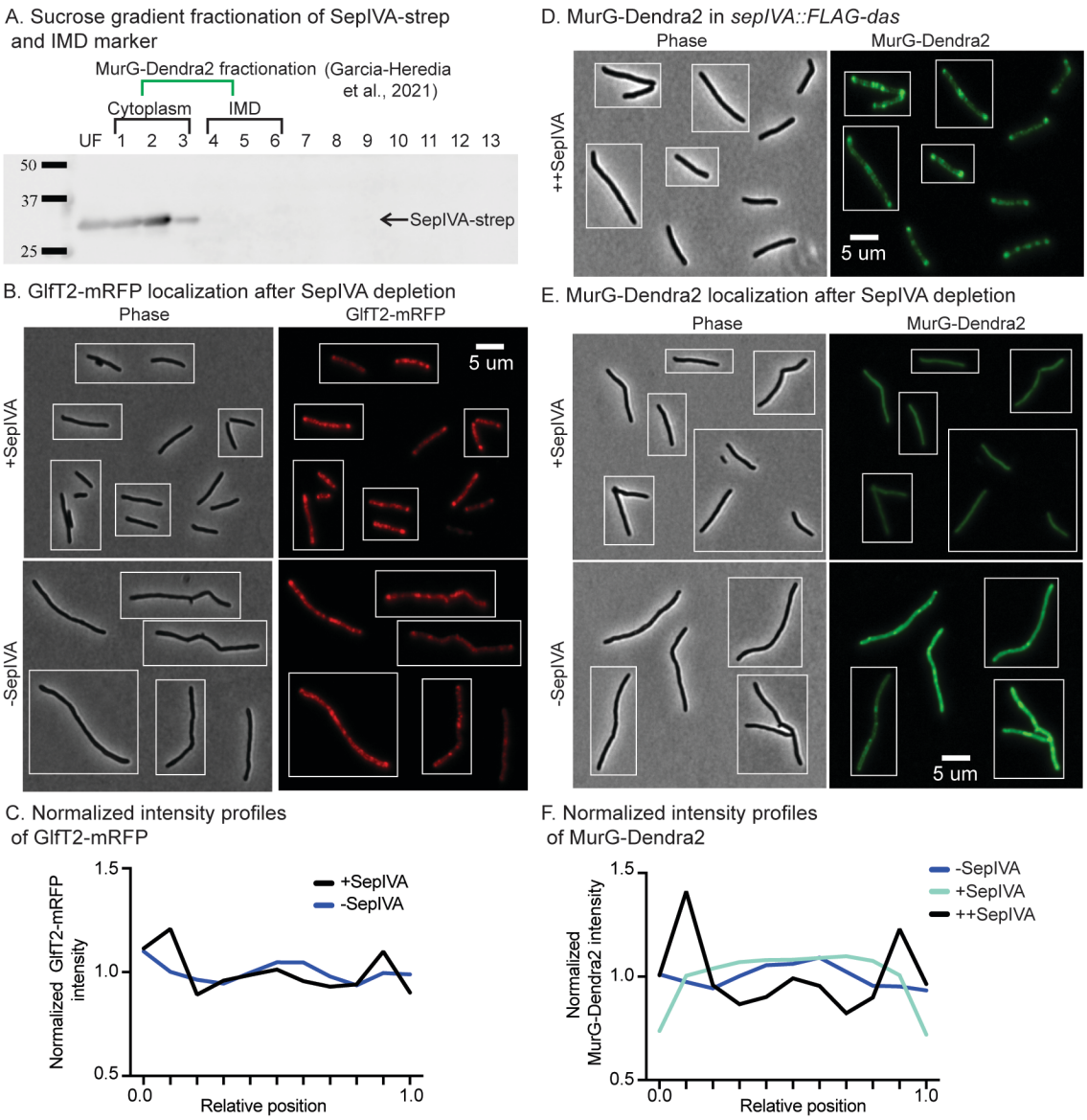

Figure 2.9. SepIVA has the same membrane association as MurG, and it affects MurG localization. (2.9a) anti-Strep western blot of sucrose gradient fractions. Fractions 4-6 contain intracellular membrane domain (IMD) proteins. The green bracket denotes fractionation of MurG-Dendra2, as shown in Garcia-Heredia *et al.* 2021. **(2.9b)** Micrographs of cells expressing or depleting SepIVA and induced for GlfT2-mRFP. Scale bar is 5 microns and applies to all images. Pictures of several cells from images processed identically were pasted together. **(2.9c)** Normalized intensity profiles of GlfT2-mRFP signal of cells expressing and depleting SepIVA and induced for GlfT2-mRFP. The solid line represents the mean intensity value across the relative position of the cell. Cells were pole-sorted such that the brighter pole in the HADA channel was set to 0 on the X axis. **(2.9d)** Micrographs of cells expressing *sepIVA::FLAG-das.* This strain lacks inducible *sspB*, therefore, SepIVA cannot be depleted in this strain. We refer to this strain as ++SepIVA. These images are 12-bit. Scale bar is 5 microns and applies to all images. Pictures of several cells from images processed identically were pasted together. **(2.9e)** Micrographs of cells expressing or depleting SepIVA while constitutively expressing MurG-

Dendra2. These images are 16-bit. Scale bar is 5 microns and applies to all images. Pictures of several cells from images processed identically were pasted together. **(2.9f)** Normalized intensity profiles of MurG-Dendra2 signal of cells expressing and depleting SepIVA. The solid line represents the mean intensity value across the relative position of the cell. Cells were pole-sorted such that the brighter pole in the HADA channel was set to 0 on the X axis.

expression, we expect a moderate decrease in SepIVA-DAS levels due to leaky SspB expression (Huang *et al.*, 2015; Costello *et al.*, 2019), and we see complete delocalization of MurG-Dendra2 (Fig. 2.9ef). When we induce SspB to strongly deplete SepIVA-DAS, MurG-Dendra2 localizes in puncta that are randomly distributed around the cell (Fig. 2.9ef).

Because SepIVA has different effects on GlfT2-RFP and MurG-Dendra2, we conclude that SepIVA does not affect IMD structure globally and is not required for IMD-association of GlfT2. Our results indicate, however, that SepIVA could have a role in modulating MurG's localization and/or association with the membrane.

2.3f Methylation site mutants on SepIVA affect polar localization of MurG

We determined that depletion of SepIVA affects localization of MurG more strongly than GlfT2 (Fig. 2.9). To determine whether arginine methylation site mutations in *sepIVA* affect MurG or GlfT2 localization, we imaged each fluorescent protein fusion in *sepIVA* wild-type and methyl-mutant strains allele swap strains. We found that the distribution of GlfT2-mRFP around the cell was unaffected by methylation site mutations (Fig. 2.10abcd). However, MurG-Dendra2 localization was less polar and more septal in the methyl-mimetic NT-M mutant (Fig. 2.10efgh) compared to the methyl-ablative mutant and the WT. This suggests that an unmethylated N-terminus of SepIVA may stimulate MurG's association with the growing pole (Fig 2.10gh), possibly by recruiting it to that site (Fig. 2.5) to promote polar peptidoglycan synthesis and polar elongation (Fig.

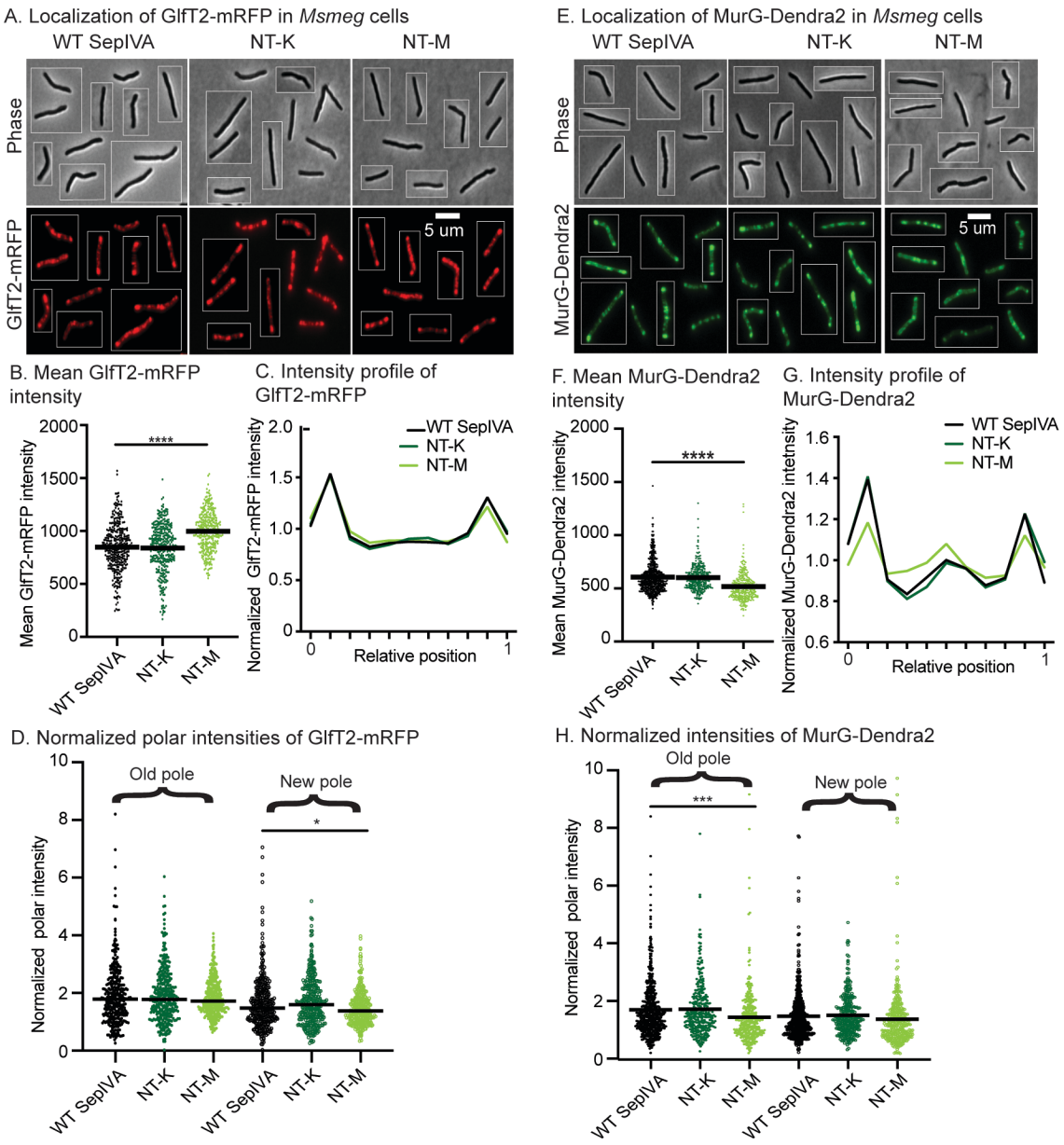

Figure 2.10. Methylation site mutations on SepIVA polar localization of MurG. (2.10a) Images of *Msmeg* cells expressing L5::*sepIVA* WT or methylation site mutants and induced for GlfT2-mRFP. Scale bar is 5 microns and applies to all images. Pictures of several cells from images processed identically were pasted together. **(2.10b)** Mean GlfT2-mRFP intensity values of *Msmeg* cells expressing *L5::sepIVA* WT or methylation site mutants and induced for GlfT2-mRFP. At least 250+ cells across three biological replicates of each mutant were analyzed in MicrobeJ. Bar represents mean intensity value. ****, *P = <0.0001.* **(2.10c)** Normalized intensity profiles of GlfT2-mRFP signal of cells expressing *L5::sepIVA* WT or methylation site mutants and induced for GlfT2-mRFP. The solid line represents the mean intensity value across the relative position of the cell. Cells were pole-sorted such that the brighter pole in the HADA channel was set to 0 on the X axis. **(2.10d)** Normalized polar GlfT2-mRFP intensities of WT and methylation site mutants. Intensity values were normalized by dividing each cell's maximum polar intensity value by the mean intensity of the whole cell. *, *P = 0.0111.* **(2.10e)** Images of

Msmeg cells expressing L5::*sepIVA* WT or methylation site mutants and constitutively expressing MurG-Dendra2. Scale bar is 5 microns and applies to all images. Pictures of several cells from images processed identically were pasted together. **(2.10f)** Mean MurG-Dendra2 intensity values of *Msmeg* cells expressing *L5::sepIVA* WT and methylation site mutants. At least 250+ cells across three biological replicates of each mutant were analyzed in MicrobeJ. Bar represents mean intensity value. *****, P = <0.0001.* **(2.10g)** Normalized intensity profiles of MurG-Dendra2 signal of cells expressing *L5::sepIVA* WT and methylation site mutants. The solid line represents the mean intensity value across the relative position of the cell. Cells were pole-sorted such that the brighter pole in the HADA channel was set to 0 on the X axis. **(2.10h)** Normalized polar MurG-Dendra2 intensities of WT and methylation site mutants. Intensity values were normalized by dividing each cell's maximum polar intensity value by the mean intensity of the whole cell. ****, P = 0.0002.* P-values were calculated using ordinary one-way ANOVA, Dunnett's multiple comparisons test, with a single pooled variance in GraphPad Prism (v9.2).

2.6, 2.7). SepIVA with a methylated N-terminus may instead decrease MurG's association to the poles (Fig. 2.10gh), which results in decreased polar peptidoglycan metabolism (Fig. 2.6cd) and elongation (Fig. 2.7c) resulting in slower growth (Fig. 2.2a). We are observing a correlation between MurG polar association (Fig. 2.10gh) and polar growth (Fig. 2.7c) in these strains, which could be due to SepIVA directly or indirectly regulating MurG.

To test if arginine methylation site mutants of *sepIVA* affect the FtsZ ring, we expressed *ftsZ-mcherry2b* in methylation mutants. Our results show that arginine methylation of SepIVA does not affect FtsZ-mcherry2B localization (Fig. 2.11).

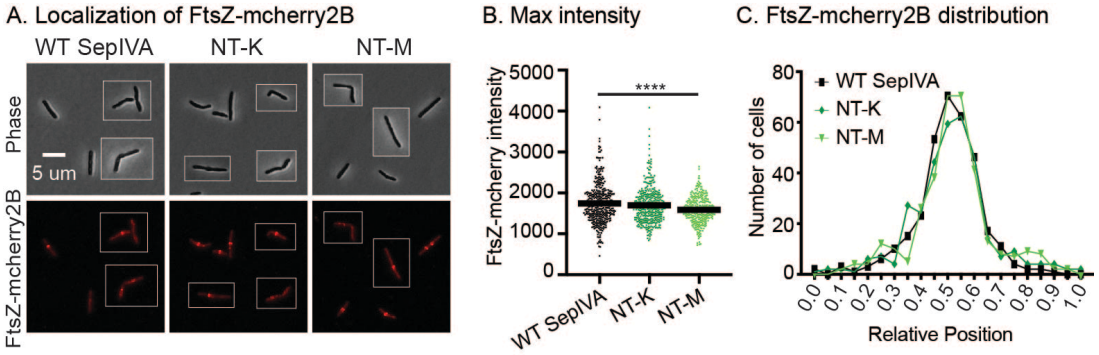

Figure 2.11. Arginine methylation of SepIVA does not affect FtsZ-mcherry2B localization. **(2.11a)** Images of cells expressing L5::*sepIVA* WT and arginine methylation mutants and TW::*ftsZ-mcherry2B.* Pictures of several cells from images processed identically were pasted

together. Scale bar applies to all images. **(2.11b)** Max intensity values of 250+ cells expressing L5::*sepIVA* WT and arginine methylation mutants and TW::*ftsZ-mcherry2B.* Bar represents mean intensity value between cells. The adjusted p-values of each mutant compared to the WT are: NT-K = 0.2925; NT-M = <0.0001; and CT-K = 0.0436. At least 2 biological replicate strains were imaged for each genotype. P-values were calculated using ordinary one-way ANOVA, Dunnett's multiple comparisons test, with a single pooled variance in GraphPad Prism (v9.2). **(2.11c)** Histogram of distribution FtsZ-mcherry2B max intensity value over the relative length of the cell. At least 250+ cells were analyzed. Relative positions of intensities were analyzed in MicrobeJ.

2.3g Residues near the C-terminus of SepIVA function in cell division

Our preliminary work on individual arginine mutations at the C-terminus of *sepIVA* indicated that these residues affect cell division (Fig. 2.2be). We further characterized the *sepIVA* R234 methylation site mutants. We observed the methyl-ablative methylation site mutant, R234K, is like the WT in growth rate and cell length, while the methyl-mimetic R234M has slower growth, longer cell length and cell branching compared to the WT (Fig. 2.12abc). Cell branching is typical of mutants with cell division defects in mycobacteria (Wu *et al.*, 2018). The *sepIVA* R234M cells also elongate slightly more than the WT (Fig. 2.12d), though this is likely to be from the increased age of poles in cells with inhibited cell division, as in fig. 2.7b. Thus, the *sepIVA* R234M strain displays inhibited cell division. The R234M strain has higher net peptidoglycan metabolism, as measured by NADA staining, than the WT, while the R234K has lower peptidoglycan metabolism than the WT (Fig. 2.12e). Because the two R234 mutants have opposing phenotypes, they may mimic the methylated and unmethylated states of SepIVA at R234. The data from these mutants suggests that arginine methylation at R234 inhibits division, while the unmethylated divides like the WT, suggesting that in the conditions measured, SepIVA is likely not methylated at this residue. The *sepIVA* R234 mutant strains both have increased MurG-Dendra2

fluorescence signal, but comparable distributions to the wild-type. Here, MurG signal does not correlate with difference in cell wall metabolism or growth (Fig. 2.12bcdgh), suggesting that regulation of cell division through the C-terminus of SepIVA does not involve regulating MurG localization. Our data show that the R234 methylation site is crucial for SepIVA's role in cell division.

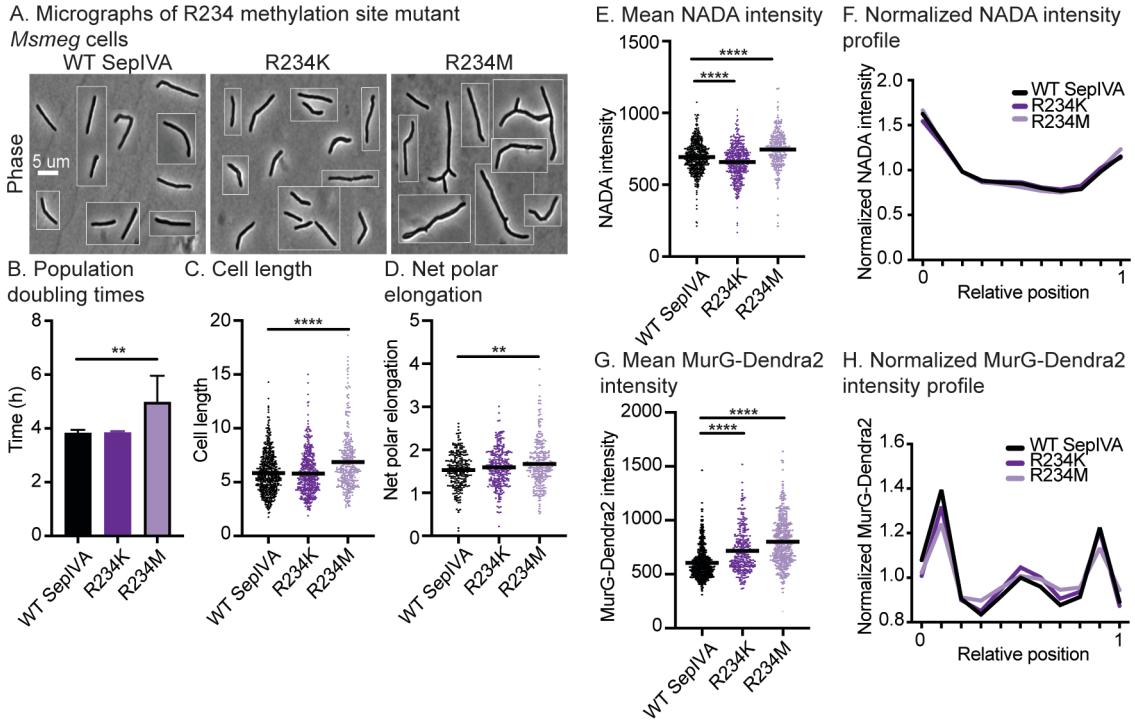

Figure 2.12. Methylation site R234 of SepIVA affects cell division. (2.12a) Images of *Msmeg* cells expressing L5::*sepIVA* WT and R234 methylation site mutants. Scale bar is 5 microns and applies to all images. Pictures of several cells from images processed identically were pasted together. **(2.12b)** Doubling time of *Msmeg* cells expressing WT or R234 methylation site mutants of SepIVA. No outline, darker color bars represent methyl-ablative methylation site mutants. Black outline bars represent methyl-mimetic methylation site mutants. At least 3 biological replicates of each strain were used. Error bars represent standard deviation. **, *P = 0.0012.* **(2.12c)** Cell lengths of SepIVA WT or R234 methylation site mutants. Bars represent mean. At least 300 cells over three biological replicates of each strain were analyzed. ****, *P = <0.0001.* **(2.12d)** Net polar elongation after 1.5 hours in cells expressing *L5::sepIVA* WT or R234 methylation site mutants. Bar represents mean polar elongation. At least 100 cells across three biological replicates were analyzed. **, *P = 0.0066.* **(2.12e)** Mean NADA intensity values of *Msmeg* cells expressing *L5::sepIVA* WT or R234 methylation site mutants. Bar represents mean intensity value. At least 250+ cells across three biological replicates of each mutant were analyzed in MicrobeJ. *P = <0.0001.* **(2.12f)** Normalized intensity profiles of NADA signal of cells expressing *L5::sepIVA* WT or R234 methylation site mutants. The solid line represents the

mean intensity value across the relative position of the cell. Cells were pole-sorted such that the brighter pole in the NADA channel was set to 0 on the X axis. **(2.12g)** Mean MurG-Dendra2 intensity values of *Msmeg* cells expressing *L5::sepIVA* WT or R234 methylation site mutants. Bar represents mean intensity value. At least 250+ cells across three biological replicates of each mutant were analyzed in MicrobeJ. ****, *P = <0.0001.* All P-values were calculated using ordinary one-way ANOVA, Dunnett's multiple comparisons test, with a single pooled variance in GraphPad Prism (v9.2). **(2.12h)** Normalized intensity profiles of MurG-Dendra2 signal of cells expressing *L5::sepIVA* WT or R234 methylation site mutants. The solid line represents the mean intensity value across the relative position of the cell. Cells were pole-sorted such that the brighter pole in the HADA channel was set to 0 on the X axis.

2.4 Discussion

Although SepIVA is a DivIVA-like protein, the preliminary data on this factor indicate that its function is distinct from other described DivIVA proteins. All other described DivIVA proteins localize specifically to the curved membranes at poles and septa (Ramamurthi and Losick, 2009). SepIVA has some localization to the septum, but it mostly localizes in a ring around the cell near the pole, but not at the pole tip (Wu *et al.*, 2018) (Fig. 2.5). This shows that SepIVA is not associated primarily with curved membranes like other DivIVA proteins. Other described DivIVA proteins have been shown to have functions in promoting polar elongation (Kang *et al.*, 2008; Letek *et al.*, 2008; Hempel *et al.*, 2008; Melzer *et al.*, 2018), helping to inhibit cell division (Marston and Errington, 1999; Eswara *et al.*, 2018) and/or to bind and regulate transcription factors (Eswaramoorthy *et al.*, 2014), cell wall enzymes (Cleverley *et al.*, 2019), cell division regulators (Eswara *et al.*, 2018), and an envelope saccharide transporter (Hammond *et al.*, 2022). None of these DivIVA proteins are essential for cell division, as SepIVA is (Wu *et al.*, 2018). While some individual residues on DivIVA homologs have been characterized as being involved in these functions, none of these residues are conserved in SepIVA. The low conservation between SepIVA and other DivIVA

proteins, the difference in localization, and the wide variety of functions and binding partners across species make it impossible to use homology to predict how SepIVA promotes cell division and regulates elongation.

Mycobacteria must regulate peptidoglycan precursor synthesis in coordination with cell wall expansion and remodeling needs. Our data indicate that SepIVA likely helps regulate the peptidoglycan layer (Fig. 2.6) possibly partly through control of MurG (Fig. 2.9, 2.10), which is the final enzyme in the construction of lipidII before it is flipped into the periplasm (Gee *et al.*, 2012; Egan *et al.*, 2020). In *E. coli*, MurG interacts with both elongation and division factors (Laddomada *et al.*, 2016; Egan *et al.*, 2020). According to our data, mild SepIVA depletion results in even dispersion of MurG throughout the cell, and strong SepIVA depletion results in mislocalization of MurG into large foci distributed randomly in the cell instead of near the poles (Fig. 2.9ef). We speculate that SepIVA is somehow affecting MurG's association with the Intracellular Membrane Domain (IMD) (Hayashi *et al.*, 2016; García-Heredia *et al.*, 2021) or other regulators that help cell wall metabolism transition between septal and elongative modes – our data do not indicate whether this regulation is direct or indirect. A third possibility is that SepIVA depletion is causing the type of cell wall damage that has previously been shown to cause MurG to re-localize to the lateral walls (Melzer *et al.*, 2021). The arginine methylation sites on the N-terminus of SepIVA appear to toggle its effect on MurG localization in a way that correlates with polar elongation: the strain with the *sepIVA* N-terminal methyl-mimetic mutations have less polar growth (Fig. 2.7c) and less MurG at the poles (Fig. 2.10f). If SepIVA's role in elongation regulation is to regulate MurG's association and dispersal from the IMD domain at the poles - directly or

indirectly - then it appears that when SepIVA is methylated at the N-terminus, it is more active in dispersing MurG from the poles.

Arginine methylation sites near the C-terminus of SepIVA, specifically R234, seem to play a role in regulating cell division (Fig. 2.12). The methyl-mimetic R234M mutant showed inhibited division (Fig. 2.12) while the methyl-ablative, R234K, did not. Methylation at this arginine residue could be inhibiting cell division. These effects on cell division revealed through mutations at the C-terminus appear to be independent of MurG localization (Fig. 2.12g).

Studies on protein arginine methylation done in eukaryotes support its importance in cell cycle progression (Biggar and Li, 2015; Raposo and Piller, 2018). Our data establish that protein arginine methylation sites on SepIVA affect the mycobacterial cell cycle as well. We have found that the arginine methylation sites on SepIVA affect both the elongation and division stages of the cell cycle. This work establishes protein arginine methylation as a physiologically important post-translational modification in bacteria and identifies SepIVA as a potential mediator between the elongation and division processes.

2.5 Methods and Materials

2.5a Bacterial strains and culture conditions.

Mycobacterium smegmatis (mc^2155) was cultured in 7H9 medium (Becton, Dickinson, Franklin Lakes, NJ) with 5 g/L bovine serum albumin (BSA), 2 g/L glucose, 0.85 g/L NaCl, 0.003 g/L catalase, 0.2% glycerol, and 0.05% Tween 80 or plated on LB agar. For *M. smeg* cultures, antibiotic concentrations were: 20 µg/mL nourseothricin, 20

μg/mL zeocin, 20 μg/mL streptomycin, 25 μg/mL kanamycin, 50 μg/mL hygromycin, and 30 μg/mL apramycin. For *E. coli* cultures, antibiotic concentrations were: 40 μg/mL nourseothricin, 25 μg/mL zeocin, 50 μg/mL streptomycin, 50 μg/mL kanamycin, 100 μg/mL hygromycin, and 50 μg/mL apramycin *E. coli* TOP10 or DH5α were used for cloning.

2.5b Strain construction

Because it is essential in *M. smegmatis, sepIVA* mutants were constructed by first integrating an additional copy of *sepIVA* at the L5 integration site. After complementing *sepIVA* at the L5 site, *sepIVA* at its native locus was knocked out via recombineering (van Kessel and Hatfull, 2008), as previously described (Boutte *et al.*, 2016). Mutant copies of *sepIVA* replaced wildtype *sepIVA* at the L5 site via allelic exchange (Pashley and Parish, 2003; Kieser *et al.*, 2015).

sepIVA depletion strains were constructed as previously described (Wu *et al.*, 2018). Merodiploid expression constructs of GlfT2-mRFP, FtsZ-mcherry2B, and MurG-Dendra2 were integrated at the Tweety integrase site (Pham *et al.*, n.d.). The merodiploid construct expressing GFPmut3-SepIVA was integrated at the L5 integrase site.

2.5c Growth rate assay

Biological replicates of *sepIVA* arginine mutants were grown to log phase in 7H9 medium. Cultures were diluted to OD_{600} = 0.1 in 200 μL 7H9 medium in a non-treated 96-well plate. Optical density at 600 nm was measured over the next 18-24 hours using a plate reader (BioTek Synergy neo2 multi-mode reader) at 37°C, shaking continuously. Population doubling times were determined using the exponential growth equation and

least squares regression fitting method in GraphPad Prism (version 9.2). P values were calculated using ordinary one-way ANOVA, Dunnett's multiple comparisons test, with a single pooled variance.

2.5d Western blots

Log phase cultures (10 mL) were pelleted and resuspended in 500 µL PBS + 1 mM phenylmethylsulfonyl fluoride (PMSF). Cells were lysed using glass beads (MiniBeadBeater-16, model 607, Biospec). Supernatants from cell lysates were run on 4–12% NuPAGE Bis Tris precast gels (Life Technologies, Beverley, MA) using MES running buffer (Life Technologies, Beverly, MA). Proteins were transferred onto polyvinylidene difluoride (PVDF) membranes (GE Healthcare). Strep-tagged proteins were detected using rabbit anti-Strep-tag II antibody (1:1000, Abcam, ab76949) in Tris-buffered saline with Tween 20 (TBST) with 0.5% BSA and goat anti-rabbit IgG (H+L) horseradish peroxide (HRP)-conjugated secondary antibody (1:10,000, Thermo Fisher Scientific 31460) in TBST. Tagged proteins were visualized using chemiluminescent reagents (Thermo Fisher Scientific 34579).

2.5e Microscopy

Cells were imaged using a Nikon Ti-2 widefield epifluorescence microscope with a Photometrics Prime 95B camera and a Plan Apo 100X, 1.45 -numerical-aperture objective. Green-fluorescent images for GFPmut3 or Dendra2 localization or NADA staining were taken with a 470/40nm excitation filter and a 525/50nm emission filter. Blue-fluorescent images for HADA staining were taken with a 350/50nm excitation filter and a 460/50nm emission filter. Red-fluorescent images for mRFP and mcherry2B localization were taken with a 560/40nm excitation filter and a 630/70 emission filter.

Images were captured using NIS Elements software. Images were analyzed using FIJI and MicrobeJ (Ducret *et al.*, 2016). For cell detection using MicrobeJ, parameters for width and area were set. V-snapping cells were cut at the septum so daughter cells could be detected as individual cells. Overlapping cells were excluded from analysis.

Cell lengths, mean intensities, maximum intensities, and minimum intensities of at least 250 cells per genotype were quantified using MicrobeJ. Mean intensity profiles were plotted using the "XStatProfile" plotting tool in MicrobeJ. P-values were calculated using ordinary one-way ANOVA, Dunnett's multiple comparisons test, with a single pooled variance using GraphPad Prism (v9.2).

2.5f Localization of cell wall proteins upon SepIVA depletion.

For depletion of SepIVA, log phase cells (10 mL) were incubated (37°C) with 500 ng/mL Anhydrotetracycline (ATc) for 7-9 hours. For induction of GlfT2-mRFP, 1 ng/mL IVN were added, and cells were incubated (37°C) for 5 hours. Cells were fixed for microscopy. Cells were fixed for microscopy with 1.6% paraformaldehyde for 10 minutes and then washed and resuspended in PBS tween80. Microscopy images were analyzed in ImageJ and MicrobeJ. P-values calculated by unpaired t-test using GraphPad Prism (v9.2).

2.5g Fluorescent staining

HADA (ThermoFisher) and NADA (ThermoFisher) fluorescent D-alanine amino acids were used to stain the peptidoglycan cell wall layer (Kuru *et al.*, 2012). For PG analysis, NADA stain was added to 1 mL exponentially growing cells at a final concentration of 1 ug/mL for 3 minutes at room temperature before washing twice in PBST. For pulse-chase experiments, HADA (1 ug/mL) was added for 15 minutes before

cells were washed twice in 7H9, incubated (37°C) for 1.5 hours, and stained again using NADA (1 ug/mL) for 3 minutes at room temperature. Cells were washed twice in PBST and imaged. Images were analyzed in ImageJ (NIH). The length of the poles and the length of the entire cell were measured manually for each cell.

2.5h Sucrose Density Gradient Fractionation

Sucrose density gradient fractionation was performed as previously described (Hayashi *et al.*, 2016). In brief, cells were grown to log phase and lysed by nitrogen cavitation. Lysate was then placed on top of a 20-50% sucrose gradient and centrifuged at 35,000 rpm for 6 hours at 4°C. Twelve one-mL fractions were collected and analyzed.

2.5i Immunoprecipitation and mass spectrometry

We previously performed LCQ-MS/MS to identify peptides from *Mtb* cell lysates (Garces *et al.*, 2010). Here, we re-analyzed those data to search for modifications in peptides, using Andromeda software.

SepIVA-strep was immunoprecipitated from CB1223. Cells were grown to late log. phase, pelleted and resuspended in PBS with PMSF at 1 mM, lysed by bead beating, and clarified by centrifugation. Immunoprecipitation was performed with MagStrep type 3 XT beads (Iba Life Sciences, Gottingen, Germany) according to the manufacturers protocol. Liquid was evaporated from the immunoprecipitants, and then digested by Trypsin/Lys-C Mix, Mass Spec Grade protease (Promega), according to the manufacturer's protocols for reduction, alkylation and two-step in-solution digestion of proteolytically resistant proteins. The digested peptide solution was then cleaned by C18-Ziptips (Sigma Aldrich) according to the manufacturers protocol.

LC-MS analysis was performed on LTQ Velos pro mass spectrometer (Thermo Scientific, CA, USA) combined with a UHPLC (UltiMate 3000, Dionex, USA). The digested peptides were separated by a nano viper analytical C18 column. (Acclaim pepMap, 150 mm × 75μm, 2μm, 100 Å, Thermo Scientific, CA, USA). A 60 min gradient method was used to separate the digested peptides (0–3 min 4.0%B, 3–50 min 4.0–50.0% B, 50–50.1 min 50–90% B,50.1–55 min 90% B, 55–55.1 min 90–4% B, 55.1–60 min 4% B; mobile phase A: 0.1% FA in water; mobile phase B: 0.1% FA in 95% acetonitrile, 5% water). 5μL of digested samples was injected at 300 nL/min flow. The nano-electrospray ionization (ESI) source used with a fixed spray voltage at 2.4 kV and a heated capillary temperature at 275 °C. A full MS spectrum obtained in normal scan mode from 350 to 2000 m/z mass range. The data-dependent acquisition was performed to get the MS/MS spectra for the 5 most abundant ions. The software Proteome Discoverer (Thermo Scientific, USA) was used to search and identify the peptides. LC-MS was performed at the Shimadzu Center for Advanced Analytical Chemistry at UT Arlington.

Chapter 3: Methylation site R230 is important for molecular function of SepIVA in *Mycobacterium smegmatis*

Angela Freeman[1], Cara Boutte[1]

[1]Department of Biology, University of Texas at Arlington, Arlington, Texas, USA

3.1 Abstract

Mycobacteria have a distinct cell wall that is strictly regulated to tolerate stressful environments. Many of the factors involved in regulating the mycobacterial cell wall are unknown. Our previous work characterized methylation sites on the cell division regulator, SepIVA. While our results suggest that arginine methylation on SepIVA helps the protein balance regulation of elongation and septation, the molecular function of SepIVA is still unknown. One methylation site, R230, on SepIVA proved to be an arginine residue that is essential for SepIVA's function in cell division. Here, we characterize the R230 methyl-ablative and methyl-mimetic mutants. Our work shows that this residue is crucial for SepIVA to regulate cell division, regardless of methylation state.

3.2 Introduction

The genus *Mycobacteria* includes the pathogenic bacterium, *Mycobacterium tuberculosis (Mtb),* the causative agent of tuberculosis (TB). A key challenge in the TB epidemic is the tolerance of the bacillus to stress, including antibiotics. This phenomenon is partly responsible for the lengthy treatment regimen required to treat TB (World Health Organization, 2022). Rifampin is currently one of four drugs used to treat drug-susceptible TB infections. However, many TB infections are rifampin-resistant (World Health Organization, 2022). Developing better treatments for TB will require understanding how mycobacterial cells adapt to environmental stresses, like those seen in infection. When mycobacteria encounter stress, the cell wall is heavily remodeled, and cells decrease in size (Wu *et al.*, 2016). Cell wall remodeling requires strict regulation of the cell wall. While plenty of research has been done to identify the

enzymes involved in construction of the cell wall, how these enzymes are regulated is still largely unknown. There is evidence that proteins like Wag31 (Jani *et al.*, 2010), CwlM (Boutte *et al.*, 2016) and SepIVA (Wu *et al.*, 2018) have a role in cell division, even though they lack enzymatic function. This supports that these proteins are regulators of cell wall enzymes and could mediate cell wall changes in stress.

SepIVA is an essential division factor conserved among the Corynebacteria (Jani *et al.*, 2010; Wu *et al.*, 2018). SepIVA contains a DivIVA-domain. Proteins containing DivIVA-domains typically localize to cell poles and function by recruiting and regulating other proteins at the poles (Cha and Stewart, 1997). DivIVA in *B. subtillis* is involved in septal site establishment, and it works by recruiting septal inhibitors to the poles (Edwards and Errington, 1997). SepIVA localizes to the septum, indicating that SepIVA is part of the divisome (Wu *et al.*, 2018), like DivIVA in *B. subtilis* and Wag31, the other DivIVA homolog in mycobacteria (Kang *et al.*, 2008). While DivIVA and SepIVA both co-localize with the divisome, SepIVA proteins are more evenly disbursed throughout the cell, versus Wag31, which localizes as puncta near the poles and midcell (Kang *et al.*, 2008; Habibi Arejan *et al.*, 2023). Wag31 and SepIVA have opposing phenotypes when depleted, therefore, the proteins are not-functionally redundant, despite both having DivIVA domains (Kang *et al.*, 2008; Jani *et al.*, 2010; Wu *et al.*, 2018). To understand the function of SepIVA without depleting the protein, we investigated the effects of post-translational modifications of SepIVA.

Our data in chapter 2 show that SepIVA is post-translationally modified via protein arginine methylation. In chapter 2, we concluded which arginine methylation sites on SepIVA help *Mycobacterium smegmatis* balance elongation and septation. In

chapter 3, we characterized arginine methylation site R230 in both methyl-ablative and methyl-mimetic states. We also perform a suppressor mutation screen in search of potential pathways that SepIVA may be involved in. Our work shows that R230 is important for SepIVA's role in cell division, regardless of methylation state.

3.3 Results

3.3a R230 is crucial for SepIVA's molecular function in cell division

When SepIVA is depleted, cells become long and filamentous, suggesting that septation is not being activated (Wu *et al.*, 2018). While investigating the role of arginine methylation sites on SepIVA, discussed in chapter 2, I discovered that both methyl-ablative and methyl-mimetic R230 site mutations lead to similar growth phenotypes. These growth defects were less severe compared to when SepIVA is depleted (Wu *et al.*, 2018). The doubling times of R230K (methyl-ablative) and R230M (methyl-mimetic) were both significantly greater than the WT (Fig. 3.1b). Looking under the microscope, I saw that R230 mutant cells were greater in length compared to the WT (Fig. 3.1ac). Since both methylation state mutants were longer in length and grew slower than the WT, we concluded that this residue was crucial to SepIVA's regulation of cell division, rather than methylation of R230.

To investigate whether R230 helped SepIVA regulate polar elongation, as well as division, I measured how much cells elongated in 1.5 hours. My results suggested that R230 mutants elongated more in 1.5 hours compared to the WT (Fig. 3.1d). However, because division is clearly inhibited in these cells, there is no new pole formation. As mycobacteria elongate from the poles, with the pole established after a division cycle

growing slower than the older pole (Kieser and Rubin, 2014), if no new pole is ever established, then only old poles will be measured. Since the old pole elongates faster than the new pole, only measuring old poles would lead to the appearance of greater elongation versus measuring both old and new poles. This led us to conclude that R230 is needed for SepIVA's role in division versus elongation.

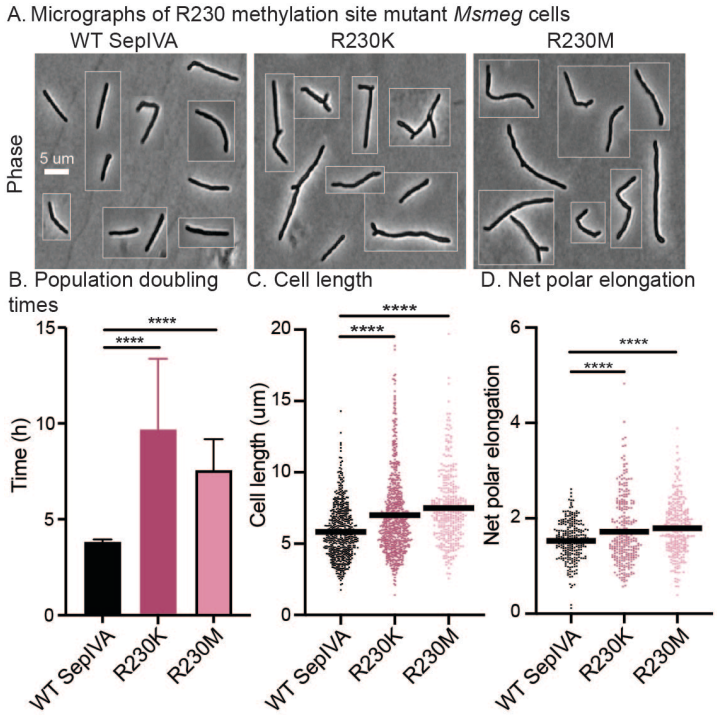

Figure 3.1. R230 on SepIVA is needed for its function in cell division. (3.1a) Images of *Msmeg* cells expressing L5::*sepIVA* WT and R230 methylation site mutants. Scale bar is 5 microns and applies to all images. Pictures of several cells from images processed identically were pasted together. **(3.1b)** Doubling time of *Msmeg* cells expressing WT or R230 methylation site mutants of SepIVA. No outline, darker color bars represent methyl-ablative methylation site mutants. Black outline bars represent methyl-mimetic methylation site mutants. At least 3 biological replicates of each strain were used. Error bars represent standard deviation. ****, *P = <0.0001.* **(3.1c)** Cell lengths of SepIVA WT or R230 methylation site mutants. Bars represent mean. At least 300 cells over three biological replicates of each strain were analyzed. ****, *P = <0.0001.* **(3.1d)** Net polar elongation after 1.5 hours in cells expressing *L5::sepIVA* WT or R230 methylation site mutants. Bar represents mean polar elongation. At least 100 cells across three biological replicates were analyzed. ****, *P = <0.0001.* All P-values were calculated using ordinary one-way ANOVA, Dunnett's multiple comparisons test, with a single pooled variance in GraphPad Prism (v9.2).

3.3b R230 on SepIVA contributes to antibiotic resistance

A key challenge to fighting the TB epidemic is the increasing number of cases of multi-drug resistant infections (World Health Organization, 2022). Since one of the ways drug resistances can develop is strict regulation of the mycobacterial cell wall, we tested our SepIVA R230 mutants for increased susceptibility to antibiotics. We determined the minimum inhibitory concentration (MIC) of two beta-lactam antibiotics, meropenem (Pryka and Haig, 1994) and cefoxitin (Wallick and Hendlin, 1974), and rifampin, which inhibits RNA synthesis (Hinkle *et al.*, 1972). Our results showed increased susceptibility to all three antibiotics tested, compared to the WT (Fig. 3.2).

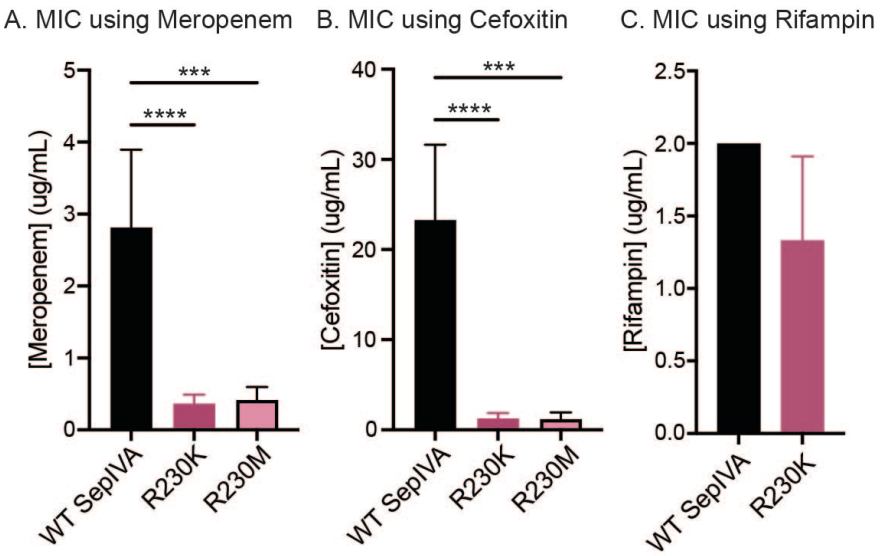

Figure 3.2 R230 methylation site has a role in antibiotic susceptibility. (3.2a) MIC of meropenem against WT and R230 methylation site mutants. Mean MIC of WT = 2.8 ug/mL. Mean MIC of R230K = 0.36 ug/mL. Mean MIC of R230M = 0.42 ug/mL. ***, *P = 0.0008.* ****, *P = <0.0001.* **(3.2b)** MIC of cefoxitin against WT and R230 methylation site mutants. Mean MIC of WT = 23.27 ug/mL. Mean MIC of R230K = 1.25 ug/mL. Mean MIC of R230M = 1.17 ug/mL. ***, *P = 0.0001.* ****, *P = <0.0001.* **(3.2c)** MIC of rifampin against WT and R230K methylation site mutant. Mean MIC of WT = 2 ug/mL. Mean MIC of R230K = 1.33 ug/mL. MIC of rifampin against R230M site mutant was not performed. P-values were calculated using ordinary one-way ANOVA, Dunnett's multiple comparisons test, with a single pooled variance in GraphPad Prism (v9.2).

Despite differences in MIC of the three antibiotics tested between the WT and R230 mutants, it should be noted that statistically significant differences were only seen with beta-lactam antibiotics (Fig 3.2ab). Since it seems that R230 is needed for SepIVA function, this finding supports our conclusion in chapter 2, that SepIVA broadly regulates the peptidoglycan layer of the cell wall (Fig. 2.6).

3.3c Suppressor mutations in R230K strains restore slow growth rate to WT

To further investigate the molecular mechanism of SepIVA, I performed suppressor screens of R230K mutants. Since R230K strains have similar phenotypes to strains with depleted SepIVA protein, this mutant was an ideal candidate for suppressor mutations in pathways that SepIVA could be involved in. To perform the suppressor screen, I passaged cultures of three R230K parent strains for 10 days (Fig. 3.3a). I performed growth curves on individual colonies grown from streak plates of each of the passaged cultures to find isolates with growth rates comparable to the WT (Fig. 3.3b). If isolates had restored growth rates to the WT rate, they were sent for whole genome sequencing to look for suppressor mutations (Fig. 3.3b, isolates marked with '*'). Our suppressor screen showed mutations in *MSMEG_2739, MSMEG_5872, MSMEG_6828* and an unknown MSMEG gene, with the most compelling mutations in *MSMEG_2739* (Fig. 3.3c).

Msmeg_2739 is a protein of unknown function with a transmembrane domain (Yates *et al.*, 2022) and is non-essential for cell viability (DeJesus *et al.*, 2017). Conserved domain analysis showed that Msmeg_2739 contains a Leu-Gly-Phe-Pro (LGFP) repeat domain (Lu *et al.*, 2020). While the function of LGFP domains remains unknown, other proteins with this domain interact with cell wall components, such as

MytA in *Corynebacterium glutamicum*, which interacts with arabinogalactan and peptidoglycan polymers (Dietrich *et al.*, 2020). If the LGFP domain of Msmeg_2739 was

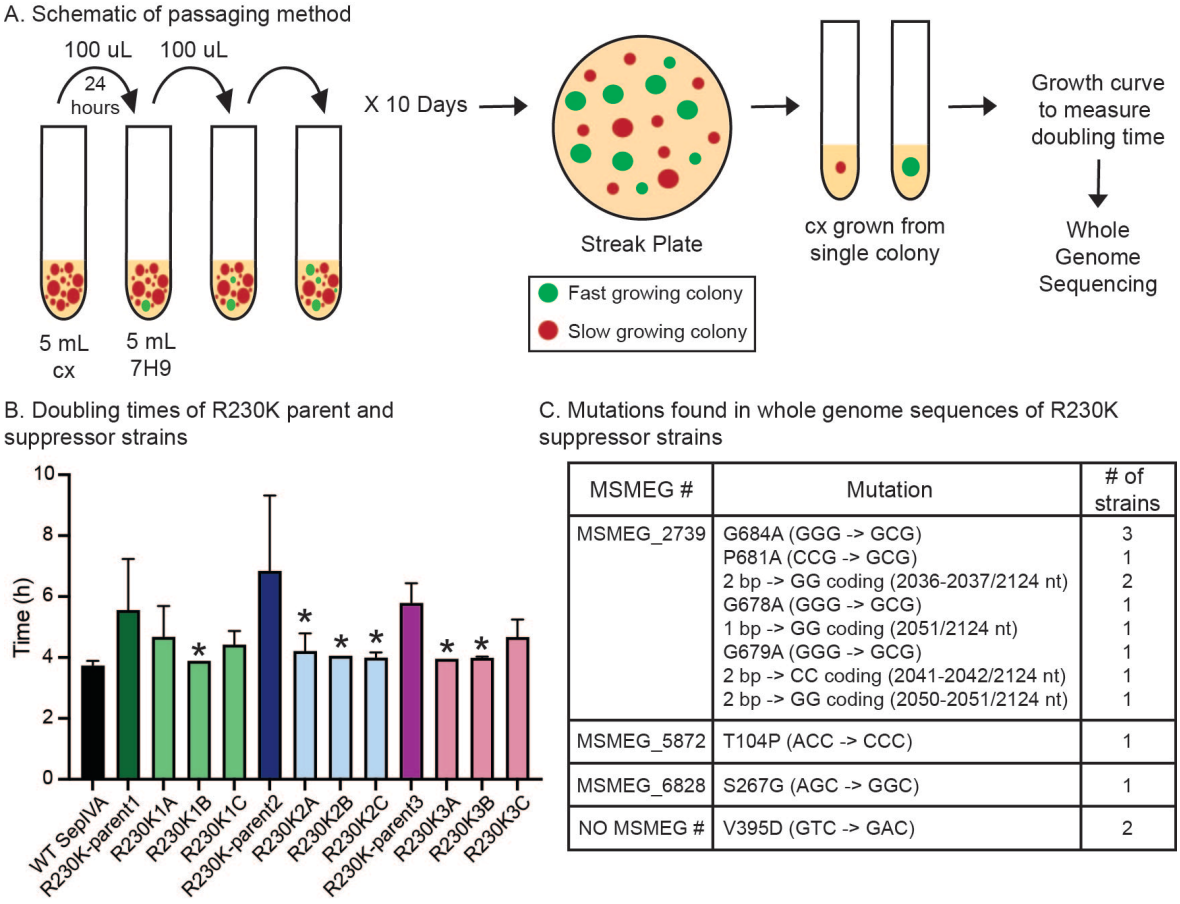

MSMEG #	Mutation	# of strains
MSMEG_2739	G684A (GGG -> GCG) P681A (CCG -> GCG) 2 bp -> GG coding (2036-2037/2124 nt) G678A (GGG -> GCG) 1 bp -> GG coding (2051/2124 nt) G679A (GGG -> GCG) 2 bp -> CC coding (2041-2042/2124 nt) 2 bp -> GG coding (2050-2051/2124 nt)	3 1 2 1 1 1 1 1
MSMEG_5872	T104P (ACC -> CCC)	1
MSMEG_6828	S267G (AGC -> GGC)	1
NO MSMEG #	V395D (GTC -> GAC)	2

Figure 3.3 R230K suppressor screen methodology and results. (3.3a) Schematic of passaging method used to promote suppressor mutation formation. **(3.3b)** Doubling times of R230K parent (dark color) and suppressor strains (light color). Isolates with doubling times like the WT were sent for whole genome sequencing, denoted with '*'. **(3.3c)** Chart depicting mutations found in whole genome sequences of R230K suppressor strains when compared to the WT genome. Nucleotide insertions are denoted as "# bp ->" followed by nucleotide(s) inserted and insertion site.

interacting with cell wall components, then SepIVA could be regulating Msmeg_2739 and its role in cell growth. However, further investigation of the relationship between SepIVA and Msmeg_2739 would have to be done. All genes found in our suppressor mutations and their potential functions can be found in table 3.1.

Table 3.1 Potential suppressors of sepIVA R230K growth defect

MSMEG #	Gene name	Protein function	Essential? (y/n)
MSMEG_2739	-	Transmembrane alanine and glycine rich protein	No
MSMEG_5872	*phoP*	DNA-binding response regulator	No
MSMEG_6828	-	Transcriptional regulator	No
NO MSMEG #	-	Diol dehydratase reactivase	-

3.4 Discussion

In this chapter, we characterized the R230 methylation site found near SepIVA's C-terminus. Our results suggest that this arginine residue is essential for SepIVA's function in cell division, regardless of methylation state. This provided us with insight into the overall function of SepIVA. Based on the inhibited cell division (Fig. 3.1abc) and the increased susceptibility to beta-lactam antibiotics (Fig. 3.2ab), SepIVA could be regulating specifically the peptidoglycan layer of the cell wall. This is supported by our findings in chapter 2, specifically figures 2.6 and the effects on MurG localization seen in figure 2.9.

Because our suppressor screen largely uncovered uncharacterized proteins, it is difficult to make concrete conclusions about this data. I speculate that the LGFP domain of Msmeg_2739 interacts with cell wall components, such as arabinogalactan or peptidoglycan polymers. If this is true, SepIVA could be regulating this protein and its interaction with cell wall components. However, a lot of work would need to be done to confirm this speculation.

3.5 Methods and Materials

3.5a Bacterial strains and culture conditions.

Mycobacterium smegmatis (mc^2155) was cultured in 7H9 medium (Becton, Dickinson, Franklin Lakes, NJ) with 5 g/L bovine serum albumin (BSA), 2 g/L glucose, 0.85 g/L NaCl, 0.003 g/L catalase, 0.2% glycerol, and 0.05% Tween 80 or plated on LB agar. For *M. smeg* cultures, antibiotic concentrations were: 20 µg/mL nourseothricin, 20 µg/mL zeocin, and 25 µg/mL kanamycin. For *E. coli* cultures, antibiotic concentrations were: 40 µg/mL nourseothricin, 25 µg/mL zeocin, and 50 µg/mL kanamycin. *E. coli* TOP10 or DH5α were used for cloning.

3.5b Strain construction

Because it is essential in *M. smegmatis, sepIVA* R230 mutants were constructed by first integrating an additional copy of *sepIVA* at the L5 integration site. After complementing *sepIVA* at the L5 site, *sepIVA* at its native locus was knocked out via recombineering (van Kessel and Hatfull, 2008), as previously described (Boutte *et al.*, 2016). Mutant copies of *sepIVA* replaced wildtype *sepIVA* at the L5 site via allelic exchange (Pashley and Parish, 2003; Kieser *et al.*, 2015).

3.5c Growth rate assay

Biological replicates of *sepIVA* arginine mutants were grown to log phase in 7H9 medium. Cultures were diluted to OD_{600} = 0.1 in 200 µL 7H9 medium in a non-treated 96-well plate. Optical density at 600 nm was measured over the next 18-24 hours using a plate reader (BioTek Synergy neo2 multi-mode reader) at 37°C, shaking continuously. Population doubling times were determined using the exponential growth equation and least squares regression fitting method in GraphPad Prism (version 9.2). P values were

calculated using ordinary one-way ANOVA, Dunnett's multiple comparisons test, with a single pooled variance.

3.5d Microscopy

Cells were imaged using a Nikon Ti-2 widefield epifluorescence microscope with a Photometrics Prime 95B camera and a Plan Apo 100X, 1.45 -numerical-aperture objective. Images were captured using NIS Elements software. Images were analyzed using FIJI and MicrobeJ (Ducret *et al.*, 2016). For cell detection using MicrobeJ, parameters for width and area were set. V-snapping cells were cut at the septum so daughter cells could be detected as individual cells. Overlapping cells were excluded from analysis.

Cell lengths of at least 250 cells per genotype were quantified using MicrobeJ. P-values were calculated using ordinary one-way ANOVA, Dunnett's multiple comparisons test, with a single pooled variance using GraphPad Prism (v9.2).

3.5e Fluorescent staining

HADA (ThermoFisher) and NADA (ThermoFisher) fluorescent D-alanine amino acids were used to stain the peptidoglycan cell wall layer (Kuru *et al.*, 2012). For pulse-chase experiments, HADA (1 ug/mL) was added for 15 minutes before cells were washed twice in 7H9, incubated (37°C) for 1.5 hours, and stained again using NADA (1 ug/mL) for 3 minutes at room temperature. Cells were washed twice in PBST and imaged. Images were analyzed in ImageJ (NIH). The length of the poles and the length of the entire cell were measured manually for each cell.

3.5f Passaging of strains to allow for suppressor mutations

Three biological replicates of SepIVA R230K methylation site mutants were grown in 7H9 media from frozen stocks. Once in log phase, 100 uL of culture was transferred into fresh 5 mL of 7H9. This was repeated daily for 10 days to allow for suppressor mutations to form. On day 10, 100 uL of each culture was plated on LB agar plates and incubated at 37°C for 3 days. From each plate, 3 larger colonies were grown up in 7H9 for growth rate analysis.

3.5g Genomic DNA isolation for whole genome sequencing

The genomic DNA (gDNA) was isolated from six fast-growing suppressor strains. gDNA isolation was done according to the phenol:chloroform:isoamyl alcohol (15:24:1) method(Sambrook and Russel, 2001). Samples were prepped according to guidelines set by SeqCenter (PA, USA). Samples were sent to SeqCenter for whole genome sequencing and variant calling. Genome sequences were compared to genome sequence of mc^2155 *ΔsepIVA::zeoR L5::sepIVA-strep.* Differences between WT and R230K genomes were considered potential suppressor mutations.

3.5h Minimum inhibitory concentration determination

Three biological replicates of SepIVA WT and R230K methylation site mutants were grown in 7H9 media from frozen stocks. Once in log phase, cultures were diluted back to OD = 0.002. Antibiotics were diluted by half between each column of wells on 96-well plate, from highest concentration on the left to lowest on the right. Two control columns were used, one with no antibiotic and one with no bacteria and highest antibiotic concentration. To each well, 100 uL of media and 100 uL of culture were added. Plates were incubated at 37°C for 48 hours, shaking continuously. To measure

any metabolic activity, a 0.02% solution of Alamar Blue (resazurin) was made. 20 uL were added to each well and plates were incubated at 37°C for 24 hours, shaking continuously. After incubation, color change from blue to purple or pink were recorded as growth. The lowest concentration of antibiotic that did not permit growth was considered the MIC. P values were calculated using ordinary one-way ANOVA, Dunnett's multiple comparisons test, with a single pooled variance.

Chapter 4: Investigating the role of SepIVA in the DNA damage response in *Mycobacterium smegmatis*

Angela Freeman[1], Cara Boutte[1], Anusuya Nepal[1]

[1]Department of Biology, University of Texas at Arlington, Arlington, Texas, USA

4.1 Abstract

The environment inside the human lung is full of stressors stemming from the host's immune defense against infections like tuberculosis (TB). Some of these stressors include reactive oxygen species which cause DNA damage in bacterial cells. *Mycobacterium tuberculosis (Mtb),* the causative agent of TB, has tools, such as nucleotide excision repair, to combat DNA damage and maintain integrity of the genome. Additionally, mycobacteria can strictly regulate cell division in response to environmental stress. In this chapter, we investigate the relationship between the cell division regulator, SepIVA and DNA damage repair protein, UvrA. Our findings suggest that SepIVA and UvrA are both involved in the cell's response to DNA damage. However, the two proteins appear to be involved in separate DNA damage repair pathways.

4.2 Introduction

4.2a Coupling cell division and DNA replication

For bacterial cell division to occur, the chromosome must be fully replicated and segregated. This checkpoint, mediated by FtsK, results in two intact chromosomes, fully separated into two daughter cells (Sherratt *et al.*, 2010). If DNA damage occurs, cell division will be halted until the chromosome can be repaired. While division is downregulated, elongation continues, resulting in long, filamentous cells (Raghunathan *et al.*, 2020). In *E. coli*, division is inhibited by SlmA, which interacts with Min system proteins and FtsZ to prevent Z-ring formation when DNA is damaged (Bernhardt and de Boer, 2005). Additionally, *E. coli* cells can inhibit division in response to DNA damage through the Z-ring antagonist SulA. SulA destabilizes FtsZ polymers to inhibit division,

specifically in the presence of damaged DNA(Mukherjee *et al.*, 1998; Burby and Simmons, 2019; Vedyaykin *et al.*, 2020). Since mycobacteria lack both the Min system and SulA, there are still many questions about how mycobacterial cells down regulate division when DNA is damaged.

4.2b DNA damage repair in mycobacteria

One of the multiple ways that mycobacteria fix DNA damage is through nucleotide-excision repair (NER). NER is highly conserved across prokaryotes and consists of Uvr proteins, UvrABCD (Hu *et al.*, 2017). Damaged DNA is recognized by UvrA and UvrB, prompting UvrA to disassociate with UvrB (Van Houten and Snowden, 1993). UvrB interacts with excinuclease, UvrC, which excises 12 or 13 bp fragments from the chromosome around the damaged DNA. UvrB and UvrC are bumped out of place by DNA helicase, UvrD. UvrD and DNA polymerase I then fill the 12 to 13 bp gap in DNA, with intact DNA, and the chromosome is repaired (Husain *et al.*, 1985; Sibghat-Ullah *et al.*, 1990; Singh, 2017; Thakur *et al.*, 2020). The Uvr proteins are highly characterized in *E. coli*, but in mycobacteria, characterization of these proteins and their connection to cell division is still being investigated.

Our work in chapter four aims to link DNA damage repair systems, specifically NER, to cell division. We found that multiple Uvr proteins are potential interactors with cell division regulator, SepIVA. Our results show that SepIVA is involved in regulating division in response to DNA damage. However, we believe that SepIVA's connection to DNA damage is through a different repair system than those involving Uvr proteins.

4.3 Results

4.3a UvrAB are potential interactors of SepIVA

There are many environmental factors that can cause cell division regulators, like SepIVA, to modify division. In search of pathways that SepIVA could be involved in, we looked for SepIVA interactors. We immunoprecipitated SepIVA-strep and identified interactors via mass spectrometry (Schmidt and Skerra, 2007). Interestingly, our results included multiple Uvr proteins as potential SepIVA interactors, with UvrA being the most abundant (Table 4.1). This led us to hypothesize that SepIVA is regulating cell division when DNA is damaged through its relationship with UvrA.

Table 4.1 SepIVA-strep pulldown data[1]

Protein	Description	IP abundance (control)	IP abundance (SepIVA-IP)	Ratio
UvrA	UvrABC system protein A	283304.8926	16380160.28	57.81813
UvrB	UvrABC system protein B	2649133.141	13300662.06	5.02076
UvrC	UvrABC system protein C	-	430190.5938	-

[1] IP abundance (control) indicates amount of peptide from strain without SepIVA-strep. IP abundance (SepIVA-IP) indicates amount of peptide from SepIVA-strep strain. Ratio equals abundance of protein from SepIVA-IP divided by control-IP.

4.3b UvrA promotes survival in DNA damage

To investigate the relationship between SepIVA and UvrA, I constructed a Δ*uvrA::hygR* strain via recombineering (Murphy *et al.*, 2015). DNA damage was induced using the cancer drug, mitomycinC (mitoC), which causes damage by crosslinking DNA (Iyer and Szybalski, 1963; Sinawe and Casadesus, 2022). We tracked how WT and Δ*uvrA* strains survived over 24 hours in the presence of DNA damage. Our results show

that UvrA promotes survival in DNA damage (Fig. 4.1). This led us to investigate whether SepIVA played a role in the DNA damage response.

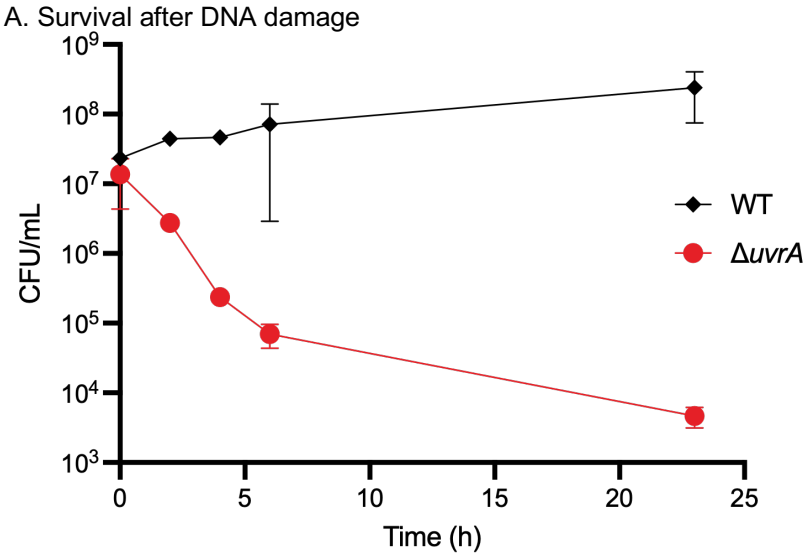

Figure 4.1 Survival of WT and *ΔuvrA* strains after DNA damage. Colony forming units/mL of WT and Δ*uvrA* strains over 24 hours after addition of mitomycin C (25 ng/mL). Three biological replicates were used for each strain.

4.3c DNA damage, but not UvrA, affects GFPmut3-SepIVA localization

Our findings in chapter 2 suggest that SepIVA has both a role in elongation and septation. When DNA has been damaged, septation is down regulated, while elongation continues (Raghunathan *et al.*, 2020). SepIVA localizes to the septum late in the cell cycle, presumably to activate septation, since septation does not occur when SepIVA is depleted (Wu *et al.*, 2018). To determine if SepIVA localization changes when division is down regulated due to DNA damage, we localized GFPmut3-SepIVA after mitoC treatment for 5 hours. Our results show that GFPmut3-SepIVA localization is largely near the cell poles and less septal after DNA damage (Fig. 4.2ab). This is consistent with previous work that suggests SepIVA is activating septation (Wu *et al.*, 2018), since without SepIVA located at the septum, division is inhibited. We also observed GFPmut3-SepIVA localization with and without *uvrA* in the presence of DNA damage.

Our results showed that GFPmut3-SepIVA re-localization in DNA damage is not affected by Δ*uvrA* (Fig. 4.2c). This further supports that SepIVA and UvrA are independently involved in DNA damage responses, versus working in the same pathway.

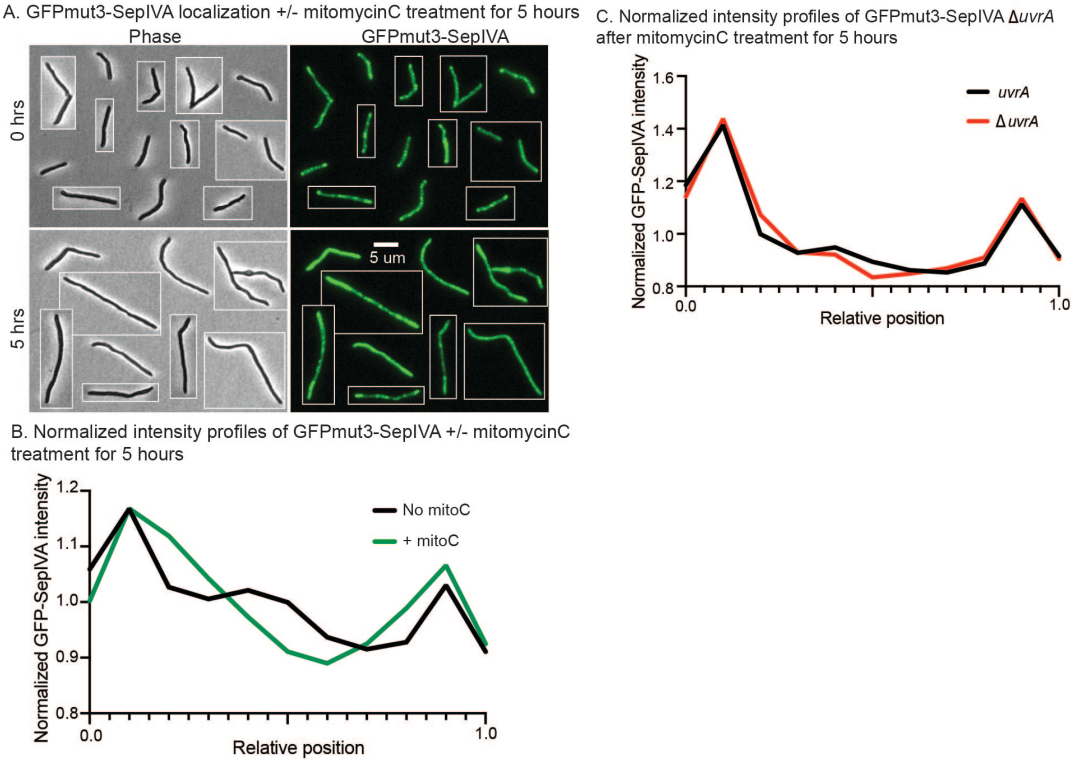

Figure 4.2. DNA damage, but not UvrA, affects septal localization of SepIVA. (4.2a) Images of *Msmeg* cells expressing L5::*GFPmut3-sepIVA* WT. Strains are merodiploid. Phase images are in the left column. Fluorescence images of GFPmut3-SepIVA are in the right column. Scale bar applies to all images. Pictures of several cells from images processed identically were pasted together. **(4.2b)** Normalized Intensity profiles of GFPmut3-SepIVA signal of WT SepIVA +/- mitomycin C treatment. MitoC was added at 50 ng/mL and incubated at 37°C for 5 hours. The solid line represents the mean intensity value across the relative position of the cell. Normalized intensity values were generated by dividing each position's intensity value by the mean intensity value. Cells were pole-sorted such that the brighter pole in the HADA channel (not shown) was set to 0 on the X axis. **(4.2c)** Normalized Intensity profiles of GFPmut3-SepIVA signal of WT SepIVA +/- *uvrA.* The solid line represents the mean intensity value across the relative position of the cell. Normalized intensity values were generated by dividing each position's intensity value by the mean intensity value. Cells were pole-sorted such that the brighter pole in the HADA channel (not shown) was set to 0 on the X axis.

4.3d Δ*uvrA* affects mean cell length after DNA damage, but not doubling time of SepIVA arginine methylation site mutants

We looked for growth defects in our SepIVA arginine methylation site mutants with and without UvrA. We then tested the same mutants after addition of mitoC. Our results showed that all mutants had a greater doubling time after induction of DNA damage, and that SepIVA arginine methylation site mutants had an even greater doubling time compared to WT SepIVA (Fig. 4.3a) However, differences in doubling time seemed to be independent of UvrA (Fig. 4.3a), meaning that strains that grew slower were likely due to mutations in SepIVA, not UvrA.

To determine if differences in growth were due to changes in elongation or division, I measured the cell length of SepIVA arginine methylation site mutants with and without *uvrA* and before and after mitoC treatment. Cultures were treated with mitoC at 25 ng/mL for 5.5-6 hours. In the presence of DNA damage, all strains were longer in length compared to untreated strains (Fig. 4.3b). This is consistent with the downregulation of septation when DNA is damaged, while elongation continues. Notably, all Δ*uvrA*, SepIVA arginine methylation mutants were longer in length after DNA damage, compared to WT SepIVA apart from the Δ*uvrA*, WT SepIVA strain (Fig. 4.3b). This suggests that UvrA and SepIVA both contribute the DNA damage response, but likely through different mechanisms of action. When WT SepIVA is present, UvrA is not needed to recover from DNA damage. However, if *sepIVA* is mutated, then cells may need to rely on other DNA damage response pathways, such as NER, involving UvrA. When SepIVA arginine methylation sites are mutated in a Δ*uvrA* background, two DNA damage response systems are impaired, supported by the additive effect on cell

lengths. If SepIVA and UvrA were working in the same pathway, knocking out *uvrA* and mutating *sepIVA* would have equal effects when DNA is damaged.

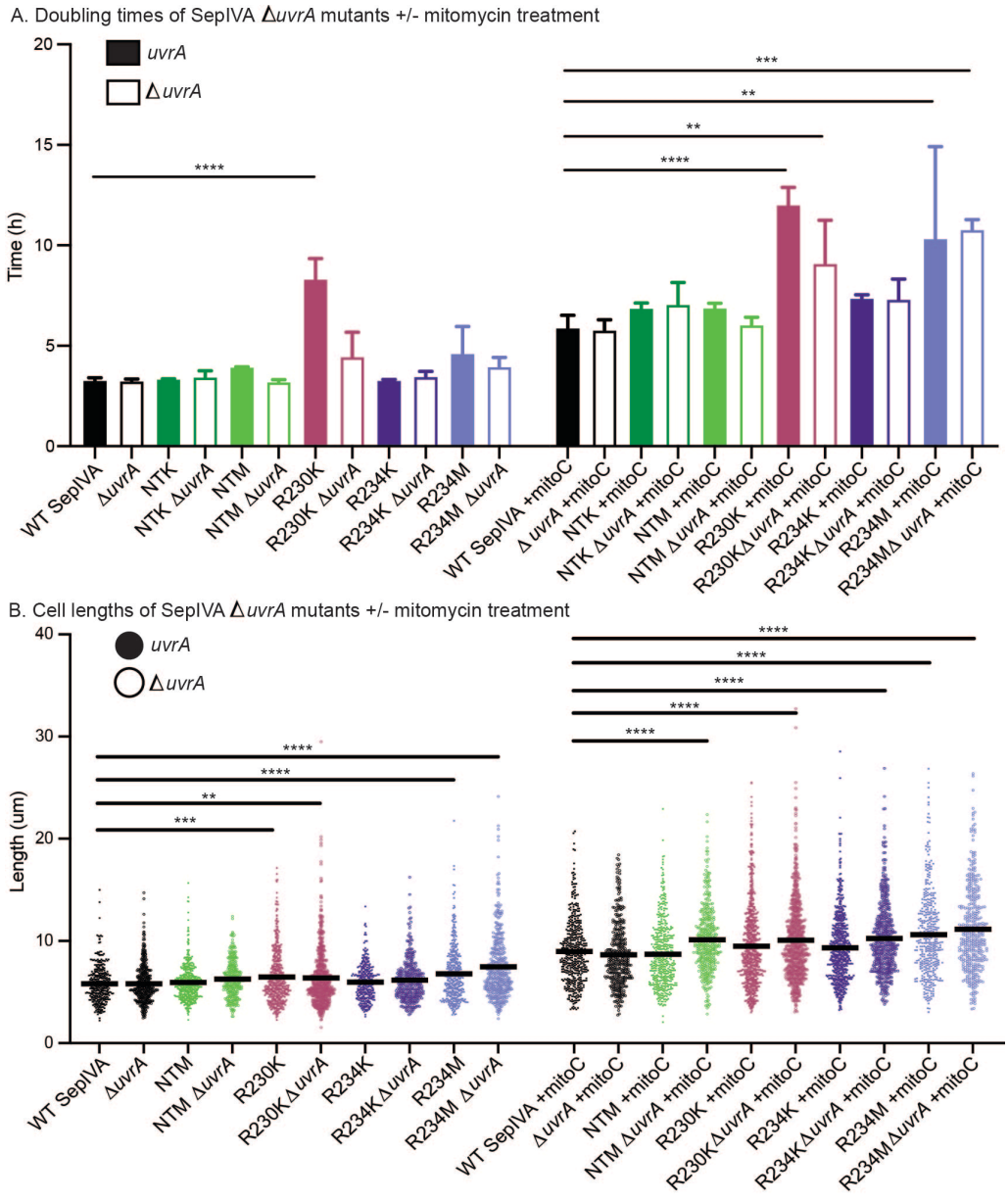

Figure 4.3 ΔuvrA and SepIVA arginine methylation site mutants affect cell length, but not doubling time in the presence of DNA damage. (4.3a) Doubling times of allele-swap *M. smeg* cells expressing *uvrA or ΔuvrA* and WT or arginine methylation site mutants of SepIVA, with and without mitomycin C treatment. MitoC was added at 25 ng/mL at t=0 of growth curve. Filled in bars represent *uvrA* strains. Outlined bars represent *ΔuvrA* strains. Left: doubling times without mitoC treatment, right: doubling times after mitoC treatment. At least 3 biological replicates of each strain were used. Error bars represent standard deviation. ****, *P = <0.0001.* WT SepIVA +mitoC vs. R230K *ΔuvrA* +mitoC*, **, P = 0.0057.* WT SepIVA +mitoC vs. R234M +mitoC, **, *P =*

0.0014. WT SepIVA +mitoC vs. R234M *ΔuvrA* +mitoC, ***, *P = 0.0004.* **(4.3b)** Cell lengths of cells expressing *uvrA or ΔuvrA* and SepIVA WT or arginine methylation site mutants. Bars represent mean. Left: length without mitoC treatment, right: lengths after mitoC treatment at 25 ng/mL for 5.5-6 hours. At least 300 cells over three biological replicates of each strain were analyzed. WT SepIVA vs. R230K, ***, *P = 0.0006,* WT SepIVA vs. *ΔuvrA* R230K, **, *P = 0.0015.* ****, *P = <0.0001.* P-values were calculated using ordinary one-way ANOVA, Dunnett's multiple comparisons test, with a single pooled variance in GraphPad Prism (v9.2).

4.3e UvrA and SepIVA have individual roles in susceptibility to DNA damage agents

To further determine if SepIVA and UvrA work together or independently to response to DNA damage, we tested the minimum inhibitory concentration (MIC) of mitoC needed to prevent growth. Our results showed that SepIVA arginine methylation site mutants only grew at mitoC concentrations considerably lower than the WT (Fig. 4.4). Furthermore, Δ*uvrA* SepIVA methylation site mutants only grew at even lower concentrations of mitoC, compared to those with *uvrA* present (Fig. 4.4).

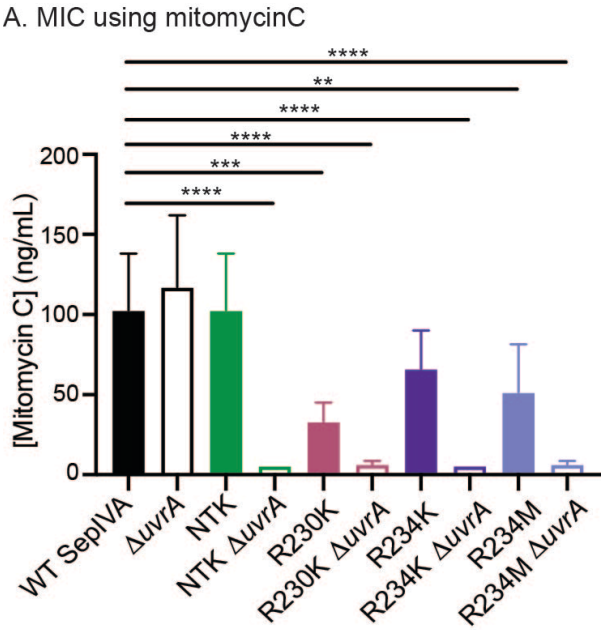

Figure 4.4 MIC of mitomycin C against Δ*uvrA* and SepIVA arginine methylation site mutants. Mean MIC of WT SepIVA = 102 ng/mL. Mean MIC of *ΔuvrA* = 117 ng/mL. Mean MIC of NTK = 102.5 ng/mL. Mean MIC of NTK *ΔuvrA* = 5.5 ng/mL. Mean MIC of R230K = 33 ng/mL. Mean MIC of R230K *ΔuvrA* = 6.4 ng/mL. Mean MIC of R234K = 66 ng/mL. Mean MIC of R234K

ΔuvrA = 5.5 ng/mL. Mean MIC of R234M = 51.3 ng/mL. Mean MIC of R234M *ΔuvrA* = 6.4 ng/mL. **, *P = 0.0062. ***, P = 0.0001. ****, P = <0.0001.* P-values were calculated using ordinary one-way ANOVA, Dunnett's multiple comparisons test, with a single pooled variance in GraphPad Prism (v9.2).

Interestingly, WT SepIVA and Δ*uvrA* strains were able to grow at relatively high concentrations of mitoC (Fig. 4.4, black bars). This suggests that even without UvrA, WT SepIVA is enough for growth to continue in DNA damage. Our results further support that SepIVA and UvrA respond to DNA damage through separate pathways, based on the additive effects seen.

4.3f N-terminus and C-terminus arginine methylation sites on SepIVA have different roles in balancing septation and elongation after DNA damage

We previously determined that arginine methylation sites near the N-terminus of SepIVA are involved in polar elongation while C-terminus methylation sites are mostly involved in septation. To determine how cell wall metabolism may be affected by DNA damage, we looked at peptidoglycan (PG) layer staining in our SepIVA arginine methylation site mutants, with and without *uvrA,* after mitomycin C treatment for 6 hours. Our results showed that after induction of DNA damage, polar PG signal was increased compared to the non-treated strains (Fig. 4.5). This suggests that while division is down regulated when DNA is damaged, elongation continues. Notably, the NT-M mutant, showed even greater polar PG signal after mitoC treatment, compared to the WT (Fig 4.5). This is contrary to what is seen in non-stress induced environments (Fig. 2.6), suggesting that N-terminus methylation sites may be needed to properly regulate PG synthesis and elongation in response to certain stressors. The NT-M Δ*uvrA* mutant had less PG intensity at the poles, after mitoC treatment, compared to the NT-M mutant (Fig. 4.5). Since UvrA is involved in detection of DNA damage, it's possible that

the Δ*uvrA* strain struggles to fully detect DNA damage and induce a response, resulting in increased polar PG signal compared to non-treated cells, but less polar PG signal than those with UvrA present.

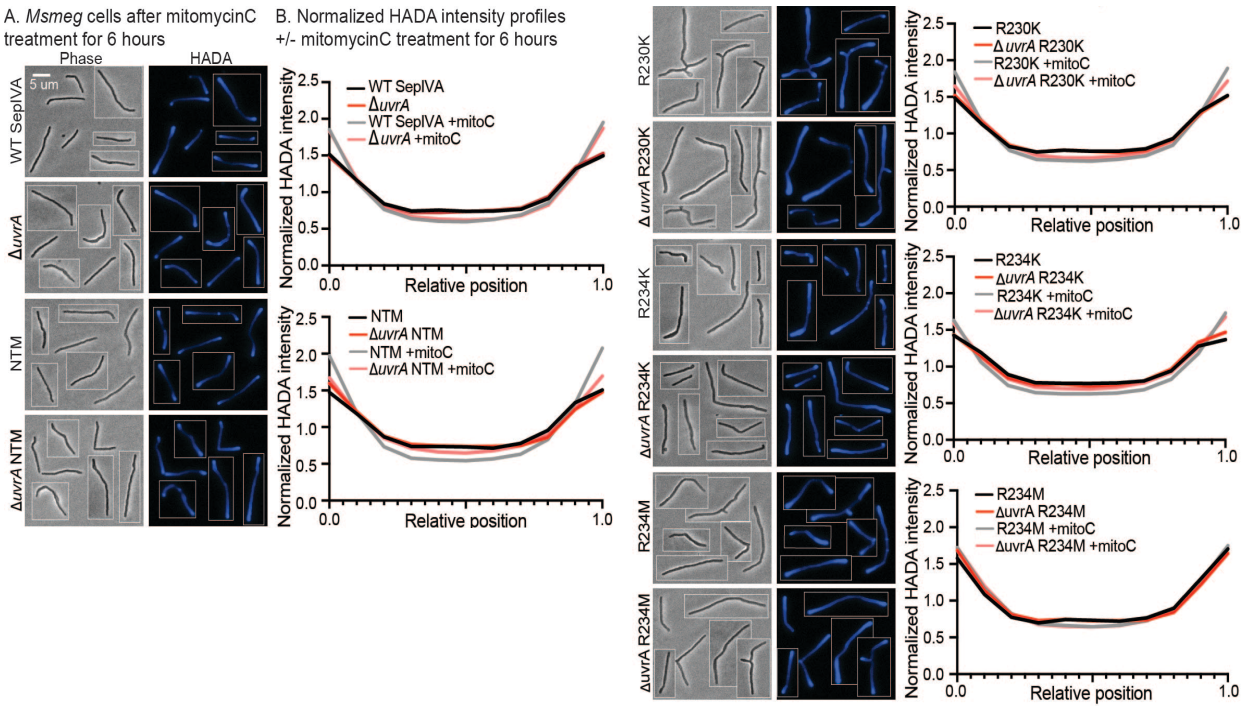

Figure 4.5 N-terminus and C-terminus arginine methylation sites on SepIVA have different roles in balancing elongation and septation in DNA damage. (4.5a) Images of M. smeg cells expressing *L5::sepIVA* WT and methylation site mutants +/- *uvrA* after mitoC treatment at 25 ng/mL for 6 hours. Scale bar applies to all images. Pictures of several cells from images processed identically were pasted together. **(4.5b)** Normalized intensity profiles of NADA signal of WT and methylation mutants +/- *uvrA* before and after mitoC treatment at 25 ng/mL for 6 hours. The solid line represents the mean intensity value across the relative position of the cell. Intensity values were normalized by dividing each strain's intensity value by its mean intensity value. Cells were pole-sorted such that the brighter pole in the HADA channel was set to 0 on the X axis.

In chapters 2 and 3, we concluded that methylation sites near SepIVA's C-terminus, R230 and R234, promote SepIVA regulation of septation. Specifically, the R230K and R234M methylation site mutants have inhibited septation in non-stressful environments (Fig. 2.12, 3.1). Interestingly, there is no differences in PG signal

distribution in the R234M mutant with and without mitoC treatment (Fig. 4.5). This suggests that R234 methylation site may have a role in down regulating septation in response to stressors, such as DNA damage. If septation is already inhibited in the R234M mutant without DNA damage, then it does not need to be additionally down regulated when DNA is damaged. This is supported by the decreased polar PG signal in the R234K mutant compared to the WT (Fig. 4.5). While the R234K mutant had similar growth phenotypes to the WT without stress (Fig. 2.12), maybe this mutation now matters in the presence of DNA damage. These findings are largely independent of *uvrA,* further supporting that SepIVA and UvrA respond to DNA damage through different pathways.

4.4 Discussion

In chapter 4, we investigated the relationship between SepIVA and DNA damage. Initially, we thought SepIVA could be regulating division in response to DNA damage through interaction with UvrA. While the two proteins could still be potential interactors, our data suggests that SepIVA and the Uvr proteins respond to DNA damage through different pathways. Our conclusion is supported by the additive effects on mitomycin C susceptibility (Fig. 4.4) and cell length (4.3b). If the two proteins were working together to respond to DNA damage, then knocking out *uvrA* and mutating arginine methylation sites on SepIVA, especially those essential to SepIVA function, would result in indistinguishable phenotypes. However, our results do support that SepIVA does regulate division in response to DNA damage.

After treatment with mitomycin C, SepIVA localization is no longer at the midcell, but more frequently at the poles (Fig. 4.2ab). Data from previous chapters (Fig. 2.12,

3.1) and Wu *et al.* 2018, suggest that SepIVA activates septation at the midcell. Our SepIVA localization after DNA damage also supports this (Figure 4.2ab), as division is down regulated and SepIVA no longer localizes to the septum.

SepIVA C-terminus methylation sites are important for SepIVA's role in cell division (Fig. 2.12, 3.1). Since R234M already has inhibited septation in stress-free environments, inhibition of septation due to DNA damage may not be observable. However, since R234M mutants are longer after treatment with mitoC (4.3b), compared to non-treated cells, this suggests that elongation is being up regulated or that there are multiple checkpoints for division that are not passed by these cells, causing division to occur even less often than non-treated R234M cells. Based on the increased cell length (4.3b) and lower MIC of mitoC of the R234K (Fig. 4.4), compared to the WT, R234 could have a specific role in SepIVA's regulation of division in response to stress. This is supported by the lack of growth defects seen in the R234K strain in stress-free environments (Fig. 2.12). While it's possible that methylation on R234 is mediating SepIVA's regulation of cell division in response to stressors, like DNA damage, more work would need to be done to confirm this hypothesis.

4.5 Methods and Materials

4.5a Bacterial strains and culture conditions.

Mycobacterium smegmatis (mc^2155) was cultured in 7H9 medium (Becton, Dickinson, Franklin Lakes, NJ) with 5 g/L bovine serum albumin (BSA), 2 g/L glucose, 0.85 g/L NaCl, 0.003 g/L catalase, 0.2% glycerol, and 0.05% Tween 80 or plated on LB agar. For *M. smeg* cultures, antibiotic concentrations were: 20 µg/mL nourseothricin, 20

μg/mL zeocin, 25 μg/mL kanamycin, and 50 μg/mL hygromycin. For *E. coli* cultures, antibiotic concentrations were: 40 μg/mL nourseothricin, 25 μg/mL zeocin, 50 μg/mL kanamycin, and 100 μg/mL hygromycin, *E. coli* TOP10 or DH5α were used for cloning.

4.5b Strain construction

Because it is essential in *M. smegmatis, sepIVA* mutants were constructed by first integrating an additional copy of *sepIVA* at the L5 integration site. After complementing *sepIVA* at the L5 site, *sepIVA* at its native locus was knocked out via recombineering (van Kessel and Hatfull, 2008; Murphy *et al.*, 2015), as previously described (Boutte *et al.*, 2016). Mutant copies of *sepIVA* replaced wildtype *sepIVA* at the L5 site via allelic exchange (Pashley and Parish, 2003; Kieser *et al.*, 2015).

Recombineering was also used to build the Δ*uvrA* strain (Murphy *et al.*, 2015). *uvrA* at its native locus was replaced with a *hygR* cassette. Unlike *sepIVA, uvrA* is non-essential, so an additional copy of *uvrA* elsewhere in the genome was not necessary.

4.5c Growth rate assay

Biological replicates of *sepIVA* arginine mutants were grown to log phase in 7H9 medium. Cultures were diluted to OD_{600} = 0.1 in 200 μL 7H9 medium in a non-treated 96-well plate. Optical density at 600 nm was measured over the next 18-24 hours using a plate reader (BioTek Synergy neo2 multi-mode reader) at 37°C, shaking continuously. Mitomycin C was added to wells of 96-well plate at 25 ng/mL at t=0 of growth curve. Population doubling times were determined using the exponential growth equation and least squares regression fitting method in GraphPad Prism (version 9.2). P values were calculated using ordinary one-way ANOVA, Dunnett's multiple comparisons test, with a single pooled variance.

4.5d Minimum inhibitory concentration determination

Three biological replicates of SepIVA WT and arginine methylation site mutants +/- *uvrA* were grown in 7H9 media from frozen stocks. Once in log phase, cultures were diluted back to OD = 0.002. Antibiotics were diluted by half between each column of wells on 96-well plate, from highest concentration on the left to lowest on the right. Two control columns were used, one with no antibiotic and one with no bacteria and highest antibiotic concentration. To each well, 100 uL of media and 100 uL of culture were added. Plates were incubated at 37°C for 48 hours, shaking continuously. To measure any metabolic activity, a 0.02% solution of Alamar Blue (resazurin) was made. 20 uL were added to each well and plates were incubated at 37°C for 24 hours, shaking continuously. After incubation, color change from blue to purple or pink were recorded as growth. The lowest concentration of antibiotic that did not permit growth was considered the MIC. P values were calculated using ordinary one-way ANOVA, Dunnett's multiple comparisons test, with a single pooled variance.

4.5e Microscopy

Cells were imaged using a Nikon Ti-2 widefield epifluorescence microscope with a Photometrics Prime 95B camera and a Plan Apo 100X, 1.45 -numerical-aperture objective. Green-fluorescent images for GFPmut3 localization were taken with a 470/40nm excitation filter and a 525/50nm emission filter. Blue-fluorescent images for HADA staining were taken with a 350/50nm excitation filter and a 460/50nm emission filter. Images were analyzed using FIJI and MicrobeJ (Ducret *et al.*, 2016). For cell detection using MicrobeJ, parameters for width and area were set. V-snapping cells

were cut at the septum so daughter cells could be detected as individual cells. Overlapping cells were excluded from analysis.

Cell lengths, mean intensities, maximum intensities, and minimum intensities of at least 250 cells per genotype were quantified using MicrobeJ. Mean intensity profiles were plotted using the “XStatProfile” plotting tool in MicrobeJ. P-values were calculated using ordinary one-way ANOVA, Dunnett’s multiple comparisons test, with a single pooled variance using GraphPad Prism (v9.2).

To induce DNA damage, cells were treated with mitomycin C at 25 ng/mL and incubated at 37°C, rolling, for 5.5 to 6 hours.

4.5f Fluorescent staining

HADA (ThermoFisher) fluorescent D-alanine amino acids was used to stain the peptidoglycan cell wall layer (Kuru *et al.*, 2012). For PG analysis, HADA stain was added to 1 mL exponentially growing cells at a final concentration of 1 ug/mL for 10 minutes at 37°C, rolling, before washing twice in Phosphate buffer saline with tween80 (PBST). Cells were fixed with 16% paraformaldehyde (PFA) and incubated at room temp for 10 minutes. Cells were washed once more in PBST and imaged. Images were analyzed in ImageJ (NIH).

4.5g Immunoprecipitation and mass spectrometry

To look for potential SepIVA interactors, 1 L cultures of SepIVA-strep strain and a WT control strain were grown up to OD = 0.8. Cells were spun down and washed x1 in 50 mL PBST + 1 mL 16% PFA. Cells were spun down again and resuspended in 50 mL PBST + 1 mL 16% PFA and let incubate at 37°C for 1.25 hrs. Cells were spun down and resuspended in 20 mL buffer W (100 mM Tris pH 8.0, 150 mM NaCl, 1 mM EDTA)

+ 200 uL PMSF. Cells were lysed by bead beating 4x 2 mins, icing for 5 mins in between. Lysates were pelleted at 15k rpm for 10 minutes in the cold rom. Supernatant was poured into 15 mL conical and incubated, rocking in the cold room with 450 uL of Streptactin beads added for 2 hrs. Beads were washed x3 with buffer W. Added 200 uL buffer BXT to beads. Vortexed and incubated at RT for 10 mins. Put on magnet and removed supt. This step was repeated and supts were combined. Added 100 uL 100% TCA (precipitates protein) to combined elutions, put in fridge overnight. Spun ppt'd protein in the cold room at 15k rpm for 15 mins. Pellet was resuspended in acetone and incubated at 27°C for 60 mins. Pellet was spun down in the cold room at 15k rpm for 15 mins. Acetone was aspirated off, making sure not to disturb the pellet. Pellet was spun down at RT for 5 seconds. Remaining acetone was aspirated off. Tubes were left open on benchtop for 25 minutes to let remaining acetone evaporate. Pellet was resuspended in 25 uL 1x Laemmli buffer. Sample was loaded into gel and run at 135 V until sample reached interface between stacking and resolving gel. Gel slice was cut into 1 cm pieces and sent to UT Southwestern Proteomics Core Facility for mass spec. Results were sorted by their abundance in the SepIVA-strep strain pulldown versus the control strain pulldown.

4.5h Survival Assay

Three biological replicates of SepIVA WT and Δ*uvrA* were grown in 7H9 media from frozen stocks. Once in log phase, cultures were diluted back to OD = 0.1. CFU/mL were measured at t = 0, 2, 4, 6 and 24 hours. CFU/mL were measured on LB plates with kanamycin.

Chapter 5: Conclusions

5.1 Preface

This chapter revisits the questions asked in this dissertation (section 1.7) and how our findings answer them. In chapter 2, we addressed SepIVA's role in regulating cell division and how post-translational modifications on SepIVA affect its functionality. We also discuss how SepIVA may be mediating the switch from division to elongation at the cell poles in chapter 2. In chapter 3, we characterize a single arginine methylation site, R230, near SepIVA's C-terminus. This arginine residue is crucial to SepIVA's function in cell division, implicating the R230K mutant as an ideal candidate to study the molecular mechanism of SepIVA. In chapter 4, we looked for potential SepIVA interactors, which suggested that SepIVA may have a role in DNA damage repair. Chapter 5 aims to summarize our conclusions and discuss additional theories about the cell division regulator, SepIVA.

5.2 SepIVA, cell division regulator

Based on our findings in chapters 2, 3 and 4, as well as previous literature (Wu *et al.*, 2018), SepIVA activates septation in mycobacteria. Cells are unable to divide when SepIVA is depleted, resulting in long, filamentous cells (Fig. 2.9). SepIVA was originally discovered as a potential FtsQ interactor (Wu *et al.*, 2018; Jain *et al.*, 2018). SepIVA could be regulating cell division through its interaction with FtsQ. However, validation of this interaction has yet to be done. To determine what step of division SepIVA is functioning in, the effects of localization of divisome factors (FtsZ, FtsEX, FtsK, FtsQLB, FtsI and FtsW) when SepIVA is depleted could be investigated. The divisome factors upstream from SepIVA should localize as expected. But factors downstream of SepIVA

should be delocalized, pinpointing which step of division SepIVA functions in. The effects of N-terminus arginine methylation on FtsZ-mRFP localization are done in chapter 2, where FtsZ appears to localize to the midcell as expected (Fig. 2.11). This data, in addition to previous literature (Wu *et al.*, 2018), suggest that SepIVA's role in cell division is not in Z-ring formation or stabilization, but downstream from FtsZ in divisome assembly. These localization experiments could answer how SepIVA is activating cell division.

5.2a SepIVA functions in both polar elongation and division

Mycobacteria elongate from their poles. Once the cell is ready to divide, it splits at the midcell, creating two new poles. These new poles must then switch growth modes from division to elongation. How this switch in growth modes is regulated is unknown. Our results suggest that SepIVA regulates both polar elongation and division (Fig. 2.2, 2.7, 2.8, 2.12, 3.1). SepIVA depletion also has a notable effect on MurG localization (Fig. 2.9). In *E. coli,* MurG associates with both elongasome and divisome factors (Mohammadi *et al.*, 2007), which is to be expected as lipid II is needed for elongation and building the new septum before division. MurG localization to the division site is dependent on FtsQ, in *E. coli* (Mohammadi *et al.*, 2007). If SepIVA's role in division has to do with its interaction with FtsQ, then depletion of SepIVA may result in delocalization of FtsQ. If FtsQ in mycobacteria is delocalized, then MurG may also be delocalized, like what is seen in *E. coli*. This could explain why we see delocalization of MurG when SepIVA is depleted.

As previously stated, MurG also interacts with elongation factors and division factors. SepIVA could also be interacting with PG synthesis activators for polar

elongation. In *E. coli,* MurG interacts with MreB, which governs where new PG is incorporated into the sidewall during elongation (Shih *et al.*, 2003; Mohammadi *et al.*, 2007; Shi *et al.*, 2018). Mycobacteria lack an MreB homolog, meaning mycobacteria have distinct machinery regulating new PG incorporation at the cell poles. SepIVA could be involved in this regulation. This is supported by our results that suggest SepIVA is involved in polar elongation and broadly regulates PG synthesis (Fig. 2.6, 2.7, 2.8).

5.3 The N-terminus of SepIVA

Our results in chapter 2 show that arginine methylation sites near the N-terminus of SepIVA are involved in polar elongation. Specifically, methyl-mimetic mutations of N-terminus methylation sites (referred to as, NT-M), has a greater doubling time (Fig. 2.2), decreased PG incorporation at the poles (Fig. 2.6) and elongates slower than the WT (Fig. 2.7). Since this strain has a similar cell length as the WT (Fig. 2.2), this suggests that cell division is still occurring once the cell has reached a given length, meaning polar elongation is inhibited in this mutant. While this data supports the N-terminus of SepIVA's broad regulation in PG synthesis, our work has yet to directly tie the molecular mechanism of SepIVA to the PG layer. There are two speculative theories I have come up with based on data already discussed and preliminary data shown here.

5.3a N-terminus of SepIVA regulates elongation in stationary phase

To cope with stationary phase stress, mycobacteria down regulate elongation but continue to divide, resulting in shorter cells (Smeulders *et al.*, 1999; Wu *et al.*, 2016). While investigating the effects of stationary phase on MurG localization (not shown), I found that N-terminus methyl-mimetic SepIVA mutants (NT-M) were longer in length

compared to the methyl-ablative (NT-K) and WT. Like our conclusion that N-terminus methylation regulates polar elongation in log phase (Fig. 2.7), the N-terminus may also down regulate of elongation in stationary phase. To further investigate this phenomenon, polar elongation of N-terminus methylation site mutants in stationary phase needs to be measured and compared to the WT.

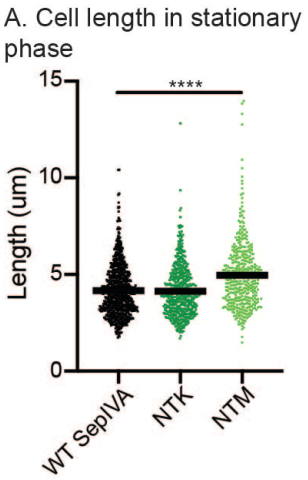

Figure 5.1 Cell lengths of SepIVA WT or N-terminus arginine methylation site mutants. Bars represent mean. At least 300 cells over three biological replicates of each strain were analyzed. *****, P = <0.0001.* P-values were calculated using ordinary one-way ANOVA, Dunnett's multiple comparisons test, with a single pooled variance in GraphPad Prism (v9.2).

5.3b SepIVA interacts with itself through N-terminus residues

The N-terminus of SepIVA is interesting because mutating three arginine residues near the N-terminus does not cause all SepIVA function to be lost. While studying the SepIVA protein, I utilized the protein structure prediction tool, AlphaFold, to predict tertiary structures of SepIVA as a monomer (Fig. 2.1), a dimer, and a trimer (Jumper *et al.*, 2021). I used ChimeraX to visualize these predictions (Pettersen *et al.*, 2021). According to AlphaFold, SepIVA may function as a dimer (Fig. 5.2). When I ran SepIVA as a dimer through AlphaFold, all predicted models showed SepIVA to interact with itself (Fig. 5.2a). However, when I ran SepIVA as a trimer through AlphaFold,

predicted models showed a SepIVA-SepIVA dimer and a non-interacting third SepIVA protein (Fig. 5.2b).

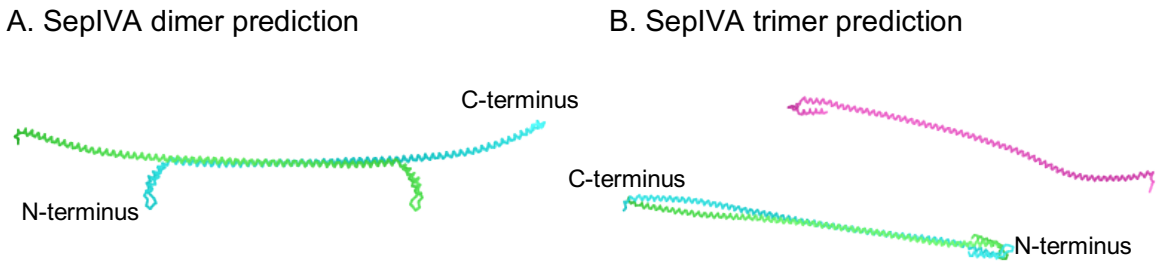

Figure 5.2. Predicted SepIVA structures. Tertiary structure of SepIVA protein as predicted by AlphaFold and visualized using UCSF ChimeraX. Models shown are the highest-ranking models out of 5. **(5.2a)** Tertiary structure of SepIVA-SepIVA dimer as predicted by Alphafold. **(5.2b)** Tertiary structure of SepIVA-SepIVA-SepIVA trimer as predicted by Alphafold.

Because N-terminus mutations do not render SepIVA fully non-functional, it is possible, although speculative, that SepIVA is interacting with itself via its N-terminus. In eukaryotes, protein arginine methylation promotes protein-protein interactions (Fig. 1.4) in response to certain stressors, like DNA damage (Auclair and Richard, 2013). Arginine methylation at the N-terminus of SepIVA could be promoting its interaction with itself. N-terminus methylation site mutants would have a harder time regulating SepIVA self-interaction. This could inhibit some of SepIVA's functions without rendering the entire protein useless. It's possible that SepIVA dimerization promotes its function in polar elongation or PG synthesis. A lot of work, including verifying that SepIVA acts as a dimer, would need to be done to investigate this theory.

5.4 The C-terminus of SepIVA

In response to Pickford *et al.*, 2020, I constructed a *sepIVA* C-terminus truncation mutant, removing the last 90 amino acids from SepIVA. I constructed this mutant using the allelic exchange system at the L5 site and was able to grow colonies on LB agar plates. However, only about half of these colonies grew in liquid culture and grew at highly variable rates, likely due to suppressor mutations (Fig. 2.4). This told me that the C-terminus of *sepIVA* is not only essential for SepIVA function, but for cell viability. Suppressor mutation screening of these strains could identify other proteins with similar functions to SepIVA, helping to pinpoint the molecular mechanism of SepIVA.

Arginine methylation sites near the C-terminus of SepIVA have opposing roles from those near the N-terminus of SepIVA. Depletion of SepIVA results in long, filamentous cells that are unable to divide, suggesting that SepIVA is an activator of septation (Wu *et al.*, 2018). Mutations of both the R230 and R234 methylation sites result in similar phenotypes to SepIVA depletion (Fig. 2.12, 3.1). Our characterization of these two arginine methylation sites on SepIVA in chapters 2, 3 and 4 led us to conclude that the C-terminus of SepIVA is key to SepIVA's regulation of cell division.

5.4a R230 is needed for SepIVA's function in cell division

In chapter 3, we thoroughly characterize R230 on SepIVA. We conclude that this arginine is important for SepIVA's function in cell division. However, we still do not know how this residue contributes to the molecular mechanism of SepIVA. We know that the SepIVA is still stable when R230 is mutated to R230K or R230M (Fig. 2.2f), meaning that the effects of this mutation are not simply destabilizing SepIVA. However, these mutations could still cause a conformation change of SepIVA. This conformational

change could block interaction or active sites on SepIVA. Both methyl-ablative and methyl-mimetic mutations of R230 have similar phenotypes, suggesting that arginine methylation at this site is not important for SepIVA function, but rather the arginine residue itself. R230 mutants are great candidates to study SepIVA function, since *sepIVA* is an essential gene and R230 mutants remain viable. While out of the scope of this dissertation, protein crystallography of SepIVA and R230 mutants would determine if loss of SepIVA function is due to conformational changes. Performing immunoprecipitations and mass spectrometry of R230 mutants and WT SepIVA could determine if R230 is mediating any SepIVA interactions.

5.4b Methylation of R234 near SepIVA's C-terminus regulates division

When characterizing arginine methylation sites on SepIVA, many individual methylation site mutations showed little to no changes in phenotype compared to the WT (Fig. 2.2de, 2.8). One arginine methylation site, R234, acted like the WT when mutated to the methyl-ablative (R234K), but showed significant growth defects when mutated to the methyl-mimetic (R234M). Since studying protein arginine methylation in prokaryotes is relatively new, these results gave us confidence that our methyl-ablative (R->K) and methyl-mimetic (R->M) mutants were a great model to study the effects of arginine methylation.

Based on our findings about R234 in chapters 2 and 4, we concluded that arginine methylation on R234 inhibits cell division (Fig 2.2de, 2.12, 4.1). In stress free environments, there is no reason to inhibit cell division, so, presumably, R234 remains un-methylated. However, in response to stress, such as DNA damage, R234 may be methylated to signal to SepIVA to inhibit cell division. This theory is supported by the

lack of growth defects seen with the R234K mutant in stress free environments. But when DNA damage occurs and division needs to be down regulated, R234K is unable to be methylated, resulting in growth defects like increased cell length (Fig. 4.3b) and increased susceptibility to mitomycin C (Fig. 4.4). In other types of stress, such as stationary phase stress, division is not inhibited like in DNA damage stress. To test whether methylation on R234 of SepIVA inhibits division due to certain stressors, cell length and polar elongation of R234K and R234M in stationary phase could be measured. We expect cells to down regulate elongation, but not division, in stationary phase. If R234M cells are not elongating but have increased length compared to the R234K and WT, this implies that methylation on R234 is inhibiting division in response to specific stressors.

5.5 SepIVA and UvrA work independently to respond to DNA damage

In chapter 4, we characterized the role of SepIVA and its potential interactor, UvrA, in the DNA damage response. Since *uvrA* is a non-essential gene, I constructed a Δ*uvrA* strain and used the allelic exchange system to swap in arginine methylation site mutant versions of *sepIVA,* at the L5 site. To investigate how these mutants tolerated DNA damage, I looked for growth defects after treating them with the DNA damage agent, mitomycin C. Our results, particularly figure 4.4, showed additive growth defects when SepIVA arginine methylation sites were mutated in a Δ*uvrA* background. In short, by hindering both SepIVA and UvrA pathways, growth defects were greater than when just one pathway was hindered. This suggests that SepIVA and UvrA respond to DNA damage individually, versus together. If the two contributed to the same DNA damage

response pathway, growth defects would be the same whether UvrA or SepIVA was rendered useless.

SepIVA's re-localization away from the midcell after DNA damage supports our conclusion that SepIVA is activating division (Fig. 4.2). One of our original hypotheses about the relationship between UvrA and SepIVA was that upon detection of DNA damage, UvrA disassociates with UvrB and interacts with SepIVA, signaling the protein to inhibit division. While UvrA is clearly not fulfilling this role, another DNA damage repair protein could be. It's possible that this other DNA repair protein is interacting with the protein arginine methyltransferase (PRMT) that methylates SepIVA. Perhaps, when this DNA repair protein interacts with SepIVA's PRMT, R234 is methylated, causing SepIVA to re-localize and not activate division. While localization of SepIVA was investigated in figures 2.5 and 4.2, how R234K and R234M mutations affect SepIVA localization has yet to be investigated. Finding the PRMT that methylates SepIVA, as well as when in the cell cycle SepIVA is methylated, would really help to understand the role of methylation on SepIVA, in addition to its overall function.

Literature cited

Addinall, S.G., Cao, C., and Lutkenhaus, J. (1997) FtsN, a late recruit to the septum in Escherichia coli. *Molecular Microbiology* **25**: 303–309.

Alderwick, L.J., Harrison, J., Lloyd, G.S., and Birch, H.L. (2015) The Mycobacterial Cell Wall—Peptidoglycan and Arabinogalactan. *Cold Spring Harb Perspect Med* **5** https://www.ncbi.nlm.nih.gov/pmc/articles/PMC4526729/. Accessed May 5, 2020.

Aldridge, B.B., Fernandez-Suarez, M., Heller, D., Ambravaneswaran, V., Irimia, D., Toner, M., and Fortune, S.M. (2012) Asymmetry and Aging of Mycobacterial Cells Lead to Variable Growth and Antibiotic Susceptibility. *Science* **335**: 100–104.

Attaibi, M., and Blaauwen, T. den (2022) An Updated Model of the Divisome: Regulation of the Septal Peptidoglycan Synthesis Machinery by the Divisome. *Int J Mol Sci* **23**: 3537.

Auclair, Y., and Richard, S. (2013) The role of arginine methylation in the DNA damage response. *DNA Repair (Amst)* **12**: 459–465.

Baranowski, C., Rego, E.H., and Rubin, E.J. (2019) The Dream of a Mycobacterium. *Microbiology Spectrum* **7** http://www.asmscience.org/content/journal/microbiolspec/10.1128/microbiolspec.GPP3-0008-2018. Accessed April 29, 2019.

Baranowski, C., Welsh, M.A., Sham, L.-T., Eskandarian, H.A., Lim, H.C., Kieser, K.J., *et al.* (2018) Maturing Mycobacterium smegmatis peptidoglycan requires non-canonical crosslinks to maintain shape. *eLife* **7**: e37516.

Baum, E.Z., Montenegro, D.A., Licata, L., Turchi, I., Webb, G.C., Foleno, B.D., and Bush, K. (2001) Identification and Characterization of New Inhibitors of the Escherichia coli MurA Enzyme. *Antimicrob Agents Chemother* **45**: 3182–3188.

Benson, T.E., Walsh, C.T., and Hogle, J.M. (1996) The structure of the substrate-free form of MurB, an essential enzyme for the synthesis of bacterial cell walls. *Structure* **4**: 47–54.

Bernhardt, T.G., and Boer, P.A.J. de (2005) SlmA, a Nucleoid-Associated, FtsZ Binding Protein Required for Blocking Septal Ring Assembly over Chromosomes in E. coli. *Molecular Cell* **18**: 555–564.

Biggar, K.K., and Li, S.S.-C. (2015) Non-histone protein methylation as a regulator of cellular signalling and function. *Nat Rev Mol Cell Biol* **16**: 5–17.

Boer, P.A. de, Crossley, R.E., Hand, A.R., and Rothfield, L.I. (1991) The MinD protein is a membrane ATPase required for the correct placement of the Escherichia coli division site. *EMBO J* **10**: 4371–4380.

Boer, P.A.J. de, Crossley, R.E., and Rothfield, L.I. (1989) A division inhibitor and a topological specificity factor coded for by the minicell locus determine proper placement of the division septum in E. coli. *Cell* **56**: 641–649.

Boes, A., Kerff, F., Herman, R., Touze, T., Breukink, E., and Terrak, M. (2020) The bacterial cell division protein fragment EFtsN binds to and activates the major peptidoglycan synthase PBP1b. *Journal of Biological Chemistry* **295**: 18256–18265.

Boes, A., Olatunji, S., Breukink, E., and Terrak, M. (2019) Regulation of the Peptidoglycan Polymerase Activity of PBP1b by Antagonist Actions of the Core Divisome Proteins FtsBLQ and FtsN. *mBio* **10** http://mbio.asm.org/lookup/doi/10.1128/mBio.01912-18. Accessed February 6, 2019.

Born, P., Breukink, E., and Vollmer, W. (2006) In Vitro Synthesis of Cross-linked Murein and Its Attachment to Sacculi by PBP1A from Escherichia coli. *Journal of Biological Chemistry* **281**: 26985–26993.

Boutte, C.C., Baer, C.E., Papavinasasundaram, K., Liu, W., Chase, M.R., Meniche, X., *et al.* (2016) A cytoplasmic peptidoglycan amidase homologue controls mycobacterial cell wall synthesis. *eLife* **5**: e14590.

Boyle, D.S., and Donachie, W.D. (1998) mraY Is an Essential Gene for Cell Growth in Escherichia coli. *J Bacteriol* **180**: 6429–6432.

Brown, P.J.B., Pedro, M.A. de, Kysela, D.T., Van der Henst, C., Kim, J., De Bolle, X., *et al.* (2012) Polar growth in the Alphaproteobacterial order Rhizobiales. *Proceedings of the National Academy of Sciences* **109**: 1697–1701.

Burby, P.E., and Simmons, L.A. (2019) Regulation of Cell Division in Bacteria by Monitoring Genome Integrity and DNA Replication Status. *J Bacteriol* **202**: e00408-19, /jb/202/2/JB.00408-19.atom.

Cabré, E.J., Monterroso, B., Alfonso, C., Sánchez-Gorostiaga, A., Reija, B., Jiménez, M., *et al.* (2015) The Nucleoid Occlusion SlmA Protein Accelerates the Disassembly of the FtsZ Protein Polymers without Affecting Their GTPase Activity. *PLoS One* **10** https://www.ncbi.nlm.nih.gov/pmc/articles/PMC4423959/. Accessed April 29, 2020.

Cameron, T.A., Zupan, J.R., and Zambryski, P.C. (2015) The essential features and modes of bacterial polar growth. *Trends in Microbiology* **23**: 347–353.

Cha, J.H., and Stewart, G.C. (1997) The divIVA minicell locus of Bacillus subtilis. *J Bacteriol* **179**: 1671–1683.

Cho, H., McManus, H.R., Dove, S.L., and Bernhardt, T.G. (2011) Nucleoid occlusion factor SlmA is a DNA-activated FtsZ polymerization antagonist. *Proceedings of the National Academy of Sciences* **108**: 3773–3778.

Cho, H., Wivagg, C.N., Kapoor, M., Barry, Z., Rohs, P.D.A., Suh, H., *et al.* (2016) Bacterial cell wall biogenesis is mediated by SEDS and PBP polymerase families functioning semi-autonomously. *Nat Microbiol* **1**: 16172.

Chodisetti, P.K., and Reddy, M. (2019) Peptidoglycan hydrolase of an unusual cross-link cleavage specificity contributes to bacterial cell wall synthesis. *Proc Natl Acad Sci USA* **116**: 7825–7830.

Cleverley, R.M., Rutter, Z.J., Rismondo, J., Corona, F., Tsui, H.-C.T., Alatawi, F.A., *et al.* (2019) The cell cycle regulator GpsB functions as cytosolic adaptor for multiple cell wall enzymes. *Nat Commun* **10**: 261.

Contreras-Martel, C., Martins, A., Ecobichon, C., Trindade, D.M., Matteï, P.-J., Hicham, S., *et al.* (2017) Molecular architecture of the PBP2–MreC core bacterial cell wall synthesis complex. *Nat Commun* **8**: 776.

Corbin, B.D., Wang, Y., Beuria, T.K., and Margolin, W. (2007) Interaction between cell division proteins FtsE and FtsZ. *J Bacteriol* **189**: 3026–3035.

Costello, A., Lao, N.T., Gallagher, C., Capella Roca, B., Julius, L.A.N., Suda, S., *et al.* (2019) Leaky Expression of the TET-On System Hinders Control of Endogenous miRNA Abundance. *Biotechnol J* **14**: 1800219.

Dajkovic, A., Lan, G., Sun, S.X., Wirtz, D., and Lutkenhaus, J. (2008) MinC Spatially Controls Bacterial Cytokinesis by Antagonizing the Scaffolding Function of FtsZ. *Current Biology* **18**: 235–244.

Datta, P., Dasgupta, A., Singh, A.K., Mukherjee, P., Kundu, M., and Basu, J. (2006) Interaction between FtsW and penicillin-binding protein 3 (PBP3) directs PBP3 to mid-cell, controls cell septation and mediates the formation of a trimeric complex involving FtsZ, FtsW and PBP3 in mycobacteria. *Molecular Microbiology* **62**: 1655–1673.

DeJesus, M.A., Gerrick, E.R., Xu, W., Park, S.W., Long, J.E., Boutte, C.C., *et al.* (2017) Comprehensive Essentiality Analysis of the *Mycobacterium tuberculosis* Genome via Saturating Transposon Mutagenesis. *mBio* **8** http://mbio.asm.org/lookup/doi/10.1128/mBio.02133-16. Accessed February 6, 2019.

Dietrich, C., Li de la Sierra-Gallay, I., Masi, M., Girard, E., Dautin, N., Constantinesco-Becker, F., *et al.* (2020) The C-terminal domain of Corynebacterium glutamicum mycoloyltransferase A is composed of five repeated motifs involved in cell wall binding and stability. *Molecular Microbiology* **114**: 1–16.

Dragset, M.S., Ioerger, T.R., Zhang, Y.J., Mærk, M., Ginbot, Z., Sacchettini, J.C., *et al.* (2019) Genome-wide Phenotypic Profiling Identifies and Categorizes Genes Required for Mycobacterial Low Iron Fitness. *Sci Rep* **9**: 11394.

Du, S., Henke, W., Pichoff, S., and Lutkenhaus, J. (2019) How FtsEX localizes to the Z ring and interacts with FtsA to regulate cell division. *Mol Microbiol* **112**: 881–895.

Ducret, A., Quardokus, E.M., and Brun, Y.V. (2016) MicrobeJ, a tool for high throughput bacterial cell detection and quantitative analysis. *Nature Microbiology* **1**: 16077.

Edwards, D.H., and Errington, J. (1997) The Bacillus subtilis DivIVA protein targets to the division septum and controls the site specificity of cell division. *Molecular Microbiology* **24**: 905–915.

Egan, A.J.F., Errington, J., and Vollmer, W. (2020) Regulation of peptidoglycan synthesis and remodelling. *Nat Rev Microbiol* **18**: 446–460.

Egan, A.J.F., Jean, N.L., Koumoutsi, A., Bougault, C.M., Biboy, J., Sassine, J., *et al.* (2014) Outer-membrane lipoprotein LpoB spans the periplasm to stimulate the peptidoglycan synthase PBP1B. *Proc Natl Acad Sci U S A* **111**: 8197–8202.

El Zoeiby, A., Sanschagrin, F., and Levesque, R.C. (2003) Structure and function of the Mur enzymes: development of novel inhibitors. *Molecular Microbiology* **47**: 1–12.

Eswara, P.J., Brzozowski, R.S., Viola, M.G., Graham, G., Spanoudis, C., Trebino, C., *et al.* (2018) An essential Staphylococcus aureus cell division protein directly regulates FtsZ dynamics. *eLife* **7** https://elifesciences.org/articles/38856. Accessed February 6, 2019.

Eswaramoorthy, P., Winter, P.W., Wawrzusin, P., York, A.G., Shroff, H., and Ramamurthi, K.S. (2014) Asymmetric Division and Differential Gene Expression during a Bacterial Developmental Program Requires DivIVA. *PLoS Genet* **10**: e1004526.

Flores, A.R., Parsons, L.M., and Pavelka, M.S. (2005) Characterization of Novel Mycobacterium tuberculosis and Mycobacterium smegmatis Mutants Hypersusceptible to -Lactam Antibiotics. *Journal of Bacteriology* **187**: 1892–1900.

Fu, G., Huang, T., Buss, J., Coltharp, C., Hensel, Z., and Xiao, J. (2010) In Vivo Structure of the E. coli FtsZ-ring Revealed by Photoactivated Localization Microscopy (PALM). *PLOS ONE* **5**: e12680.

Garces, A., Atmakuri, K., Chase, M.R., Woodworth, J.S., Krastins, B., Rothchild, A.C., *et al.* (2010) EspA Acts as a Critical Mediator of ESX1-Dependent Virulence in Mycobacterium tuberculosis by Affecting Bacterial Cell Wall Integrity. *PLOS Pathogens* **6**: e1000957.

García-Heredia, A., Kado, T., Sein, C.E., Puffal, J., Osman, S.H., Judd, J., *et al.* (2021) Membrane-partitioned cell wall synthesis in mycobacteria. *eLife* **10**: e60263.

García-Heredia, A., Pohane, A.A., Melzer, E.S., Carr, C.R., Fiolek, T.J., Rundell, S.R., *et al.* (2018) Peptidoglycan precursor synthesis along the sidewall of pole-growing mycobacteria. *eLife* **7** https://www.ncbi.nlm.nih.gov/pmc/articles/PMC6191288/. Accessed May 23, 2019.

Garde, S., Chodisetti, P.K., and Reddy, M. (2021) Peptidoglycan: Structure, Synthesis, and Regulation. *EcoSal Plus* **9** https://www.asmscience.org/content/journal/ecosalplus/10.1128/ecosalplus.ESP-0010-2020. Accessed January 26, 2021.

Gee, C.L., Papavinasasundaram, K.G., Blair, S.R., Baer, C.E., Falick, A.M., King, D.S., *et al.* (2012) A Phosphorylated Pseudokinase Complex Controls Cell Wall Synthesis in Mycobacteria. *Sci Signal* **5**: ra7–ra7.

Gegnas, L.D., Waddell, S.T., Chabin, R.M., Reddy, S., and Wong, K.K. (1998) Inhibitors of the bacterial cell wall biosynthesis enzyme Mur D. *Bioorganic & Medicinal Chemistry Letters* **8**: 1643–1648.

Geissler, B., Elraheb, D., and Margolin, W. (2003) A gain-of-function mutation in ftsA bypasses the requirement for the essential cell division gene zipA in Escherichia coli. *Proc Natl Acad Sci U S A* **100**: 4197–4202.

Gerding, M.A., Ogata, Y., Pecora, N.D., Niki, H., and Boer, P.A.J.D. (2007) The trans-envelope Tol–Pal complex is part of the cell division machinery and required for proper outer-membrane invagination during cell constriction in E. coli. *Molecular Microbiology* **63**: 1008–1025.

Goehring, N.W., Gueiros-Filho, F., and Beckwith, J. (2005) Premature targeting of a cell division protein to midcell allows dissection of divisome assembly in Escherichia coli. *Genes Dev* **19**: 127–137.

Gola, S., Munder, T., Casonato, S., Manganelli, R., and Vicente, M. (2015) The essential role of SepF in mycobacterial division: Essential role of SepF in mycobacterial division. *Molecular Microbiology* **97**: 560–576.

Habibi Arejan, N., Ensinck, D., Diacovich, L., Patel, P.B., Quintanilla, S.Y., Emami Saleh, A., *et al.* (2023) Polar protein Wag31 both activates and inhibits cell wall metabolism at the poles and septum. *Front Microbiol* **13**: 1085918.

Halbedel, S., and Lewis, R.J. (2019) Structural basis for interaction of DivIVA/GpsB proteins with their ligands. *Molecular Microbiology* **111**: 1404–1415.

Hale, C.A., and Boer, P.A.J. de (1997) Direct Binding of FtsZ to ZipA, an Essential Component of the Septal Ring Structure That Mediates Cell Division in E. coli. *Cell* **88**: 175–185.

Hale, C.A., and Boer, P.A.J. de (2002) ZipA Is Required for Recruitment of FtsK, FtsQ, FtsL, and FtsN to the Septal Ring in *Escherichia coli*. *J Bacteriol* **184**: 2552–2556.

Hale, C.A., Meinhardt, H., and Boer, P.A.J. de (2001) Dynamic localization cycle of the cell division regulator MinE in Escherichia coli. *EMBO J* **20**: 1563–1572.

Hale, C.A., Rhee, A.C., and Boer, P.A.J. de (2000) ZipA-Induced Bundling of FtsZ Polymers Mediated by an Interaction between C-Terminal Domains. *J Bacteriol* **182**: 5153–5166.

Hammond, L.R., Khan, S.J., Sacco, M.D., Spanoudis, C., Hough, A., Chen, Y., and Eswara, P.J. (2021) GpsB coordinates cell division and cell surface decoration by wall teichoic acids in *Staphylococcus aureus*. Microbiology, . http://biorxiv.org/lookup/doi/10.1101/2021.09.29.462461. Accessed October 4, 2021.

Hammond, L.R., Sacco, M.D., Khan, S.J., Spanoudis, C., Hough-Neidig, A., Chen, Y., and Eswara, P.J. (2022) GpsB Coordinates Cell Division and Cell Surface Decoration by Wall Teichoic Acids in Staphylococcus aureus. *Microbiol Spectr* **10**: e01413-22.

Hammond, L.R., White, M.L., and Eswara, P.J. (2019) ¡vIVA la DivIVA! *J Bacteriol* JB.00245-19, jb;JB.00245-19v1.

Hansen, F.G., and Atlung, T. (2018) The DnaA Tale. *Front Microbiol* **9** https://www.ncbi.nlm.nih.gov/pmc/articles/PMC5835720/. Accessed April 29, 2020.

Hayashi, J.M., Luo, C.-Y., Mayfield, J.A., Hsu, T., Fukuda, T., Walfield, A.L., *et al.* (2016) Spatially distinct and metabolically active membrane domain in mycobacteria. *PNAS* **113**: 5400–5405.

Hayashi, J.M., Richardson, K., Melzer, E.S., Sandler, S.J., Aldridge, B.B., Siegrist, M.S., and Morita, Y.S. (2018) Stress-Induced Reorganization of the Mycobacterial Membrane Domain. *mBio* **9** http://mbio.asm.org/lookup/doi/10.1128/mBio.01823-17. Accessed February 6, 2019.

Heijenoort, J. v. (2001) Formation of the glycan chains in the synthesis of bacterial peptidoglycan. *Glycobiology* **11**: 25R-36R.

Hempel, A.M., Wang, S. -b., Letek, M., Gil, J.A., and Flardh, K. (2008) Assemblies of DivIVA Mark Sites for Hyphal Branching and Can Establish New Zones of Cell Wall Growth in Streptomyces coelicolor. *Journal of Bacteriology* **190**: 7579–7583.

Hett, E.C., and Rubin, E.J. (2008) Bacterial Growth and Cell Division: a Mycobacterial Perspective. *Microbiology and Molecular Biology Reviews* **72**: 126–156.

Hinkle, D.C., Mangel, W.F., and Chamberlin, M.J. (1972) Studies of the binding of Escherichia coli RNA polymerase to DNA: IV. The effect of rifampicin on binding and on RNA chain initiation. *Journal of Molecular Biology* **70**: 209–220.

Hu, J., Selby, C.P., Adar, S., Adebali, O., and Sancar, A. (2017) Molecular mechanisms and genomic maps of DNA excision repair in Escherichia coli and humans. *J Biol Chem* **292**: 15588–15597.

Hu, Z., Mukherjee, A., Pichoff, S., and Lutkenhaus, J. (1999) The MinC component of the division site selection system in *Escherichia coli* interacts with FtsZ to prevent polymerization. *Proc Natl Acad Sci USA* **96**: 14819–14824.

Hu, Z., Saez, C., and Lutkenhaus, J. (2003) Recruitment of MinC, an Inhibitor of Z-Ring Formation, to the Membrane in Escherichia coli: Role of MinD and MinE. *J Bacteriol* **185**: 196–203.

Huang, H.-H., Seeger, C., Helena Danielson, U., and Lindblad, P. (2015) Analysis of the leakage of gene repression by an artificial TetR-regulated promoter in cyanobacteria. *BMC Res Notes* **8**: 459.

Husain, I., Van Houten, B., Thomas, D.C., Abdel-Monem, M., and Sancar, A. (1985) Effect of DNA polymerase I and DNA helicase II on the turnover rate of UvrABC excision nuclease. *Proc Natl Acad Sci U S A* **82**: 6774–6778.

Ikeda, M., Wachi, M., Jung, H.K., Ishino, F., and Matsuhashi, M. (1991) The Escherichia coli mraY gene encoding UDP-N-acetylmuramoyl-pentapeptide: undecaprenyl-phosphate phospho-N-acetylmuramoyl-pentapeptide transferase. *J Bacteriol* **173**: 1021–1026.

Iswahyudi, Mukamolova, G.V., Straatman-Iwanowska, A.A., Allcock, N., Ajuh, P., Turapov, O., and O'Hare, H.M. (2019) Mycobacterial phosphatase PstP regulates global serine threonine phosphorylation and cell division. *Sci Rep* **9**: 8337.

Iyer, V.N., and Szybalski, W. (1963) A molecular mechanism of mitomycin action: linking of complementary dna strands*†. *Proceedings of the National Academy of Sciences* **50**: 355–362.

Jain, P., Malakar, B., Khan, M.Z., Lochab, S., Singh, A., and Nandicoori, V.K. (2018) Delineating FtsQ-mediated regulation of cell division in *Mycobacterium tuberculosis*. *Journal of Biological Chemistry* **293**: 12331–12349.

Jani, C., Eoh, H., Lee, J., Hamasha, K., Sahana, M., Han, J.-S., *et al.* (2010) Regulation of Polar Peptidoglycan Biosynthesis by Wag31 Phosphorylation in Mycobacteria. *BMC Microbiol* **10**: 327.

Jankute, M., Cox, J.A.G., Harrison, J., and Besra, G.S. (2015) Assembly of the Mycobacterial Cell Wall. *Annual Review of Microbiology* **69**: 405–423.

Jean, N.L., Bougault, C.M., Lodge, A., Derouaux, A., Callens, G., Egan, A.J.F., *et al.* (2014) Elongated Structure of the Outer-Membrane Activator of Peptidoglycan Synthesis LpoA: Implications for PBP1A Stimulation. *Structure* **22**: 1047–1054.

Jumper, J., Evans, R., Pritzel, A., Green, T., Figurnov, M., Ronneberger, O., *et al.* (2021) Highly accurate protein structure prediction with AlphaFold. *Nature* http://www.nature.com/articles/s41586-021-03819-2. Accessed August 2, 2021.

Kang, C.-M. (2005) The Mycobacterium tuberculosis serine/threonine kinases PknA and PknB: substrate identification and regulation of cell shape. *Genes & Development* **19**: 1692–1704.

Kang, C.-M., Nyayapathy, S., Lee, J.-Y., Suh, J.-W., and Husson, R.N. (2008) Wag31, a homologue of the cell division protein DivIVA, regulates growth, morphology and polar cell wall synthesis in mycobacteria. *Microbiology* **154**: 725–735.

Katayama, T., Kasho, K., and Kawakami, H. (2017) The DnaA Cycle in Escherichia coli: Activation, Function and Inactivation of the Initiator Protein. *Front Microbiol* **8** https://www.ncbi.nlm.nih.gov/pmc/articles/PMC5742627/. Accessed April 29, 2020.

Kato, J., Suzuki, H., and Hirota, Y. (1985) Dispensability of either penicillin-binding protein-la or-lb involved in the essential process for cell elongation in Escherichia coil. .

Kessel, J.C. van, and Hatfull, G.F. (2008) Mycobacterial Recombineering. *Methods in Molecular Biology (Clifton, NJ)* **435**: 203–215.

Kieser, K.J., Boutte, C.C., Kester, J.C., Baer, C.E., Barczak, A.K., Meniche, X., *et al.* (2015) Phosphorylation of the Peptidoglycan Synthase PonA1 Governs the Rate of Polar Elongation in Mycobacteria. *PLOS Pathogens* **11**: e1005010.

Kieser, K.J., and Rubin, E.J. (2014) How sisters grow apart: mycobacterial growth and division. *Nat Rev Microbiol* **12**: 550–562.

Kim, J.-H., Wei, J.-R., Wallach, J.B., Robbins, R.S., Rubin, E.J., and Schnappinger, D. (2011) Protein inactivation in mycobacteria by controlled proteolysis and its application to deplete the beta subunit of RNA polymerase. *Nucleic Acids Res* **39**: 2210–2220.

Kleckner, N.E., Chatzi, K., White, M.A., Fisher, J.K., and Stouf, M. (2018) Coordination of Growth, Chromosome Replication/Segregation, and Cell Division in E. coli. *Front Microbiol* **9** https://www.frontiersin.org/articles/10.3389/fmicb.2018.01469/full. Accessed April 23, 2020.

Kruse, T., Bork-Jensen, J., and Gerdes, K. (2005) The morphogenetic MreBCD proteins of Escherichia coli form an essential membrane-bound complex. *Molecular Microbiology* **55**: 78–89.

Kuru, E., Hughes, H.V., Brown, P.J., Hall, E., Tekkam, S., Cava, F., *et al.* (2012) In Situ Probing of Newly Synthesized Peptidoglycan in Live Bacteria with Fluorescent D -Amino Acids. *Angewandte Chemie International Edition* **51**: 12519–12523.

Kuru, E., Tekkam, S., Hall, E., Brun, Y.V., and Van Nieuwenhze, M.S. (2015) Synthesis of fluorescent D-amino acids and their use for probing peptidoglycan synthesis and bacterial growth in situ. *Nat Protoc* **10**: 33–52.

Laddomada, F., Miyachiro, M.M., and Dessen, A. (2016) Structural Insights into Protein-Protein Interactions Involved in Bacterial Cell Wall Biogenesis. *Antibiotics (Basel)* **5**: 14.

Lassak, J., Koller, F., Krafczyk, R., and Volkwein, W. (2019) Exceptionally versatile – arginine in bacterial post-translational protein modifications. *Biological Chemistry* **0** http://www.degruyter.com/view/j/bchm.ahead-of-print/hsz-2019-0182/hsz-2019-0182.xml. Accessed August 15, 2019.

Letek, M., Ordonez, E., Vaquera, J., Margolin, W., Flardh, K., Mateos, L.M., and Gil, J.A. (2008) DivIVA Is Required for Polar Growth in the MreB-Lacking Rod-Shaped Actinomycete Corynebacterium glutamicum. *Journal of Bacteriology* **190**: 3283–3292.

Liu, B., Persons, L., Lee, L., and Boer, P.A.J. de (2015) Roles for both FtsA and the FtsBLQ subcomplex in FtsN-stimulated cell constriction in Escherichia coli. *Molecular Microbiology* **95**: 945–970.

Logsdon, M.M., and Aldridge, B.B. (2018) Stable Regulation of Cell Cycle Events in Mycobacteria: Insights From Inherently Heterogeneous Bacterial Populations. *Front Microbiol* **9**: 514.

Lu, S., Wang, J., Chitsaz, F., Derbyshire, M.K., Geer, R.C., Gonzales, N.R., *et al.* (2020) CDD/SPARCLE: the conserved domain database in 2020. *Nucleic Acids Res* **48**: D265–D268.

Ma, X., Ehrhardt, D.W., and Margolin, W. (1996) Colocalization of cell division proteins FtsZ and FtsA to cytoskeletal structures in living Escherichia coli cells by using green fluorescent protein. https://www.pnas.org/doi/10.1073/pnas.93.23.12998. Accessed November 10, 2022.

Mahone, C.R., and Goley, E.D. (2020) Bacterial cell division at a glance. *J Cell Sci* **133**: jcs237057.

Marmont, L.S., and Bernhardt, T.G. (2020) A conserved subcomplex within the bacterial cytokinetic ring activates cell wall synthesis by the FtsW-FtsI synthase. *PNAS* **117**: 23879–23885.

Marrakchi, H., Lanéelle, M.-A., and Daffé, M. (2014) Mycolic Acids: Structures, Biosynthesis, and Beyond. *Chemistry & Biology* **21**: 67–85.

Marston, A.L., and Errington, J. (1999) Selection of the midcell division site in Bacillus subtilis through MinD-dependent polar localization and activation of MinC. *Molecular Microbiology* **33**: 84–96.

Melzer, E.S., Kado, T., García-Heredia, A., Gupta, K.R., Meniche, X., Morita, Y.S., *et al.* (2021) Cell wall damage reveals spatial flexibility in peptidoglycan synthesis and a non-redundant role for RodA in mycobacteria. Microbiology, . http://biorxiv.org/lookup/doi/10.1101/2021.10.26.465981. Accessed November 8, 2021.

Melzer, E.S., Sein, C.E., Chambers, J.J., and Sloan Siegrist, M. (2018) DivIVA concentrates mycobacterial cell envelope assembly for initiation and stabilization of polar growth. *Cytoskeleton* **75**: 498–507.

Mengin-Lecreulx, D., Texier, L., Rousseau, M., and Heijenoort, J. van (1991) The murG gene of Escherichia coli codes for the UDP-N-acetylglucosamine: N-acetylmuramyl-(pentapeptide) pyrophosphoryl-undecaprenol N-acetylglucosamine transferase involved in the membrane steps of peptidoglycan synthesis. *J Bacteriol* **173**: 4625–4636.

Meniche, X., Otten, R., Siegrist, M.S., Baer, C.E., Murphy, K.C., Bertozzi, C.R., and Sassetti, C.M. (2014) Subpolar addition of new cell wall is directed by DivIVA in mycobacteria. *Proceedings of the National Academy of Sciences* **111**: E3243–E3251.

Mohammadi, T., Karczmarek, A., Crouvoisier, M., Bouhss, A., Mengin-Lecreulx, D., and Blaauwen, T. den (2007) The essential peptidoglycan glycosyltransferase MurG forms a complex with proteins involved in lateral envelope growth as well as with proteins involved in cell division in Escherichia coli. *Mol Microbiol* **65**: 1106–1121.

Morgenstein, R.M., Bratton, B.P., Nguyen, J.P., Ouzounov, N., Shaevitz, J.W., and Gitai, Z. (2015) RodZ links MreB to cell wall synthesis to mediate MreB rotation and robust morphogenesis. *Proc Natl Acad Sci U S A* **112**: 12510–12515.

Mukherjee, A., Cao, C., and Lutkenhaus, J. (1998) Inhibition of FtsZ polymerization by SulA, an inhibitor of septation in Escherichia coli. *Proc Natl Acad Sci U S A* **95**: 2885–2890.

Mukherjee, P., Sureka, K., Datta, P., Hossain, T., Barik, S., Das, K.P., *et al.* (2009) Novel role of Wag31 in protection of mycobacteria under oxidative stress. *Molecular Microbiology* **73**: 103–119.

Murphy, K.C., Papavinasasundaram, K., and Sassetti, C.M. (2015) Mycobacterial Recombineering. In *Mycobacteria Protocols*. Parish, T., and Roberts, D.M. (eds). Springer New York, New York, NY. pp. 177–199 http://link.springer.com/10.1007/978-1-4939-2450-9_10. Accessed May 3, 2019.

Nelson, D.E., and Young, K.D. (2001) Contributions of PBP 5 and DD-carboxypeptidase penicillin binding proteins to maintenance of cell shape in Escherichia coli. *J Bacteriol* **183**: 3055–3064.

Park, K.-T., Du, S., and Lutkenhaus, J. (2020) Essential Role for FtsL in Activation of Septal Peptidoglycan Synthesis. *mBio* **11**: e03012-20.

Pashley, C.A., and Parish, T. (2003) Efficient switching of mycobacteriophage L5-based integrating plasmids in *Mycobacterium tuberculosis*. *FEMS Microbiology Letters* **229**: 211–215.

Peh, H.L., Toh, A., Murugasu-Oei, B., and Dick, T. (2001) In Vitro Activities of Mitomycin C against Growing and Hypoxic Dormant Tubercle Bacilli. *Antimicrob Agents Chemother* **45**: 2403–2404.

Pelicic, V., Jackson, M., Reyrat, J.-M., Jacobs, W.R., Gicquel, B., and Guilhot, C. (1997) Efficient allelic exchange and transposon mutagenesis in Mycobacterium tuberculosis. *PNAS* **94**: 10955–10960.

Pettersen, E.F., Goddard, T.D., Huang, C.C., Meng, E.C., Couch, G.S., Croll, T.I., *et al.* (2021) UCSF ChimeraX: Structure visualization for researchers, educators, and developers. *Protein Sci* **30**: 70–82.

Pham, T.T., Jacobs-Sera, D., Pedulla, M.L., Hendrix, R.W., and Hatfull, G.F.Y. 2007 Comparative genomic analysis of mycobacteriophage Tweety: evolutionary insights and construction of compatible site-specific integration vectors for mycobacteria. *Microbiology* **153**: 2711–2723.

Pichoff, S., Du, S., and Lutkenhaus, J. (2015) The bypass of ZipA by overexpression of FtsN requires a previously unknown conserved FtsN motif essential for FtsA-FtsN interaction supporting a model in which FtsA monomers recruit late cell division proteins to the Z ring. *Mol Microbiol* **95**: 971–987.

Pichoff, S., and Lutkenhaus, J. (2001) Escherichia coli Division Inhibitor MinCD Blocks Septation by Preventing Z-Ring Formation. *J Bacteriol* **183**: 6630–6635.

Pickford, H., Alcock, E., Singh, A., Kelemen, G., and Bhatt, A. (2020) A mycobacterial DivIVA domain-containing protein involved in cell length and septation. *Microbiology* https://www.microbiologyresearch.org/content/journal/micro/10.1099/mic.0.000952. Accessed July 18, 2020.

Plocinski, P., Ziolkiewicz, M., Kiran, M., Vadrevu, S.I., Nguyen, H.B., Hugonnet, J., *et al.* (2011) Characterization of CrgA, a New Partner of the Mycobacterium tuberculosis Peptidoglycan Polymerization Complexes. *Journal of Bacteriology* **193**: 3246–3256.

Pogliano, J., Pogliano, K., Weiss, D.S., Losick, R., and Beckwith, J. (1997) Inactivation of FtsI inhibits constriction of the FtsZ cytokinetic ring and delays the assembly of FtsZ rings at potential division sites. *Proc Natl Acad Sci USA* **94**: 559–564.

Prisic, S., Dankwa, S., Schwartz, D., Chou, M.F., Locasale, J.W., Kang, C.-M., *et al.* (2010) Extensive phosphorylation with overlapping specificity by Mycobacterium tuberculosis serine/ threonine protein kinases. *Proceedings of the National Academy of Sciences* **107**: 7521–7526.

Prisic, S., and Husson, R.N. (2014) Mycobacterium tuberculosis Serine/Threonine Protein Kinases. *Microbiology Spectrum* **2** http://www.asmscience.org/content/journal/microbiolspec/10.1128/microbiolspec.MGM2-0006-2013. Accessed February 6, 2019.

Pryka, R.D., and Haig, G.M. (1994) Meropenem: A New Carbapenem Antimicrobial. *Ann Pharmacother* **28**: 1045–1054.

Puffal, J., García-Heredia, A., Rahlwes, K.C., Siegrist, M.S., and Morita, Y.S. (2018) Spatial control of cell envelope biosynthesis in mycobacteria. *Pathogens and Disease* **76** https://academic.oup.com/femspd/article/doi/10.1093/femspd/fty027/4953754. Accessed February 10, 2020.

Raghunathan, S., Chimthanawala, A., Krishna, S., Vecchiarelli, A.G., and Badrinarayanan, A. (2020) Asymmetric chromosome segregation and cell division in DNA damage-induced bacterial filaments. *MBoC* **31**: 2920–2931.

Ramamurthi, K.S., and Losick, R. (2009) Negative membrane curvature as a cue for subcellular localization of a bacterial protein. *Proceedings of the National Academy of Sciences* **106**: 13541–13545.

Raposo, A.E., and Piller, S.C. (2018) Protein arginine methylation: an emerging regulator of the cell cycle. *Cell Div* **13**: 3.

Raskin, D.M., and Boer, P.A.J. de (1997) The MinE Ring: An FtsZ-Independent Cell Structure Required for Selection of the Correct Division Site in E. coli. *Cell* **91**: 685–694.

Raskin, D.M., and Boer, P.A.J. de (1999a) Rapid pole-to-pole oscillation of a protein required for directing division to the middle of *Escherichia coli*. *Proc Natl Acad Sci USA* **96**: 4971–4976.

Raskin, D.M., and Boer, P.A.J. de (1999b) MinDE-Dependent Pole-to-Pole Oscillation of Division Inhibitor MinC in Escherichia coli. *J Bacteriol* **181**: 6419–6424.

Reck, F., Marmor, S., Fisher, S., and Wuonola, M.A. (2001) Inhibitors of the bacterial cell wall biosynthesis enzyme MurC. *Bioorganic & Medicinal Chemistry Letters* **11**: 1451–1454.

Rego, E.H., Audette, R.E., and Rubin, E.J. (2017) Deletion of a mycobacterial divisome factor collapses single-cell phenotypic heterogeneity. *Nature* **546**: 153–157.

Rohs, P.D.A., Buss, J., Sim, S.I., Squyres, G.R., Srisuknimit, V., Smith, M., *et al.* (2018) A central role for PBP2 in the activation of peptidoglycan polymerization by the bacterial cell elongation machinery. *PLOS Genetics* **14**: e1007726.

Ruiz, N. (2008) Bioinformatics identification of MurJ (MviN) as the peptidoglycan lipid II flippase in *Escherichia coli*. *PNAS* **105**: 15553–15557.

Sakatos, A., Babunovic, G.H., Chase, M.R., Dills, A., Leszyk, J., Rosebrock, T., *et al.* (2018) Posttranslational modification of a histone-like protein regulates phenotypic resistance to isoniazid in mycobacteria. *Science Advances* **4**: eaao1478.

Sambrook, J., and Russel, D. (2001) *Molecular Cloning A Laboratory Manual*. 3rd ed., Cold Spring Harbour Laboratory Press, Cold Spring Harbour, New York.

Schmidt, K.L., Peterson, N.D., Kustusch, R.J., Wissel, M.C., Graham, B., Phillips, G.J., and Weiss, D.S. (2004) A Predicted ABC Transporter, FtsEX, Is Needed for Cell Division in Escherichia coli. *J Bacteriol* **186**: 785–793.

Schmidt, T.G., and Skerra, A. (2007) The Strep-tag system for one-step purification and high-affinity detection or capturing of proteins. *Nat Protoc* **2**: 1528–1535.

Sham, L.-T., Butler, E.K., Lebar, M.D., Kahne, D., Bernhardt, T.G., and Ruiz, N. (2014) MurJ is the flippase of lipid-linked precursors for peptidoglycan biogenesis. *Science* **345**: 220–222.

Shamma, F., Papavinasasundaram, K., Quintanilla, S.Y., Bandekar, A., Sassetti, C., and Boutte, C.C. (2020) Phosphorylation on PstP Regulates Cell Wall Metabolism and Antibiotic Tolerance in *Mycobacterium smegmatis*. *J Bacteriol* **203**: e00563-20, /jb/203/4/JB.00563-20.atom.

Shen, L., Viljoen, A., Villaume, S., Joe, M., Halloum, I., Chêne, L.P., *et al.* (2020) The endogenous galactofuranosidase GlfH1 hydrolyzes mycobacterial arabinogalactan. *J Biol Chem* jbc.RA119.011817.

Sherratt, D.J., Arciszewska, L.K., Crozat, E., Graham, J.E., and Grainge, I. (2010) The Escherichia coli DNA translocase FtsK. *Biochem Soc Trans* **38**: 395–398.

Shi, H., Bratton, B.P., Gitai, Z., and Huang, K.C. (2018) How to Build a Bacterial Cell: MreB as the Foreman of E. coli Construction. *Cell* **172**: 1294–1305.

Shih, Y.-L., Le, T., and Rothfield, L. (2003) Division site selection in Escherichia coli involves dynamic redistribution of Min proteins within coiled structures that extend between the two cell poles. *Proc Natl Acad Sci U S A* **100**: 7865–7870.

Sibghat-Ullah, Sancar, A., and Hearst, J.E. (1990) The repair patch of E. coli (A)BC excinuclease. *Nucleic Acids Res* **18**: 5051–5053.

Sinawe, H., and Casadesus, D. (2022) *Mitomycin*. StatPearls Publishing, . https://www.ncbi.nlm.nih.gov/books/NBK562249/. Accessed April 6, 2023.

Singh, A. (2017) Guardians of the mycobacterial genome: A review on DNA repair systems in Mycobacterium tuberculosis. *Microbiology* **163**: 1740–1758.

Singhal, A., Virmani, R., Naz, S., Arora, G., Gaur, M., Kundu, P., *et al.* (2020) Methylation of two-component response regulator MtrA in mycobacteria negatively modulates its DNA binding and transcriptional activation. *Biochemical Journal* **477**: 4473–4489.

Smeulders, M.J., Keer, J., Speight, R.A., and Williams, H.D. (1999) Adaptation of Mycobacterium smegmatis to Stationary Phase. *J Bacteriol* **181**: 270–283.

Su, Y., Li, J., Zhang, W., Ni, J., Huang, R., Wang, Z., *et al.* (2021) Methylation of PhoP by CheR Regulates *Salmonella* Virulence. *mBio* https://journals.asm.org/doi/10.1128/mBio.02099-21. Accessed September 28, 2021.

Suginaka, H., Blumberg, P.M., and Strominger, J.L. (1972) Multiple Penicillin-binding Components in Bacillus subtilis, Bacillus cereus, Staphylococcus aureus, and Escherichia coli. *Journal of Biological Chemistry* **247**: 5279–5288.

Taguchi, A., Welsh, M.A., Marmont, L.S., Lee, W., Sjodt, M., Kruse, A.C., *et al.* (2019) FtsW is a peptidoglycan polymerase that is functional only in complex with its cognate penicillin-binding protein. *Nature Microbiology* http://www.nature.com/articles/s41564-018-0345-x. Accessed February 6, 2019.

Takayama, K., Wang, C., and Besra, G.S. (2005) Pathway to Synthesis and Processing of Mycolic Acids in Mycobacterium tuberculosis. *Clin Microbiol Rev* **18**: 81–101.

Teeffelen, S. van, Wang, S., Furchtgott, L., Huang, K.C., Wingreen, N.S., Shaevitz, J.W., and Gitai, Z. (2011) The bacterial actin MreB rotates, and rotation depends on cell-wall assembly. *Proceedings of the National Academy of Sciences* **108**: 15822–15827.

Thakur, M., Badugu, S., and Muniyappa, K. (2020) UvrA and UvrC subunits of the *Mycobacterium tuberculosis* UvrABC excinuclease interact independently of UvrB and DNA. *FEBS Lett* **594**: 851–863.

Thanky, N.R., Young, D.B., and Robertson, B.D. (2007) Unusual features of the cell cycle in mycobacteria: Polar-restricted growth and the snapping-model of cell division. *Tuberculosis* **87**: 231–236.

Tsang, M.-J., and Bernhardt, T.G. (2015a) A role for the FtsQLB complex in cytokinetic ring activation revealed by an ftsL allele that accelerates division. *Mol Microbiol* **95**: 925–944.

Tsang, M.-J., and Bernhardt, T.G. (2015b) Guiding divisome assembly and controlling its activity. *Curr Opin Microbiol* **24**: 60–65.

Tsang, M.-J., Yakhnina, A.A., and Bernhardt, T.G. (2017) NlpD links cell wall remodeling and outer membrane invagination during cytokinesis in Escherichia coli. *PLOS Genetics* **13**: e1006888.

Typas, A., Banzhaf, M., Berg van Saparoea, B. van den, Verheul, J., Biboy, J., Nichols, R.J., *et al.* (2010) Regulation of Peptidoglycan Synthesis by Outer-Membrane Proteins. *Cell* **143**: 1097–1109.

Typas, A., Banzhaf, M., Gross, C.A., and Vollmer, W. (2012) From the regulation of peptidoglycan synthesis to bacterial growth and morphology. *Nature Reviews Microbiology* **10**: 123–136.

Van Houten, B., and Snowden, A. (1993) Mechanism of action of the Escherichia coli UvrABC nuclease: Clues to the damage recognition problem. *BioEssays* **15**: 51–59.

Vedyaykin, A., Rumyantseva, N., Khodorkovskii, M., and Vishnyakov, I. (2020) SulA is able to block cell division in Escherichia coli by a mechanism different from sequestration. *Biochemical and Biophysical Research Communications* **525**: 948–953.

Villanelo, F., Ordenes, A., Brunet, J., Lagos, R., and Monasterio, O. (2011) A model for the Escherichia coli FtsB/FtsL/FtsQ cell division complex. *BMC Struct Biol* **11**: 28.

Vollmer, W., and Bertsche, U. (2008) Murein (peptidoglycan) structure, architecture and biosynthesis in Escherichia coli. *Biochimica et Biophysica Acta (BBA) - Biomembranes* **1778**: 1714–1734.

Wachi, M., Doi, M., Tamaki, S., Park, W., Nakajima-Iijima, S., and Matsuhashi, M. (1987) Mutant isolation and molecular cloning of mre genes, which determine cell shape, sensitivity to mecillinam, and amount of penicillin-binding proteins in Escherichia coli. *J Bacteriol* **169**: 4935–4940.

Wallick, H., and Hendlin, D. (1974) Cefoxitin, a Semisynthetic Cephamycin Antibiotic: Susceptibility Studies. *Antimicrob Agents Chemother* **5**: 25–32.

Weibull, C., and Koffler, H. (1959) ε-N-Methyl-lysine in Bacterial Flagellar Protein | Nature. https://www.nature.com/articles/184056b0. Accessed August 9, 2019.

Weiss, D.S. (2015) Last but not least: new insights into how FtsN triggers constriction during Escherichia coli cell division. *Molecular Microbiology* **95**: 903–909.

World Health Organization (2022) *Global tuberculosis report 2022*. World Health Organization, . https://apps.who.int/iris/handle/10665/363752. Accessed January 6, 2023.

Wu, K.J., Zhang, J., Baranowski, C., Leung, V., Rego, E.H., Morita, Y.S., *et al.* (2018) Characterization of Conserved and Novel Septal Factors in *Mycobacterium smegmatis*. *Journal of Bacteriology* **200**: e00649-17, /jb/200/6/e00649-17.atom.

Wu, L.J., and Errington, J. (2012) Nucleoid occlusion and bacterial cell division. *Nature Reviews Microbiology* **10**: 8–12.

Wu, M.-L., Gengenbacher, M., and Dick, T. (2016) Mild Nutrient Starvation Triggers the Development of a Small-Cell Survival Morphotype in Mycobacteria. *Front Microbiol* **7** http://journal.frontiersin.org/Article/10.3389/fmicb.2016.00947/abstract. Accessed September 19, 2019.

Yan, Y., Munshi, S., Leiting, B., Anderson, M.S., Chrzas, J., and Chen, Z. (2000) Crystal structure of Escherichia coli UDPMurNAc-tripeptide d-alanyl-d-alanine-adding enzyme (MurF) at 2.3 Å resolution. *Journal of Molecular Biology* **304**: 435–445.

Yang, D.C., Peters, N.T., Parzych, K.R., Uehara, T., Markovski, M., and Bernhardt, T.G. (2011) An ATP-binding cassette transporter-like complex governs cell-wall hydrolysis at the bacterial cytokinetic ring. *PNAS* **108**: E1052–E1060.

Yang, D.C., Tan, K., Joachimiak, A., and Bernhardt, T.G. (2012) A conformational switch controls cell wall-remodelling enzymes required for bacterial cell division. *Molecular Microbiology* **85**: 768–781.

Yates, A.D., Allen, J., Amode, R.M., Azov, A.G., Barba, M., Becerra, A., *et al.* (2022) Ensembl Genomes 2022: an expanding genome resource for non-vertebrates. *Nucleic Acids Research* **50**: D996–D1003.

Zeng, B., Wong, K.K., Pompliano, D.L., Reddy, S., and Tanner, M.E. (1998) A Phosphinate Inhibitor of the meso-Diaminopimelic Acid-Adding Enzyme (MurE) of Peptidoglycan Biosynthesis. *J Org Chem* **63**: 10081–10085.

Zhang, M., Xu, J.-Y., Hu, H., Ye, B.-C., and Tan, M. (2018) Systematic Proteomic Analysis of Protein Methylation in Prokaryotes and Eukaryotes Revealed Distinct Substrate Specificity. *PROTEOMICS* **18**: 1700300.

Zhang, Y.-W., Zhu, J.-H., Wang, Z.-Q., Wu, Y., Meng, X., Zheng, X., and Javid, B. (2019) HspX promotes the polar localization of mycobacterial protein aggregates. *Sci Rep* **9**: 14571.

Zhou, X., Rodriguez-Rivera, F.P., Lim, H.C., Bell, J.C., Bernhardt, T.G., Bertozzi, C.R., and Theriot, J.A. (2019) Sequential assembly of the septal cell envelope prior to V snapping in Corynebacterium glutamicum. *Nature Chemical Biology* http://www.nature.com/articles/s41589-018-0206-1. Accessed February 6, 2019.

Zupan, J., Guo, Z., Biddle, T., and Zambryski, P. (2021) *Agrobacterium tumefaciens* Growth Pole Ring Protein: C Terminus and Internal Apolipoprotein Homologous Domains Are Essential for Function and Subcellular Localization. *mBio* **12**: e00764-21, /mbio/12/3/mBio.00764-21.atom.

Zupan, J.R., Grangeon, R., Robalino-Espinosa, J.S., Garnica, N., and Zambryski, P. (2019) GROWTH POLE RING protein forms a 200-nm-diameter ring structure essential for polar growth and rod shape in Agrobacterium tumefaciens. *PNAS* 201905900.